U. S. Department of Commerce
National Oceanic and Atmospheric Administration
National Weather Service
National Centers for Environmental Prediction
4700 Silver Hill Road, Mail Stop 9910
Washington, DC 20233-9910

Technical Note

Optimum Discrete Interaction Aproximations for wind waves. Part 1: mapping using inverse modeling.[†]

Hendrik L. Tolman [‡]
SAIC-GSO at
Environmental Modeling Center
Marine Modeling and Analysis Branch

April 2003

[†] MMAB Contribution No. 227.

[‡] e-mail: Hendrik.Tolman@NOAA.gov

This page is intentionally left blank.

Abstract

This report addresses the capability of previously suggested and new Discrete Interaction Approximations (DIAs) of the nonlinear wave-wave interactions for wind waves to reproduce the exact interactions source term. The investigation mainly considers inverse modeling and optimization of free parameters in such DIAs, with the aim of reproducing the exact interactions source term for test spectra. In this initial study, only deep water spectra with a single peak are considered. It is shown that an accurate description of the exact interactions source term by a DIA requires an expanded definition of the quadruplet. A new two-parameter quadruplet configuration proved adequate in this respect. A previously suggested inclusion of additional proportionality constants does not appear to improve the DIA significantly, and therefore does not seem justified. A new method, where the free parameters of the DIA are allowed to be a slowly varying function of the spectral frequency f, results in some further improvement. A strong point of this approximation is that its accuracy appears relatively insensitive to the test case considered. Unfortunately, this method proved not to result in stable model integration when applied in the WAVEWATCH III model. Very accurate results were obtained with a multiple DIA with four components and the expanded definition of the interacting quadruplets considered in the DIA. This 'multiple' DIA results in stable model integration, but requires dynamical estimation of its free parameters for optimum results. Part 2 of this study will address the capability of various DIA formulations to result in stable and realistic model integration in a full wave model.

Acknowledgments. The author thanks Henrique Alves, Mary Hart and Prof. Hashimoto for comments on early drafts of this manuscript. The present study was made possibly by funding from the Office of Naval Research (ONR) through grant N00014-00-F-0332 and by funding from the NOAA High Performance Computing and Communication (HPCC) office.

This report is available as a pdf file from

http://polar.ncep.noaa.gov/waves

Contents

This page is intentionally left blank.

1 Introduction

Ocean wave modeling has been in the center of interest for several decades. Following Hasselmann (1960) numerical models are generally based on an action or energy balance equation of the form

$$\frac{DF}{Dt} = S_{tot} = S_{in} + S_{nl} + S_{ds} \quad , \tag{1.1}$$

where F is the spectrum, and S_{tot} represents the sources and sinks, consisting of a wind input (S_{in}), nonlinear interactions (S_{nl}) and dissipation (S_{ds}) source terms. Arguably the biggest breakthrough in the understanding of wind wave generation, and hence in numerical wave modeling, occurred with the understanding of the critical role of the nonlinear interactions source term S_{nl} in the process of wave growth (Phillips, 1960; Hasselmann, 1962, 1963a,b; Hasselmann et al., 1973). The nonlinear interactions are believed to provide the lowest order mechanism to shift wave energy to longer waves, and also provide a stabilization mechanism for the shape of the spectrum. Reviews of the interactions and their impact can be found, for instance, in Masuda (1980), Phillips (1981), Young and Van Vledder (1993) or Komen et al. (1994).

The nonlinear interactions source term describes the resonant exchange of energy, momentum and action between a "quadruplet" of four spectral components with wavenumber vectors $\boldsymbol{k}_1$ through $\boldsymbol{k}_4$ and (radian) frequencies σ_1 through σ_4 ($\sigma = 2\pi f$). These satisfy the resonance following conditions (Hasselmann, 1962, 1963a) :

$$\boldsymbol{k}_1 + \boldsymbol{k}_2 = \boldsymbol{k}_3 + \boldsymbol{k}_4 \quad , \tag{1.2}$$

$$\sigma_1 + \sigma_2 = \sigma_3 + \sigma_4 \quad . \tag{1.3}$$

The interactions are conventionally expressed in terms of the rate of change of the action spectrum $n \equiv F/\sigma$ in terms of the wavenumber vector $\boldsymbol{k}$, as

$$\begin{aligned} \frac{\partial n_1}{\partial t} &= \iiint G\left(\boldsymbol{k}_1, \boldsymbol{k}_2, \boldsymbol{k}_3, \boldsymbol{k}_4\right)\ \delta_k\, \delta_\sigma \\ &\times \quad \left[n_1 n_3 \left(n_4 - n_2\right) + n_2 n_4 \left(n_3 - n_1\right)\right]\ d\boldsymbol{k}_2\, d\boldsymbol{k}_3\, d\boldsymbol{k}_4 \quad , \end{aligned} \tag{1.4}$$

where n_i is the action density at component i, $n_i = n(\boldsymbol{k}_i)$, G is a complex coupling coefficient (Webb, 1978; Herterich and Hasselmann, 1980), and δ_k and δ_σ are delta functions corresponding to the resonance conditions (1.2) and (1.3).

Due to the multidimensional integration and singularities in G the solution of (1.4) is much too expensive for application in operational wind wave models. From the perspective of operational wave modeling, a major breakthrough occurred with the development of the Discrete Interaction Approximation (DIA, Hasselmann et al., 1985), which proved sufficiently economical for application in

operational wave models. The DIA and previously suggested adaptations to this algorithm will be discussed in more detail in the following section.

The DIA made the development of the first third-generation wave model possible (WAM, WAMDIG, 1988). By definition, Eq. (1.1) is fully parameterized in third-generation wave models, without assuming the resulting spectral shape. Nevertheless, even with the success of the DIA, Hasselmann et al. (1985) recognized shortcomings in the accuracy of the DIA. It is therefore not surprising that much research has been performed in the past decades attempting to derive or construct nonlinear interactions algorithms which combine the accuracy of the full solution with the economy of the DIA.

Several different paths have been taken in this research. First, much progress has been made in optimizing the exact interactions, using various approaches. Important steps where made, for instance, by Masuda (1980), Tracy and Resio (1982), Resio and Perrie (1991), Komatsu and Masuda (1996), and Van Vledder (2000). Even with this improved efficiency, the exact interaction algorithm remains several orders of magnitude more expensive than the DIA, making it economically unacceptable for application in a practical model.

One attempt to speed up the calculation of the interactions is by applying various filtering techniques (e.g., Snyder et al., 1998; Hashimoto and Kawaguchi, 2001; Hashimoto et al., 2002). One of the methods described in the latter paper (SRIAM), is claimed to 'retain most of the [interactions] accuracy in computing the nonlinear energy transfer' at about 20 times the costs of the DIA. Unfortunately, this claim is not substantiated. Generally, any such filtering technique trades speed for accuracy.

In the same family of approaches (trading speed for accuracy), the DIA can be expanded to become more accurate. Expansions have included more complex descriptions of the interactions, more complex quadruplets, or more quadruplet combinations (e.g., Ueno and Ishizaka, 1997; Hashimoto and Kawaguchi, 2001; Van Vledder, 2001, 2002a). Several of the above papers indicate that much progress can be made while increasing the computational costs compared to the DIA by an order of magnitude or less.

Other methods employed to obtain an accurate yet economic parameterization of the nonlinear interactions have been fully parametric approaches. Some of these have been reviewed by Hasselmann et al. (1985). These methods are shown to either lack accuracy or the capability of stabilizing the shape of the spectrum. Recently some new approaches have been tried. Two recent methods that stand out are a new diffusion-operator approach by Zakharov and Pushkarev (to the knowledge of the present author still unpublished) and direct mapping methods based on Neural Networks (Krasnopolsky et al., 2002). These methods are in various stages of development, and will not be considered in detail here. The latter Neural Network (NN) approach, however, is a direct reason for starting the present study.

The Marine Modeling and Analysis Branch (MMAB) of the Environmental Modeling Center (EMC) of the National Centers for Environmental Prediction (NCEP) has gained extensive experience with the above NN approaches. This experience suggests that in order to get a robust NN algorithm to calculate non-linear interactions, it would be advisable to integrate physical aspects of the interactions into the NN. The DIA appears to be the most reduced version of S_{nl} that retains all physical aspects. A NN interaction approximation for S_{nl} based on the DIA therefore seems to be a natural choice. A first step towards such a NN/DIA is taken here by assessing the potential of various forms of the DIA to reproduce the exact interactions, mostly using inverse modeling techniques. Second, the need for dynamically adjusting the DIA will be assessed. Note that this need already appears to have been identified by Hashimoto and Kawaguchi (2001), who show in their Table 1 that the optimum choice of DIA parameters is a distinct function of spectral shape.

The layout of this report is as follows. In Section 2 presently published DIAs are presented and discussed. Based on previous work, two new modifications to the DIA are suggested. The first is an alternative layout of the quadruplet used in the DIA. The second is the so-called Variable DIA (VDIA), where free parameters in the DIA are allowed to be a function of the parameters defining the spectral space. In Section 3 the results for inverse modeling for several DIAs are presented using a single test case. The two most promising methods appear to be a single VDIA, or a multiple DIA (MDIA) with constant DIA parameters in spectral space for each component. In Section 4 the most promising methods are applied to a set different test cases to address their general applicability and to assess the need for dynamically adjusting parameter settings. The VDIA proves less accurate for very sharp spectra, and does not appear to benefit greatly from dynamically adjusting parameter settings. The MDIA can be generally accurate, but then requires dynamical adjustment of the parameter settings. In Section 5, both selected methods are incorporated in a wave model to assess if they can result in stable model integration. For the VDIA no successful integration was obtained, but for the MDIA it was. Finally, a summary and conclusions are given in Section 6.

This page is intentionally left blank.

2 Discrete Interaction Approximations

2.1 The original DIA

The Discrete Interaction Approximation (DIA) was developed by Hasselmann et al. (1985). Compared to the exact interaction of Eqs. (1.2) through (1.4), a massive speed up in computation is achieved in two ways. First, only a very small sub-set of resonant quadruplets satisfying Eqs. (1.2), (1.3) is considered, where

$$\left.\begin{array}{rcl} \boldsymbol{k}_2 & = & \boldsymbol{k}_1 \\ \sigma_3 & = & (1+\lambda)\sigma_1 \end{array}\right\} \quad , \tag{2.1}$$

where λ is a constant, and $\boldsymbol{k}_1$ corresponds to discrete spectral components only (with a minor extension of the discrete grid to high frequencies, to assure that all such quadruplets with contributions within the actual discrete spectral space are considered). For each $\boldsymbol{k}_1$, only two ('mirror image') quadruplets satisfy Eqs. (1.2), (1.3) and (2.1).

Second, the exact interaction integral is replaced by a "deep water discrete-interaction analogue" (Hasselmann et al., 1985, Eq. (5.4))

$$\left(\begin{array}{c} \delta n_1 \\ \delta n_3 \\ \delta n_4 \end{array}\right) = \left(\begin{array}{c} -2 \\ 1 \\ 1 \end{array}\right) C' g^{-8} f_1^{19} \left[n_1^2 (n_3 + n_4) - 2 n_1 n_3 n_4 \right] \Delta \boldsymbol{k} \, \Delta t \, , \tag{2.2}$$

where δn_1 is the discrete change of action density $n(\boldsymbol{k}_1)$ in time step Δt (etc.), and C' is a constant. The speed up in computation is achieved here by replacing the six-dimensional integral in (1.4) with a single loop over the discrete spectral space, and by replacing the complicated interaction coefficient G (with its singularities) with a simple constant (C').

In wave models, the wave field has conventionally been described by using the wave variance spectrum in terms of the wave frequency and direction, $F(f,\theta) = 4\pi\sigma^4 g^{-2} n(\boldsymbol{k})$ (deep water). The corresponding contribution to the nonlinear interactions $\delta S_{nl,i}$ at component i of the quadruplet becomes (Hasselmann et al., 1985, Eq. (5.5))

$$\begin{aligned} \left(\begin{array}{c} \delta S_{nl,1} \\ \delta S_{nl,3} \\ \delta S_{nl,4} \end{array}\right) &= \left(\begin{array}{c} -2\frac{\Delta f_1 \Delta\theta_1}{\Delta f_1 \Delta\theta_1} \\ (1+\lambda)\frac{\Delta f_1 \Delta\theta_1}{\Delta f_3 \Delta\theta_3} \\ (1-\lambda)\frac{\Delta f_1 \Delta\theta_1}{\Delta f_4 \Delta\theta_4} \end{array}\right) C g^{-4} f_1^{11} \times \\ &\left[F_1^2 \left(\frac{F_3}{(1+\lambda)^4} + \frac{F_4}{(1-\lambda)^4} \right) - \frac{2 F_1 F_3 F_4}{(1-\lambda^2)^4} \right] , \end{aligned} \tag{2.3}$$

where C is a preset constant, and Δf and $\Delta\theta$ are increments or band widths in the discrete spectral space. Furthermore assuming a constant discretization of

the spectral directions, and constant relative frequency increments $f_{i+1} = \alpha f_i$, the conventional expression for the DIA is found

$$\begin{pmatrix} \delta S_{nl,1} \\ \delta S_{nl,3} \\ \delta S_{nl,4} \end{pmatrix} = \begin{pmatrix} -2 \\ 1 \\ 1 \end{pmatrix} C g^{-4} f_1^{11} \times \left[F_1^2 \left(\frac{F_3}{(1+\lambda)^4} + \frac{F_4}{(1-\lambda)^4} \right) - \frac{2F_1F_3F_4}{(1-\lambda^2)^4} \right] . \quad (2.4)$$

Details of the derivation of an extended DIA can be found in Van Vledder (2001). It is important to note that the spectral grid layout is included in this formulation, and that it is constructed assuming deep water conditions. The restriction to deep water does not impact the present feasibility study, but needs to be addressed when an actual DIA is implemented in a wave model.

It should be noted that the DIA retains general conservation characteristics of the exact interactions. The distribution of the contributions $\delta S_{nl,1}$ through $\delta S_{nl,4}$ over the four components of the quadruplet in Eq. (2.3) or (2.4) guarantees the conservation of the total energy in the spectrum. If the conservation of energy is thus assured, the resonance conditions implicit to the definition of the quadruplet in turn guarantee the conservation of momentum and action (e.g., Hasselmann, 1963a; Webb, 1978). This implies that the DIA will have proper conservation properties regardless of the layout and number of quadruplets, as long as each quadruplet satisfies the resonance conditions. This furthermore implies that the conservation properties are retained regardless of the actual form of the common factors and the term in square brackets at the right side of Eq. (2.3) or (2.4). All DIAs that are considered in this study therefore retain the proper conservation characteristics of the exact interactions.

2.2 A test case

To illustrate the strengths and weaknesses of the DIA, a simple test will be set up similar to the test presented in Hasselmann et al. (1985). This test will also be used in the following sections as the basis of the inverse modeling efforts. The frequency spectrum $F(f)$ used in the test is the JONSWAP spectrum (Hasselmann et al., 1973)

$$F(f) = \phi_1 \ \phi_2 \ \phi_3 \ , \quad (2.5)$$

$$\phi_1 = \frac{ag^2}{(2\pi)^4 f_p^5} \left(\frac{f_p}{f} \right)^m \ , \quad \phi_2 = \exp\left[-\frac{m}{n} \left(\frac{f}{f_p} \right)^{-n} \right] \ ,$$

$$\phi_3 = \gamma^{\exp\left[-\frac{1}{2} \left\{ \frac{f-f_p}{\sigma f_p} \right\}^2 \right]} \ ,$$

where a is a proportionality constant, f_p is the spectral peak frequency, ϕ_1 and $m = 5$ describe the high-frequency flank of the spectrum, and ϕ_2 and $n = 4$ describe the low-frequency flank of the spectrum. ϕ_3 is the so-called peak-enhancement factor, with γ ranging from roughly 1 to 10, and σ represents the width of the peak, typically $\sigma = 0.07$. To represent a moderately peaked spectrum, typical for well developed wind seas, $\gamma = 2$ is used. Rather than using an arbitrary peak frequency and energy level a, the spectrum is normalized so that $f_p = 1$ and $F(f,\theta)_{\max} = 1$. In combination with this frequency spectrum, the directional distribution D of Hasselmann et al. (1980) is used

$$D(f,\theta) = \cos^{2s}[0.5(\theta - \bar{\theta}(f))] \quad , \tag{2.6}$$

$$s = \begin{cases} 6.97 \left(\frac{f}{f_p}\right)^{4.06} & \text{for} \quad f < 1.05 f_p \\ 9.77 \left(\frac{f}{f_p}\right)^{-2.34} & \text{for} \quad f \geq 1.05 f_p \end{cases} \quad , \tag{2.7}$$

where $\bar{\theta}$ is the mean direction, which to be consistent with the above is set to $\bar{\theta} = 0$. The full spectrum is defined from the frequency spectrum $F(f)$ and the directional distribution D as

$$F(f,\theta) = F(f) D(f,\theta) \quad . \tag{2.8}$$

As in practical numerical wave models, a parametric tail of the shape f^{-5} is used for frequencies above $3f_p$, with a smooth transition between $2.5f_p$ and $3f_p$ following Tolman and Chalikov (1996).

Finally, a benchmark nonlinear interaction is needed for the test case. Here, the interactions according to the Webb-Resio-Tracy (WRT) method are used (Webb, 1978; Tracy and Resio, 1982; Resio and Perrie, 1991), as implemented in version 4 of the portable exact S_{nl} package developed by Van Vledder (2002b). In the present and all following computations, the spectral space is discretized using 36 directions ($\Delta\theta = 10^\circ$) and with a relative frequency increment of 7% ($\alpha = 1.07$). The spectral space is described with 31 discrete frequencies ranging from 0.48 to 3.6 (normalized with f_p).

Figure 2.1 shows the exact (WRT) and DIA estimates of the nonlinear interactions for this test case. Hasselmann and Hasselmann (1985) set $\lambda = 0.25$ and $C = 3 \times 10^7$ to get an accurate representation of the positive lobe of the interactions for frequencies just below the spectral peak. Indeed, the one-dimensional, directionally integrated source term $S_{nl}(f)$ is represented fairly well for $f_p < 1$ (Fig. 2.1b, left) and shows the proper magnitude for the corresponding full interactions (compare Fig. 2.1a and b, right panels). However, this figure also shows a much broader positive lobe in frequency space for the DIA, particularly away from the mean direction. The choice to represent the low frequency lobe as accurate as possible results in major errors for higher frequencies. The negative lobe in panel d is more than three times as large as expected, and the positive lobe at

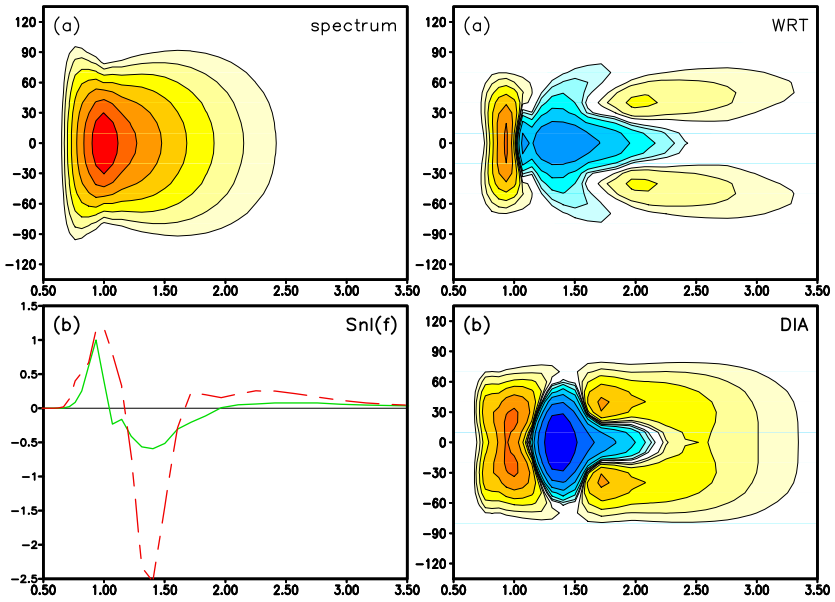

Fig. 2.1 : Nonlinear interactions for test case. Spectrum using logarithmic scaling with factor two increment and highest contour at 0.5 (panel a, left). Interactions according to WRT method (panel a, right) or original DIA (panel b, right) using logarithmic scaling with lowest contour value ± 70 *and blue identifies negative values. One dimensional interactions* $S_{nl}(f)$ *for WRT (green solid line) or DIA (red dashed line), normalized with maximum absolute value for WRT (panel b, left).*

high frequencies is also clearly overestimated. These errors were already identified in Hasselmann et al. (1985), which also shows that the use of the DIA in a numerical wave model results in a significant overestimation of the spectral wave energy at high frequencies, and a significant spurious broadening of the spectrum (figures not reproduced here).

The strength of the DIA is not its accuracy, but in its retention of many important physical characteristics of the nonlinear interactions, and its robustness when applied in a practical wave model. Equation (2.4), in combination with the resonance conditions, retains the conservation of energy, action and momentum (as discussed above); the product terms of action or energy of Eqs. (2.2) or (2.4) retain both the 'pumping' and 'diffusive' characteristics of the interactions as identified by Webb (1978). Many years of research since the introduction of the DIA have not led to even more reduced forms of S_{nl} that retain all these properties. The DIA may therefore be considered as the most basic representation of the nonlinear interactions presently available.

2.3 Previous modifications to the DIA

Several modified versions of the DIA have recently been suggested (see, for instance Ueno and Ishizaka, 1997; Van Vledder et al., 2000; Hashimoto and Kawaguchi, 2001; Van Vledder, 2001, 2002a). From these, three distinct methods for expanding the original DIA can be identified.

One modification consists of generating a composite of several DIAs with different parameter settings. In this approach (referred to here as the multiple DIA or MDIA) the DIA becomes a building block of the nonlinear interaction parameterization. It is assumed that the accuracy of the parameterization can be improved by increasing the number of degrees of freedom (adding more interacting quadruplets) at the penalty of increased costs. Hashimoto and Kawaguchi (2001) and Van Vledder (2001) both show that this approach indeed reduces the error in the DIA. The authors of these papers also suggest that with proper numerical implementation, the increase in computational costs shows asymptotic behavior with costs roughly 3 times the costs of a single DIA, even for 10 or more DIA components (2002 WISE meeting).

Another suggested modification to the original DIA (Van Vledder, 2001) is to use alternative definitions of the representative quadruplet defined by Eq. (2.1), improving the flexibility of the resulting parameterization. Van Vledder suggests the following definition for the representative quadruplet

$$\left.\begin{array}{rcc} \sigma_1 & = & \sigma \\ \sigma_2 & = & (1+\mu)\sigma \\ \sigma_3 & = & (1+\lambda)\sigma \\ \sigma_4 & = & (1-\lambda+\mu)\sigma \\ \theta_2 & = & \theta_1 \pm \Delta\theta \end{array}\right\} \quad , \tag{2.9}$$

where $\Delta\theta$ is the predescribed angular difference between the first two wavenumber vectors, and μ is an additional parameter describing the quadruplet[1]. Valid quadruplet configurations are presented in Fig. 1 and Eqs. (9) through (13) of Van Vledder (2001). Note that this quadruplet configuration reduces to the original configuration (2.1) for $\mu = 0$ and $\Delta\theta = 0$. The proper contributions of a given quadruplet to the nonlinear interaction source term cf. Eq. (2.4) is found in Eq. (21) of Van Vledder (2001)[2] (equation not reproduced here).

Finally, Ueno and Ishizaka (1997) suggest the addition of a second tunable parameter to Eq. (2.4), resulting in the following modified DIA

[1] Note that the expression for σ_4 is erroneous in Van Vledder (2001), and that both positive and negative $\Delta\theta$ need to be considered to assure symmetry.

[2] With error corresponding to the error in quadruplet description.

$$\begin{pmatrix} \delta S_{nl,1} \\ \delta S_{nl,3} \\ \delta S_{nl,4} \end{pmatrix} = \begin{pmatrix} -2 \\ 1 \\ 1 \end{pmatrix} g^{-4} f_1^{11} \times \left[C_1 F_1^2 \left(\frac{F_3}{(1+\lambda)^4} + \frac{F_4}{(1-\lambda)^4} \right) - \frac{2C_2 F_1 F_3 F_4}{(1-\lambda^2)^4} \right] . \quad (2.10)$$

where C_1 and C_2 are constants replacing C in Eq. (2.4). Equation (2.10) reduces to Eq. (2.4) for $C_1 = C_2 = C$.

Not having full access to the pertinent Japanese literature, the justification for this adaptation to the DIA is not quite clear. It appears to be rooted in an alternative version of the full interaction integral (1.4). The term in square brackets in this equation can be rewritten as

$$[n_1 n_2 (n_3 + n_4) - n_3 n_4 (n_1 + n_2)] \quad . \quad (2.11)$$

This form of the equation is used as the starting point by Ueno and Ishizaka (1997). The separate constants in Eq. (2.10) correspond to adding different weights to the two separate terms in Eq. (2.11). It is not quite clear to the present author what physical argument underlies this modification. In fact, following the argument of Webb (1978), the form of the product term as used in Eq. (1.4) identifies a separate "diffusion" and "pumping" term. If additional weights are used in the DIA, it might make more sense to split these terms, resulting in

$$\begin{pmatrix} \delta S_{nl,1} \\ \delta S_{nl,3} \\ \delta S_{nl,4} \end{pmatrix} = \begin{pmatrix} -2 \\ 1 \\ 1 \end{pmatrix} g^{-4} f_1^{11} \times \left[F_1^2 \left(\frac{C_3 F_3}{(1+\lambda)^4} + \frac{C_4 F_4}{(1-\lambda)^4} \right) - \frac{(C_3 + C_4) F_1 F_3 F_4}{(1-\lambda^2)^4} \right] , \quad (2.12)$$

where the constants are designated C_3 and C_4 to distinguish them from the constants of Ueno and Ishizaka (1997) in Eq. (2.10). This equation also reduces to Eq. (2.4) for $C_3 = C_4 = C$. Clearly, one could also consider using separate constants for all four terms in (2.11).

2.4 A more general DIA

In the present study, we will use an alternative form of the DIA that includes most of the previously suggested modifications to this parameterization, but which also reduces transparently to the original DIA.

First, a more flexible layout of the quadruplet will be used, similar to the approach used by Van Vledder (2001) [present Eq. (2.9)]. However, instead of Van Vledder's three-parameter approach, a more simple two-paramenter approach is used which proved sufficiently flexible for the present study. In this two-parameter approach, the quadruplet is defined as

$$\left.\begin{array}{rcccl} \boldsymbol{k}_1+\boldsymbol{k}_2 & = & \boldsymbol{k}_3+\boldsymbol{k}_4 & = & 2\boldsymbol{k} \\ \sigma_1 & = & (1+\mu)\sigma & & \\ \sigma_2 & = & (1-\mu)\sigma & & \\ \sigma_3 & = & (1+\lambda)\sigma & & \\ \sigma_4 & = & (1-\lambda)\sigma & & \end{array}\right\} \quad , \tag{2.13}$$

where $(\boldsymbol{k},\sigma)$ now represent the discrete spectral component, and which has four solutions like Eq. (2.9) (see Fig. 1 of Van Vledder, 2001). Adding the arbitrary requirement that $\boldsymbol{k}$ and σ satisfy the dispersion relation uniquely defines the quadruplet. This approach includes an elegant symmetry, which simplifies implementation, and has additional potential in terms of economy.

Equations (2.13) reduce to Eq. (2.1) for $\mu = 0$, or for $\lambda = 0$, and appropriate rotation of parameters and indices. Note that if the values for λ and μ are exchanged, an identical set of four quadruplets is found. Note furthermore, that for deep water, λ and μ cannot be larger than 0.5 for the dispersion relation and resonance conditions to have solutions. Finally, since sign changes of λ and μ result in identical sets of quadruplets, it is sufficient to consider only

$$0 \le \mu \le \lambda \le 0.5 \tag{2.14}$$

The proper DIA corresponding to the quadruplet (2.13), including multiple proportionality constants C, can be derived from Eq. (2.2) as

$$\begin{aligned} \begin{pmatrix} \delta S_{nl,1} \\ \delta S_{nl,2} \\ \delta S_{nl,3} \\ \delta S_{nl,4} \end{pmatrix} &= \frac{1}{2} \begin{pmatrix} -1 \\ -1 \\ 1 \\ 1 \end{pmatrix} g^{-4} f^{11} \times \\ &\left[\frac{F_1 F_2}{(1-\mu^2)^4} \left(\frac{C_3' F_3}{(1+\lambda)^4} + \frac{C_4' F_4}{(1-\lambda)^4} \right) \right. \\ &\left. - \frac{F_3 F_4}{(1-\lambda^2)^4} \left(\frac{C_1' F_1}{(1+\mu)^4} + \frac{C_2' F_2}{(1-\mu)^4} \right) \right] , \end{aligned} \tag{2.15}$$

where $2\pi f = \sigma$ is the frequency of the discrete spectral grid point considered, and C' represents the different proportionality constants. The factor $1/2$ is not strictly needed, but assures that for either $\mu = 0$ or $\lambda = 0$ this alternative DIA collapses to the conventional DIA where each quadruplet configuration has only two components instead of the four components of the new quadruplet. The

actual choice of the parameters C' defines the details of the DIA method used. The simple case

$$C'_1 = C'_2 = C'_3 = C'_4 = C \quad , \tag{2.16}$$

reproduces the conventional DIA of Hasselmann et al. (1985), with or without the extended quadruplet configuration. The form of Ueno and Ishizaka (1997) as in Eq. (2.10) is obtained when

$$C'_3 = C'_4 = C_1 \quad , \quad C'_1 = C'_2 = C_2 \quad , \tag{2.17}$$

whereas

$$C'_1 = C'_3 = C_3 \quad , \quad C'_2 = C'_4 = C_4 \quad , \tag{2.18}$$

reproduces the separate retuning of the diffusion and pumping terms of Webb (1978) as in Eq. (2.12).

A remark needs to be made about optimizing the proportionality constants C, etc. The shape stabilizing effect of the nonlinear interactions is of critical importance to numerical models. This behavior is probably due to the diffusive aspects of the nonlinear interactions as discussed by Webb (1978). If optimization results in negative values for C, this diffusive character may turn into antidiffusive behavior, with its potential for generating numerical instability. Therefore, optimizations resulting in positive values for C are preferred. Note, however, that only actual integration in a wave model can identify the robustness of any nonlinear parameterization with any value (sign) of C.

From the basic DIA defined by Eqs. (2.13) and (2.15), a multiple DIA (MDIA) with N components can simply be calculated from components $S_j(f,\theta)$ according to the above equations as

$$S_{nl}(f,\theta) = \frac{1}{N} \sum_{j=1}^{N} S_j(f,\theta) \quad . \tag{2.19}$$

The factor $1/N$ is not strictly necessary here, but is added to assure that an MDIA composed of identical components becomes identical to its components.

So far, all extensions to the original DIA are, in essence, taken from previous studies. However, close inspection of Eqs. (1.4) and (2.15) identifies a potentially more powerful adaptation to the DIA. Equations (1.4) and (2.15) incorporate a detailed balance within the nonlinear interactions (as discussed above), and hence guarantee *locally* within the spectrum the conservation of energy, action and momentum. Considering this, there is no need for assuming either λ, μ or C to be constants. It is well known that dominant wavenumber scales of interactions vary throughout the spectrum (e.g., Hasselmann, 1963b; Hasselmann and Hasselmann, 1985), particularly with frequency f. This suggests that λ and

μ should at least be a function of f. It is then only logical to also allow C to vary. Allowing λ, μ and C to vary dynamically throughout the spectrum is expected to result in a more powerful DIA. This approach will be denoted here as a variable DIA (VDIA).

Before starting with the inverse modeling of the different DIAs, implementation details of the generalized DIA will be discussed. This detailed information will later be used to estimate relative costs of different approaches based on the number of operations required, without the need of generating optimal implementations for all approaches

2.5 Implementation details

Equation (2.15) cannot be used directly in a numerical calculation, because the components of each quadruplet ($\boldsymbol{k}_1$ through $\boldsymbol{k}_4$) generally do not coincide with discrete spectral grid points. First, energy densities for the quadruplet components (F_i, where i represents component number in quadruplet) are calculated using simple linear interpolation from the spectral grid

$$F_i = \sum_{j=1}^{4} w_{i,j} F_{i,j} \quad , \tag{2.20}$$

where j is a counter for the four surrounding spectral grid points, $w_{i,j}$ are the corresponding bi-linear interpolation factors, and $F_{i,j}$ are corresponding discrete spectral energies. Similarly, source term contributions $\delta S_{nl,i}$ do not coincide with the discrete grid, and therefore need to be distributed consistently with (2.20)

$$\delta S_{nl,i,j} = w_{i,j}\, \delta S_{nl,i} \quad , \tag{2.21}$$

where $S_{nl,i,j}$ are quadruplet contributions at actual discrete spectral grid points. Note that every individual quadruplet thus generates as many as 16 discrete contributions to S_{nl}. With four quadruplets for each discrete $\boldsymbol{k}$, this corresponds to up to 64 discrete contributions for each spectral grid point. Note, furthermore, that the original DIA has only 2 quadruplets, with two components of the quadruplet that coincide with grid points, and hence has only 18 contributions for each grid point.

In third-generation wave models, the diagonal terms D of $\partial S_{nl}/\partial F$ are used in common time integration schemes for source terms (WAMDIG, 1988; Tolman, 1992). Although not strictly necessary for the present study, these derivatives will be discussed here too. Diagonal contributions in (2.15) are governed by the partial derivatives of the term in square brackets (K), with respect to F_1 through F_4

$$K'_1 = \frac{\partial K}{\partial F_1} = \frac{F_2\, S_{34}}{(1-\mu^2)^4} - \frac{C'_1 P_{34}}{(1+\mu)^4} \quad , \tag{2.22}$$

$$K_2' = \frac{\partial K}{\partial F_2} = \frac{F_1\, S_{34}}{(1-\mu^2)^4} - \frac{C_2' P_{34}}{(1-\mu)^4} \quad , \tag{2.23}$$

$$K_3' = \frac{\partial K}{\partial F_3} = \frac{C_3' P_{12}}{(1+\lambda)^4} - \frac{F_4\, S_{12}}{(1-\lambda^2)^4} \quad , \tag{2.24}$$

$$K_4' = \frac{\partial K}{\partial F_4} = \frac{C_4' P_{12}}{(1-\lambda)^4} - \frac{F_3\, S_{12}}{(1-\lambda^2)^4} \quad , \tag{2.25}$$

where

$$S_{12} = \frac{C_1' F_1}{(1+\mu)^4} + \frac{C_2' F_2}{(1-\mu)^4} \quad , \quad S_{34} = \frac{C_3' F_3}{(1+\lambda)^4} + \frac{C_4' F_4}{(1-\lambda)^4} \quad ,$$
$$P_{12} = \frac{F_1 F_2}{(1-\mu^2)^4} \quad , \quad P_{34} = \frac{F_3 F_4}{(1-\lambda^2)^4} \quad .$$

With this, the contributions to the diagonal D (δD_1 etc.) corresponding to Eq. (2.15) become

$$\begin{pmatrix} \delta D_1 \\ \delta D_2 \\ \delta D_3 \\ \delta D_4 \end{pmatrix} = \frac{2}{N} \begin{pmatrix} -K_1' \\ -K_2' \\ K_3' \\ K_4' \end{pmatrix} g^{-4} f^{11} \quad , \tag{2.26}$$

These contributions also do not coincide with the discrete spectral grid. Applying (2.20) and (2.21), discrete spectral contributions $D_{i,j}$ to the diagonal term become

$$D_{i,j} = \frac{2}{N} w_{i,j}^2 \, (\pm K_i') \, g^{-4} f^{11} \quad , \tag{2.27}$$

again resulting in (up to) 16 contributions per quadruplet, or 64 per discrete spectral grid point. In the conventional DIA, the number of contributions is again reduced to 18.

3 Inverse modeling for the test case

3.1 Introduction

In this section, the potential of several approaches to compute S_{nl} using DIAs will be assessed. Initially, a single test case will be used. Using a spectrum that is fairly representative for well developed wind seas is expected to give at least a good impression of the potential of several approaches.

The previous section leaves a large number of possible DIAs to be considered, ranging from single to multiple DIAs with constant parameters throughout the spectrum to essentially infinite possibilities of VDIAs and multiple VDIAs. Irrespective of the form of a DIA, several definitions of the layout of the representative quadruplet can be considered. A selected set of possible approaches is chosen for the following reasons.

The ultimate goal of developing DIAs is to obtain an optimal parameterization for operational wave models. Economy then is of paramount importance for the viability of such a DIA. Obviously, the cheapest methods suggested here are aggressively optimized single DIAs, where the tunable constants are constant in spectral space. Previous work also shows that similar multiple DIAs are also expected to be economically viable. Therefore, single and multiple DIAs with constant parameters will be discussed first in section 3.2.

In a variable DIA (VDIA), the tunable parameters are allowed to vary in spectral space. A VDIA therefore includes massive potential in terms of increased degrees of freedom compared to a single DIA to (in principle) fit exact interactions at almost arbitrary accuracy. Because, furthermore, a VDIA is more complex than a DIA with constant parameters, it makes no sense to even consider a multiple VDIA. Various VDIA approaches will be analyzed in section 3.3.

The following nomenclature will be used in this and following sections:

- The term 'DIA' can refer to any form of a Discrete Interaction Approximation as defined in section 2.4.
- The term 'original DIA' or 'conventional DIA' refers to the DIA as proposed by Hasselmann et al. (1985), i.e., the present DIA with $\lambda = 0.25$, $\mu = 0$ and $C = 3\,10^7$.
- The term 'MDIA' will be used for a DIA with one or more representative quadruplets, and with optimized tunable parameters that are constant in spectral space.
- The term 'VDIA' will be used for a DIA with a single representative quadruplet, and with optimized tunable parameters that are allowed to vary in spectral space.

For each MDIA or VDIA, the actual definition of the quadruplet used and which parameters are optimized will be explicitly stated in the text. Note that the

term MDIA will also be used for parameterizations with only one representative quadruplet, to distinguish them from the VDIA.

Optimization of a DIA implies the (subjective) estimate of (some of) the free parameters λ, μ, and C_1 through C_4. All DIAs are optimized by minimizing the rms error ϵ

$$\epsilon = \sqrt{\int\int \left(X_{nl}(f,\theta) - S_{nl}(f,\theta)\right)^2 \, df \, d\theta} \quad , \tag{3.1}$$

where X_{nl} is the exact interaction, to which the DIA is fit, and S_{nl} represents the DIA estimate. In the following, the normalized error (ϵ_n) is generally presented. This represents the error normalized with the corresponding error of the conventional DIA.

The parameters describing the shape of the quadruplet (λ and μ) are implicit in the formulation of the DIA, and hence cannot be estimated directly. Instead, an iterative procedure is required. The proportionality constants C, however, are an explicit part of the DIA, and can be estimated directly. Details of the optimization techniques for the MDIA are given in Appendix A, and for the VDIA in Appendix B.

3.2 Optimizing the MDIA

The MDIA will be optimized going from simple to more complex configurations. First, an MDIA with up to five components, and a single proportionality constant C as in Eq. (2.16), will be optimized. The results are presented in Table 3.1 and Figs. 3.1 through 3.3. After these results have been discussed, DIAs with dual constants C [Eq. (2.17) and (2.18)] will be considered.

Figure 3.1 shows results for MDIAs with a single component ($N = 1$) with optimum μ or with $\mu \equiv 0$. The latter case (Fig. 3.1c) represents the conventional DIA with optimized λ and C, and will be discussed first. For this MDIA, $\lambda = 0.249$ is virtually identical to $\lambda = 0.25$ in the conventional DIA. The proportionality constant C, however, is more than a factor of 3 smaller in the MDIA. The quantitative improvement gained by the optimization is dramatic, with a reduction in the error ϵ by a factor of more than 3. Note that this MDIA is close to the DIA used in the WAVEWATCH III model ($\lambda = 0.25$, $C = 10^7$; Tolman and Chalikov, 1996; Tolman, 2002). Qualitatively, however, this is not necessarily an improvement. The negative lobe in the one dimensional source terms is represented much better (compare left panels of Figs. 3.1c and d), but the positive lobe at low frequencies is severely underestimated. Considering the importance of the positive low frequency lobe for wave growth, it remains to be seen if this MDIA would result in realistic wave growth behavior in a wave model.

Figure 3.1b shows the results for a single MDIA ($N = 1$), with a quadruplet defined by both λ and μ, and with a single constant C. Compared to the

Table 3.1: Optimum parameter values of several MDIAs with a single proportionality constant as in Eq. (2.16), for $N = 1$ through 5, with or without inclusion of μ; and corresponding rms errors, normalized with error of conventional DIA (ϵ_n) in percent. C multiplied by 10^{-7}.

N	Fig.	ϵ_n (%)						
1	3.1c	29.6	$\lambda =$	0.249				
			$C =$	0.841				
2	3.2a	18.9	$\lambda =$	0.174	0.293			
			$C =$	3.17	0.903			
3	3.2b	18.6	$\lambda =$	0.172	0.280	0.363		
			$C =$	4.71	1.33	0.242		
4	3.2c	18.6	$\lambda =$	0.170	0.232	0.286	0.334	
			$C =$	6.02	0.732	1.08	0.515	
5	3.2d	17.1	$\lambda =$	0.175	0.223	0.225	0.279	0.366
			$C =$	15.1	-145.	141.	1.17	0.561
1	3.1b	20.3	$\lambda =$	0.248				
			$\mu =$	0.127				
			$C =$	1.81				
2	3.3a	12.0	$\lambda =$	0.080	0.254			
			$\mu =$	0.051	0.127			
			$C =$	19.6	3.41			
3	3.3b	8.10	$\lambda =$	0.139	0.220	0.323		
			$\mu =$	0.004	0.127	0.079		
			$C =$	2.68	5.93	0.948		
4	3.3c	5.74	$\lambda =$	0.075	0.219	0.299	0.394	
			$\mu =$	0.023	0.127	0.184	0.135	
			$C =$	8.36	7.28	3.34	0.257	
5	3.3d	5.69	$\lambda =$	0.074	0.237	0.221	0.300	0.394
			$\mu =$	0.022	0	0.127	0.180	0.092
			$C =$	10.8	-0.32	9.71	3.87	0.292

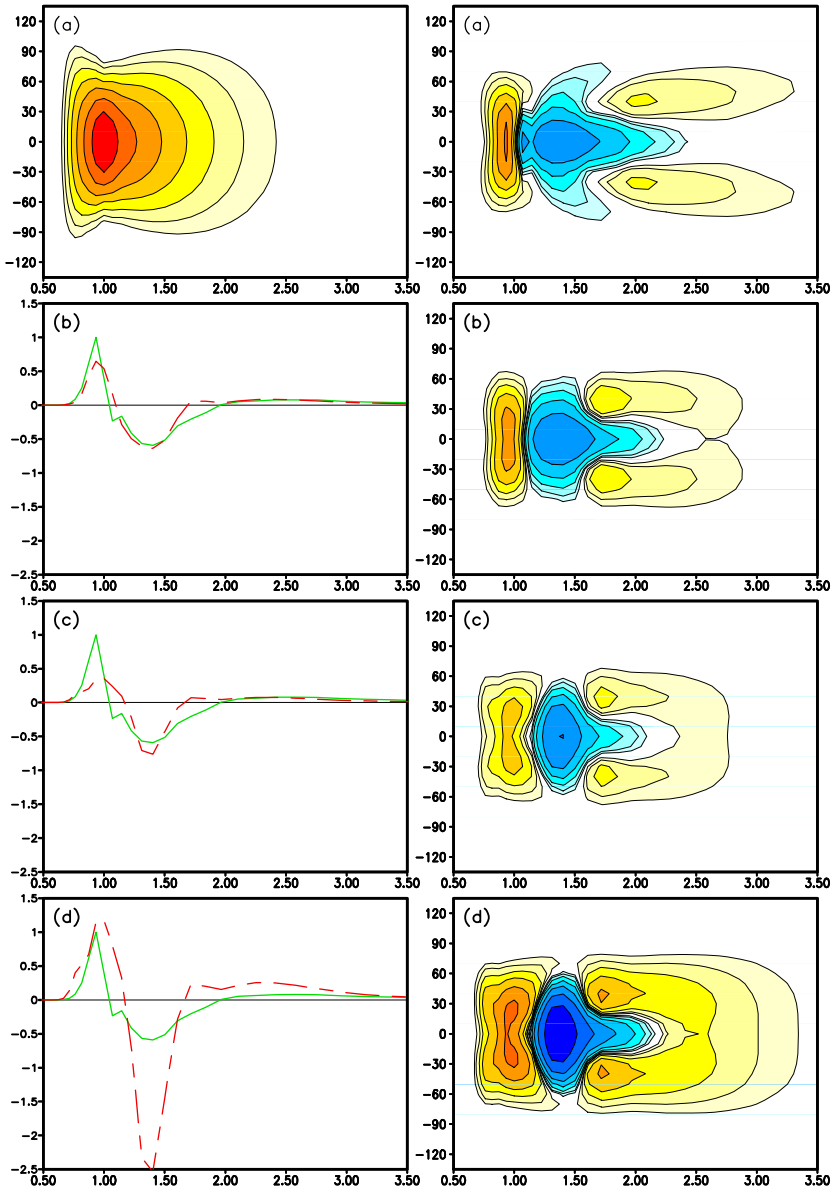

Fig. 3.1 : (a) Test spectrum (left) and exact interactions (right). (b) Single MDIA with optimum λ, μ and C. (c) Similar MDIA with $\mu \equiv 0$. (d) Original DIA. Left panels in (b) through (c) represent a comparison between the exact and estimated one-dimensional interactions $S_{nl}(f)$. Right panels show full two-dimensional interactions. Legends as in Fig. 2.1.

original DIA, the error ϵ is reduced by a factor of almost 5 (Table 3.1). This approach not only shows large quantitative improvements over the original DIA, but also significant qualitative improvements. The positive lobe at low frequencies is represented much better in the full spectral space (right panels in Fig. 3.1), although the magnitude is still somewhat underestimated, as is obvious in the one-dimensional interaction (left panel in Fig. 3.1b). The largest errors in this approach are concentrated at higher frequencies, typically $f > 1.5 f_p$.

Figure 3.2 shows the MDIA with $\mu \equiv 0$ and a single constant C, for the number of components N increasing from 2 to 5. Adding a second component to this MDIA ($N = 2$) reduces the error ϵ by another 30% compared to the single MDIA ($N = 1$, see Table 3.1). However, adding more components ($N = 3$ through 5) has little impact on the error ϵ_n. Moreover, the resulting nonlinear interactions retain some qualitative deficiencies. This MDIA systematically underestimates the magnitude of the positive lobe at low frequencies, as is clear from the one dimensional source terms in the left panels of Fig. 3.2. Furthermore, this low frequency lobe is realistically narrow in frequency space near the mean direction (compare with Fig. 3.1a), but remains spuriously broad at directions away from $\theta = 0$, resulting in an unrealistic horse shoe shape for the positive part of the interactions at low frequencies.

It is also important to note that for $N = 5$, the optimization procedure finds two near identical values for λ, with large values of C with opposite signs. The occurrence of the negative C is not desirable, as it corresponds to antidiffusive behavior as discussed in the previous section. With the present optimization approach, therefore, it is not desirable to use more than 4 components in this MDIA (for the present test). An alternative solution can be obtained when a fixed spacing is used for λ, and only the values of C and the overall spacing for λ are optimized. Such an approach has not been tried here, since it is not expected that this approach will positively improve the qualitative deficiencies of this MDIA.

Figure 3.3 shows the resulting optimum MDIA with the two-parameter quadruplet ($\lambda, \mu \neq 0$), for the number of components N increasing from 2 to 5. Adding components systematically reduces the remaining model error up to $N = 4$, where the error is reduced by a factor 17 compared to the conventional DIA ($\epsilon_n = 5.74\%$). For this configuration, the quantitative and qualitative fit to the exact interactions is excellent (compare Fig. 3.3c with Fig. 3.1a), with no apparent remaining deficiencies. Note that for $N = 5$ negative values for C appear, and hence $N > 4$ appears less desirable (as discussed in the context of Fig. 3.2).

After DIAs based on a single constant C have been analyzed, inclusion of two such constants, according to Eqs. (2.17) or (2.18), is considered. Results for such MDIAs are presented in Figs. 3.4 through 3.8. The corresponding normalized errors are presented in Table 3.2.

The quantitative impact of adding a second tunable proportionality constant

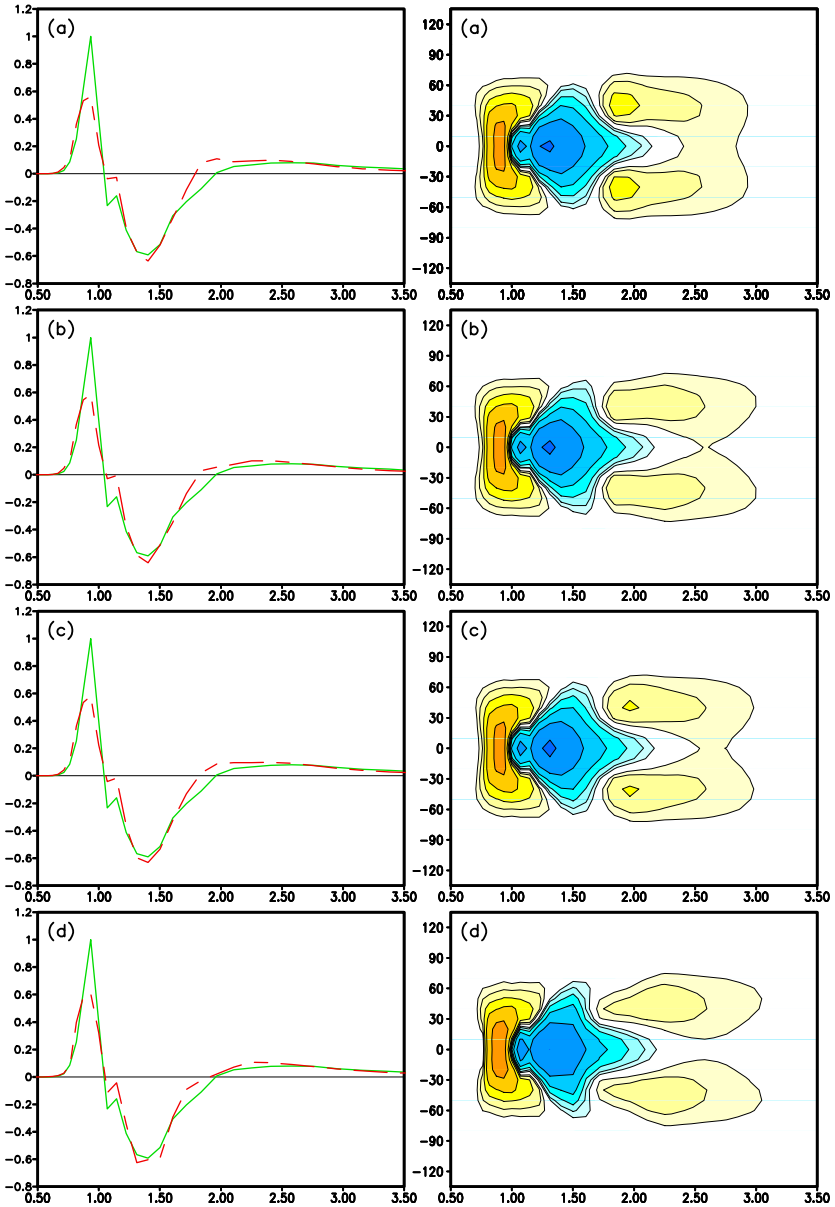

Fig. 3.2 : Test results for MDIA with optimized λ and C, and with $\mu \equiv 0$. (a) $N = 2$. (b) $N = 3$. (c) $N = 4$. (d) $N = 5$. Legends as in Fig. 2.1b.

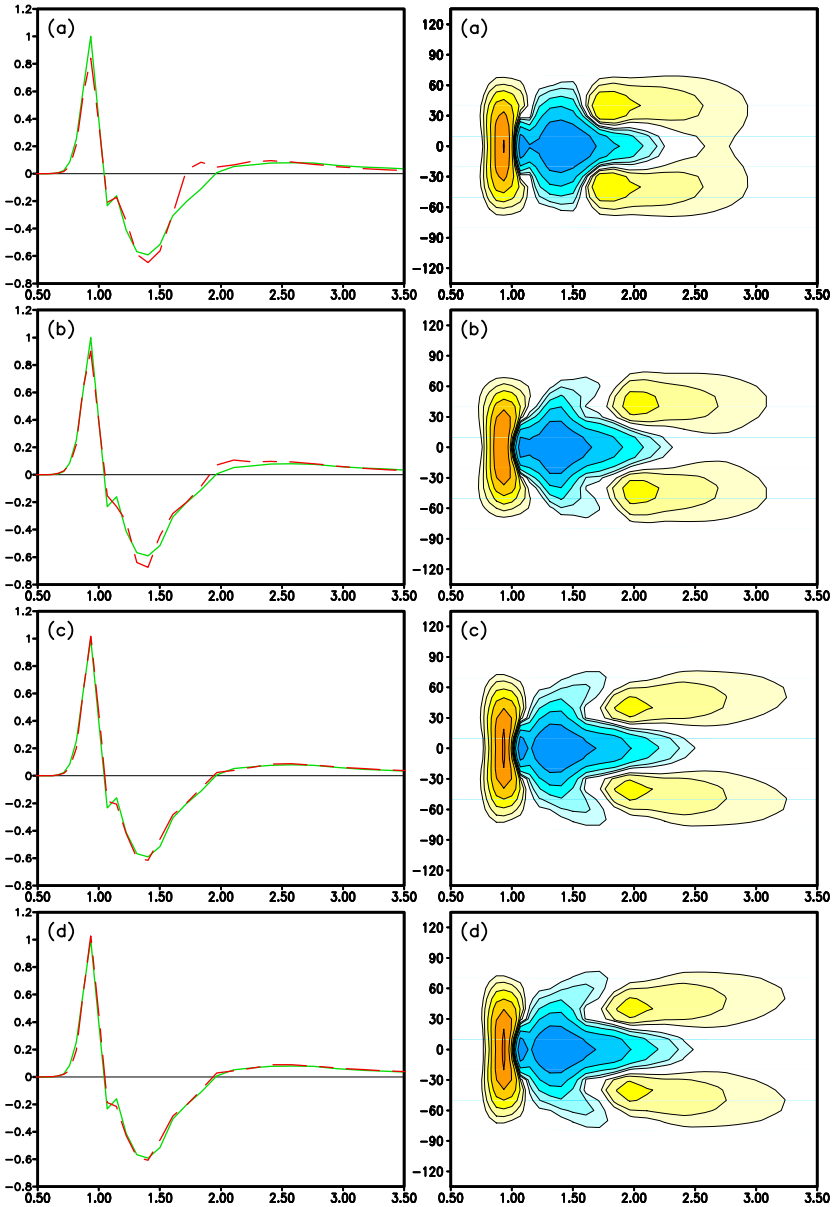

Fig. 3.3 : Test results for MDIA with optimized λ, μ, and C. (a) $N = 2$. (b) $N = 3$. (c) $N = 4$. (d) $N = 5$. Legends as in Fig. 2.1b.

Table 3.2: Normalized errors ϵ_n for MDIA with N components, and configured as indicated in the table.

	optimized λ			optimized λ and μ		
N	C	(C_1,C_2)	(C_3,C_4)	C	(C_1,C_2)	(C_3,C_4)
1	29.6	29.4	29.0	20.3	20.3	17.9
2	18.9	18.4	15.8	12.0	16.1	11.5
3	18.6	17.0	14.6	8.10	6.57	6.21
4	18.6	16.1	13.3	5.74	3.64	5.66
5	17.1	15.8	13.1	5.69	3.41	3.49

is limited (see Table 3.2). For single MDIAs, the impact is negligible; for multiple DIAs the impact is larger, but still small compared to MDIAs with a single C as discussed above. Generally, the technique where the two constants are assigned to the 'diffusion' and 'pumping' terms separately [C_3, C_4 as in Eq. (2.18)] appears to have a more positive impact on the resulting errors than the method described by Ueno and Ishizaka (1997) [C_1, C_2 as in Eq. (2.17)]. Only for $N \geq 4$, when both λ and μ optimized, does the impact of tuning C_n appear significant. Note that for isolated cases, the two parameter (C_n) results are worse than the one parameter (C) results. This is an artifact of the fairly simple optimization procedure used, and of the fact that there is no guarantee in nonlinear optimization that the absolute best fit is always found. If the best fit for one parameter is chosen as the starting point for the two parameter fit, the two parameter fit will always give better results, as would be expected.

The qualitative impact of the added tuning parameters is even less impressive. For the one parameter quadruplet ($\mu \equiv 0$), the DIA retains its undesirable horseshoe shape for the positive lobe at low frequencies (Figs. 3.4a,b, 3.5 and 3.6). For such MDIAs with larger numbers of components ($N = 3, 4$), there also appears to be a tendency to generate nonlinear interactions with spuriously broad direction characteristics in the positive lobes at high frequencies. Probably most detrimental for this approach is the occurrence of spurious 'wiggles' at low frequencies in Fig. 3.6, which could have a serious negative impact on model integration. For the two parameter quadruplet (with λ and μ optimized, Figs. 3.4c,d, 3.7 and 3.8), these deficiencies are not observed. However, a comparison with Figs. 3.1 and 3.3 shows only minor improvements in the shape of the central negative lobe. It remains to be seen if this justifies the inclusion of an additional tunable parameter, particularly when considering that additional tunable parameters generally complicate dynamical estimation of parameters.

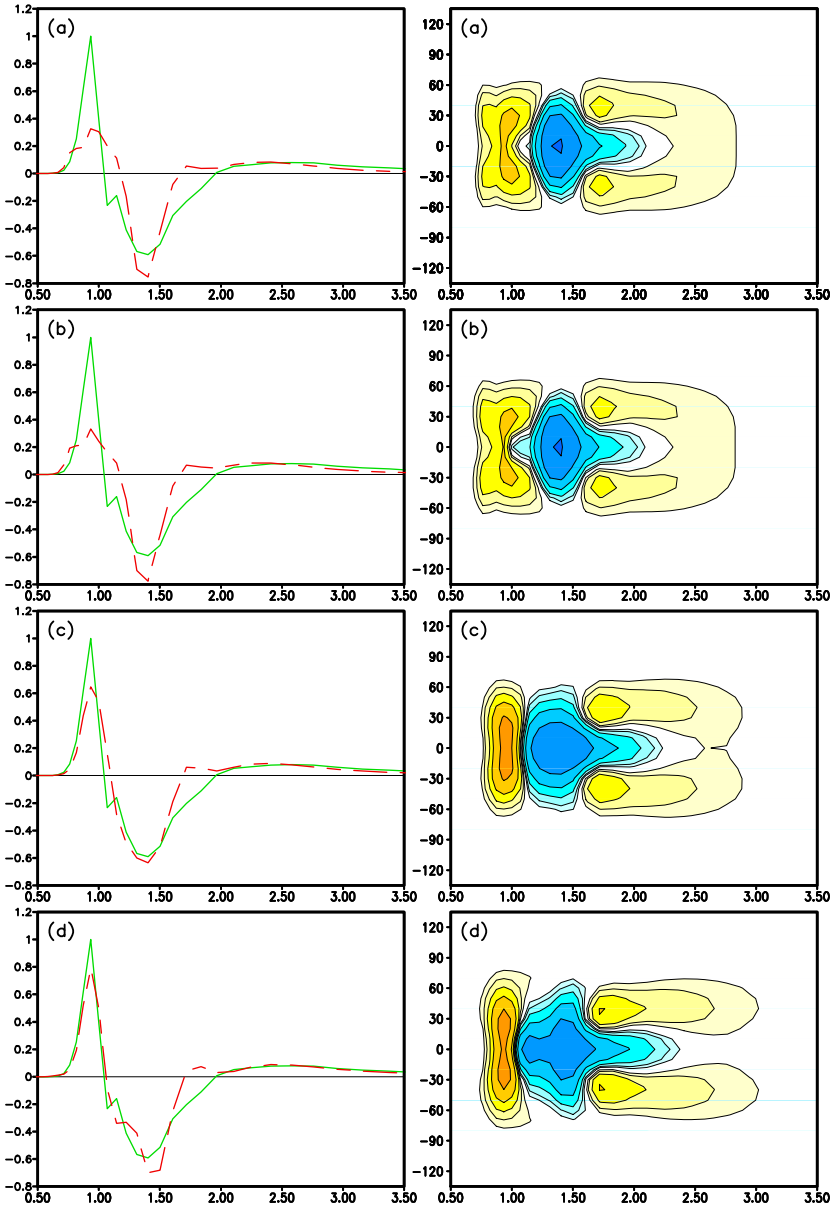

Fig. 3.4 : Test results for several single MDIAs ($N = 1$) (a) Optimized λ, C_1, and C_2. (b) Optimized λ, C_3, and C_4. (c) Optimized λ, μ, C_1, and C_2. (d) Optimized λ, μ, C_3, and C_4. Legends as in Fig. 2.1b.

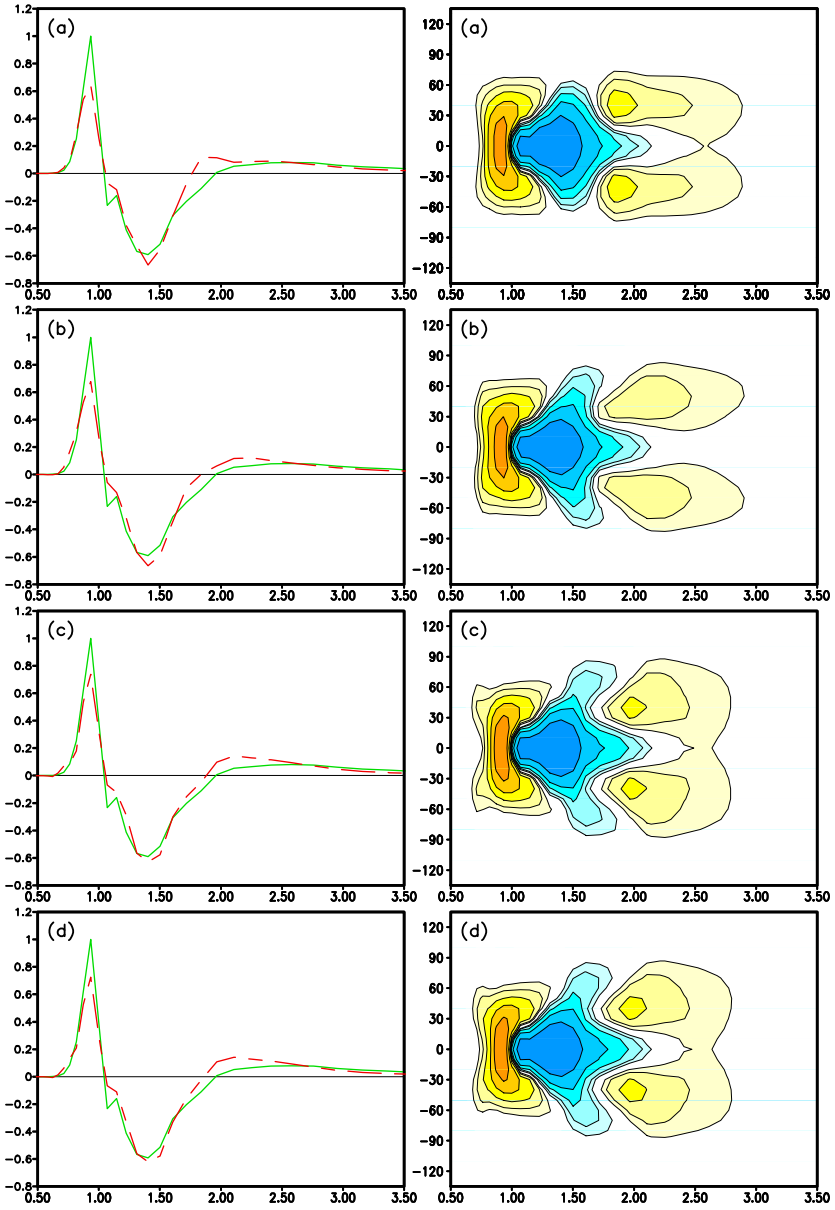

Fig. 3.5 : Test results for MDIA with optimized λ, C_1 and C_2 [Eq. (2.17)], and with $\mu \equiv 0$. (a) $N = 2$. (b) $N = 3$. (c) $N = 4$. (d) $N = 5$. Legends as in Fig. 2.1b.

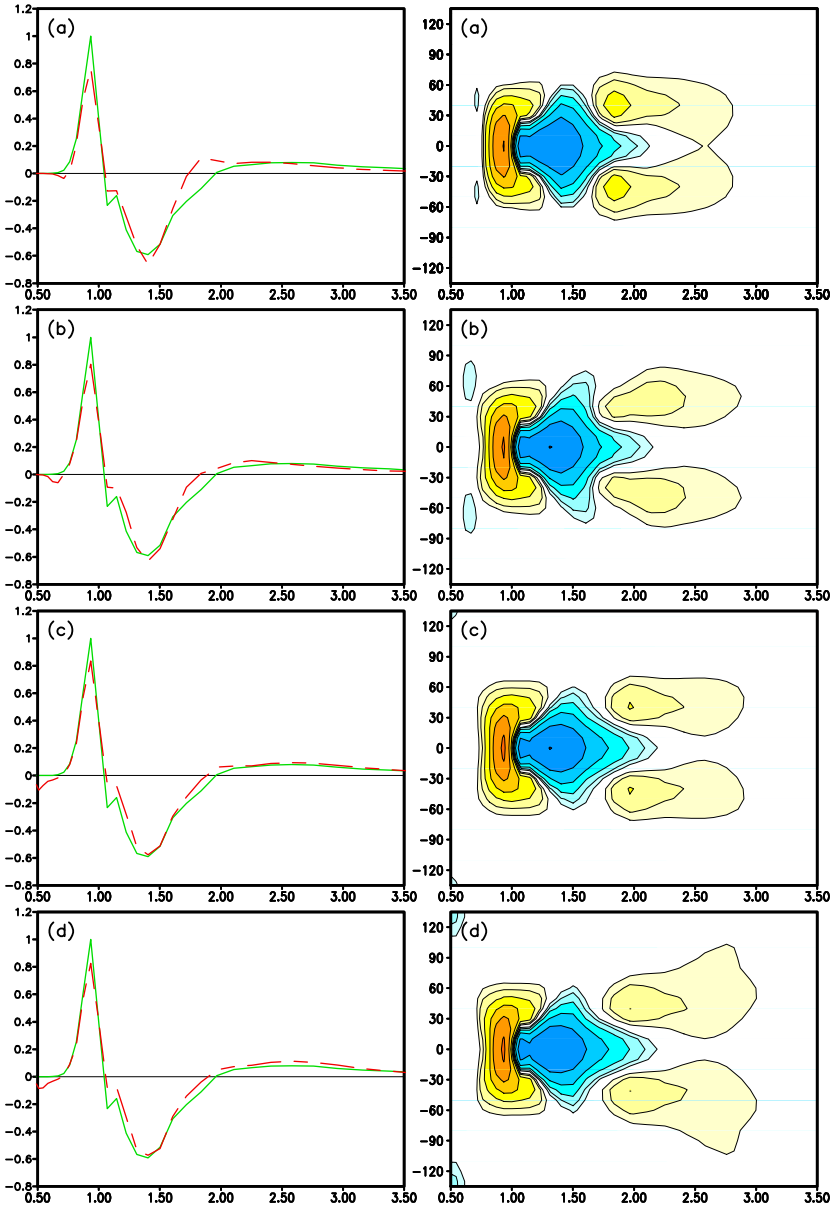

Fig. 3.6 : Test results for MDIA with optimized λ, C_3 and C_4 [Eq. (2.18)], and with $\mu \equiv 0$. (a) $N = 2$. (b) $N = 3$. (c) $N = 4$. (d) $N = 5$. Legends as in Fig. 2.1b.

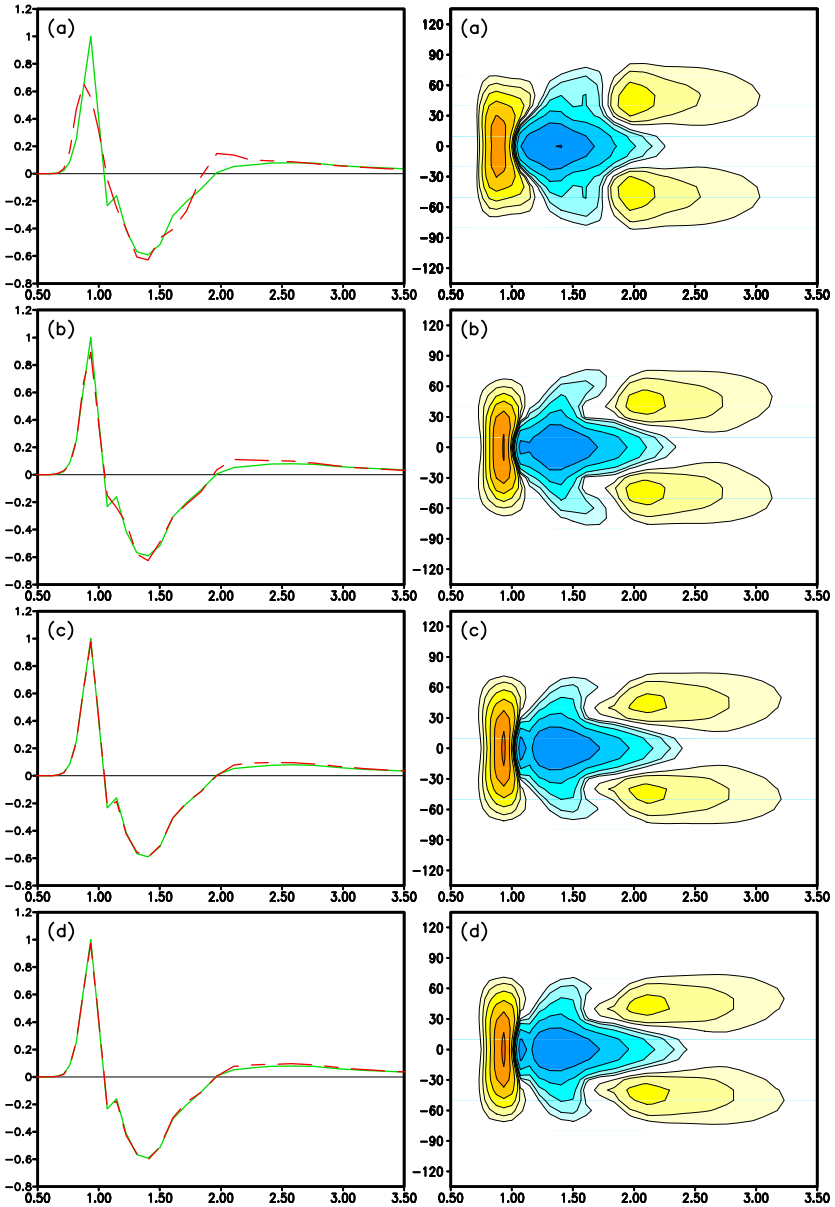

Fig. 3.7 : Test results for MDIA with optimized λ, μ, C_1 and C_2 [Eq. (2.17)]. (a) $N = 2$. (b) $N = 3$. (c) $N = 4$. (d) $N = 5$. Legends as in Fig. 2.1b.

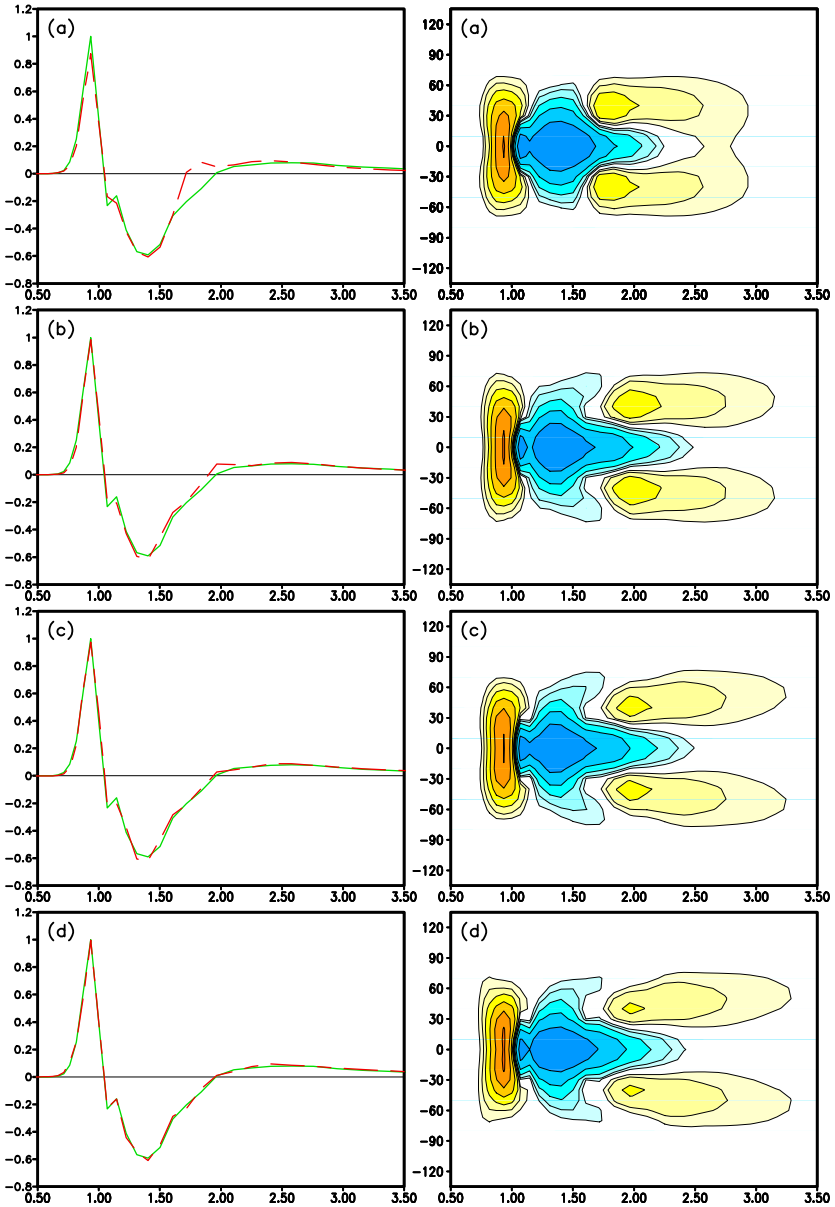

Fig. 3.8 : Test results for MDIA with optimized λ, μ, C_3 and C_4 [Eq. (2.18)]. (a) $N = 2$. (b) $N = 3$. (c) $N = 4$. (d) $N = 5$. Legends as in Fig. 2.1b.

The following conclusions can be drawn from the above experiments with specific optimized MDIAs:

- All single MDIAs ($N = 1$) show a large improvement over the conventional DIA, but are not deemed to be sufficiently accurate to realistically reproduce the exact interactions.
- MDIAs with quadruplets based on λ only ($\mu \equiv 0$) retain spurious errors in the shape of the positive lobe at low frequencies that are not deemed desirable. Adding components to this MDIA does not improve this behavior significantly.
- The replacement of the single proportionality constant C with two constants, (C_1, C_2) or (C_3, C_4), does not have a sufficiently positive impact on the resulting interactions to justify this complication of the MDIA.
- A MDIA based on optimized λ, μ and C, with approximately four components, appears to give a good representation of the exact interactions for practical purposes.

Note that these interim conclusions are solely based on accuracy. Economical considerations will be addressed in some detail in section 3.4.

3.3 Optimizing the VDIA

The ultimate goal of investigating the VDIA is to find a balance between accuracy and a minimum number of free parameters. The latter is crucial in being able to get a reliable (dynamic) estimate of the free parameters. To get to this goal, the first focus will be on addressing what is needed to get an accurate VDIA. In this, the attention will first be focused on optimizing C, because this can be done explicitly. Considering the results of the previous section, only the optimization of a single C will be considered (instead of C_n). After that, different degrees of variation of λ and μ will be examined. Details of the optimization and inverse modeling techniques used here are given in Appendix B.

Figure 3.9 shows the resulting fully variable $C(f, \theta)$, required for the VDIA with $\lambda = 0.25$ and $\mu = 0$ to reproduce the exact interactions. As expected, this method reproduces the exact interactions accurately. To achieve this, however, C requires a large variability. Some of this variability for low frequencies and for directions away from $\theta = 0$, is due to the inverse modeling problem being poorly conditioned, as discussed in Appendix B. The relatively smooth behavior of C for frequencies above the spectral peak suggests that a simpler approach (less degrees of freedom) could be expected to give reasonable results. The clear dependence of C on direction for $f > 2.5$ suggests that the quadruplet used here is not representative for the dominant scales of interaction, as expected and discussed in section 2.4. The large changes of C close to the spectral peak ($f = 1$), suggest

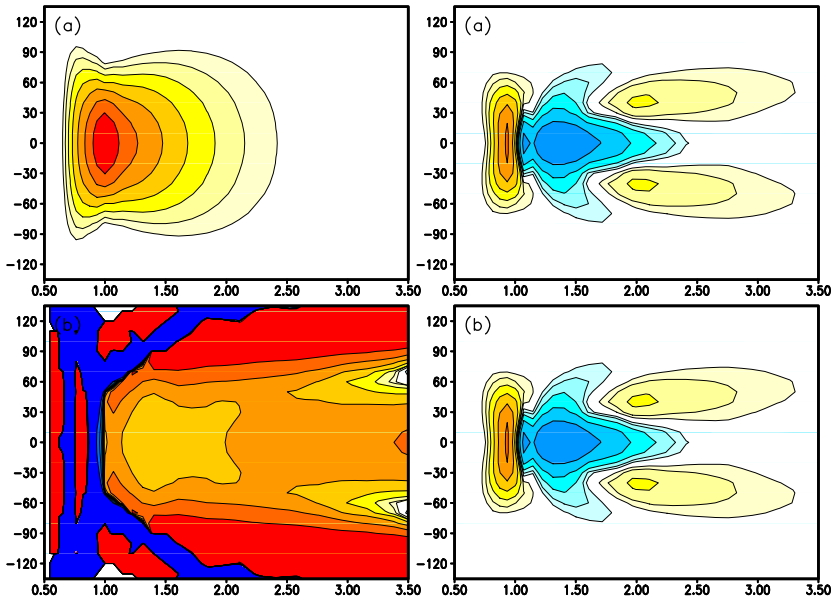

Fig. 3.9 : (a) Spectrum for test case (left) and exact interactions (WRT, right). (b) Retrieved constant $C(f,\theta)$ (left) and corresponding DIA (right) for $\lambda = 0.25$ and $\mu = 0$. Legend for spectra and source terms as in Fig. 2.1. Logarithmic scaling for C with lowest contour levels at $\pm 10^6$

that any optimum C is expected to require significant variability in this part of the frequency domain (and for this particular quadruplet) to give good results. Since a VDIA with this many degrees of freedom is not expected to be practical, it will be left as an illustration only, and will not be investigated further.

Figure 3.10 shows results for optimizing $C(f)$ (C independent of θ). This optimization is performed for the original DIA quadruplet ($\lambda = 0.25$, and $\mu = 0$, panels c) and for the previously optimized new quadruplet ($\lambda = 0.248$, and $\mu = 0.127$, panels b). In both cases the resulting errors (upper right corner of right panels) are reduced by a factor of approximately 2 when compared to the error of the corresponding MDIA with optimized constant C ($N = 1$ results in Table 3.1). Qualitatively, however, the results have deteriorated. The resulting source terms, in general, include more noise, and in particular show spurious wiggles below the peak frequency. It is potentially detrimental when such a parameterization is applied in a wave model. A positive result of this experiment is that the unrestrained $C(f)$ appears reasonably well behaved, particularly for the original quadruplet (Fig. 3.10c). This suggests that a description of $C(f)$ based on fewer degrees of freedom may also improve the model behavior. By definition, such an approach will result in a smoother estimate of $C(f)$, which is expected to result in a smoother source term.

To investigate this, a simple polynomial description of C is adopted, where

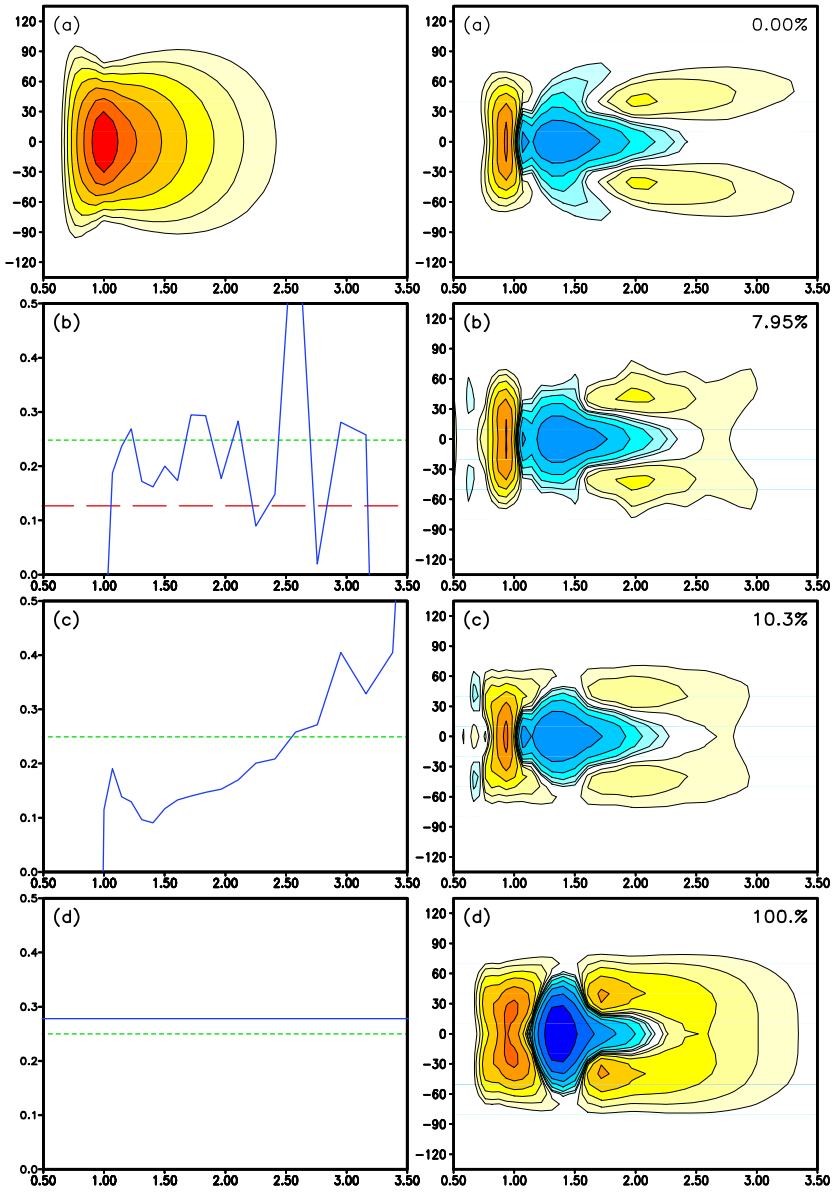

Fig. 3.10 : (a) Spectrum for test case (left) and exact interactions (WRT, right). (b) -(d) Left panels show λ (short dash, green), μ (long dash, red) and optimized $C(f) \times 10^{-8}$ (solid blue line). Right panels show the resulting source term and normalized error ϵ_n in upper right corner. (b) VDIA with $\lambda = 0.248$, $\mu = 0.127$ (c) VDIA with $\lambda = 0.25$, $\mu = 0.0$. (d) Original DIA.

the mth order polynomial is defined as

$$C(f) = c_0 + c_1 f + c_2 f^2 + \ldots + c_m f^m \quad , \tag{3.2}$$

where c_m are the factors to be optimized. Figure 3.11 shows the results for this VDIA, with constant $\lambda = 0.25$ and $\mu = 0$, for polynomials of the order 1 through 4. Figure 3.12 shows similar results for $\lambda = 0.248$ and $\mu = 0.127$. The corresponding results for a polynomial of the order 0 were already presented in Figs. 3.2a and 3.3a and in Table 3.1 ($N = 1$).

For both quadruplets (i.e., definitions of λ and μ), the increasing of the order of the polynomials has only a small effect on the resulting error. In most cases, the reduction of the error is accompanied by a clearly less realistic overall description of the source term. Only for the extended quadruplet ($\mu \neq 0$) and a polynomial of order 1 or 2 (Figs. 3.12a,b), is the reduced error accompanied by a better qualitative representation of the source term. Based on these results, it may be concluded that little is to be gained by allowing C to vary by itself. Any quantitative improvement appears to be offset by significant qualitative deteriorations in the behavior of the source term. Therefore, only low level polynomial descriptions of C will be used in the following analyses. Somewhat arbitrarily, these will be the polynomials of order 0 and 2.

The final step in analyzing the potential of a VDIA is to allow λ and μ to vary with frequency f. From the previous results, it may be expected that an unrestrained variation of these parameters will result in a smaller error, at the cost of a less realistic (noisy) source term. For completeness, this option is nevertheless investigated. Figure 3.13 shows the results for several VDIA configurations as defined in the legend of this figure. As expected, the resulting source terms are tainted by noise, but the optimum values of λ and μ appear well behaved. Therefore, a simple functional fit again will be tried for these parameters. Somewhat arbitrarily, a low order Pade approximant of the form

$$\lambda, \mu = \frac{c_0 + c_1 f}{1 + c_2 f} \tag{3.3}$$

is used. The optimum results for this approximation are presented in Fig. 3.14. For the quadruplet with $\mu \equiv 0$ (panels a and b), the quantitative improvement is again minimal, and is accompanied by a clear qualitative deterioration of the resulting interactions. For the quadruplet with optimized λ and μ, the quantitative improvements are small but notable (15% compared to the single DIA with constant parameters), and the resulting interactions also appear qualitatively better, in particular for the positive lobes at high frequencies. In the latter case, the simplest approach for C (Fig 3.14c) appears to give the best results.

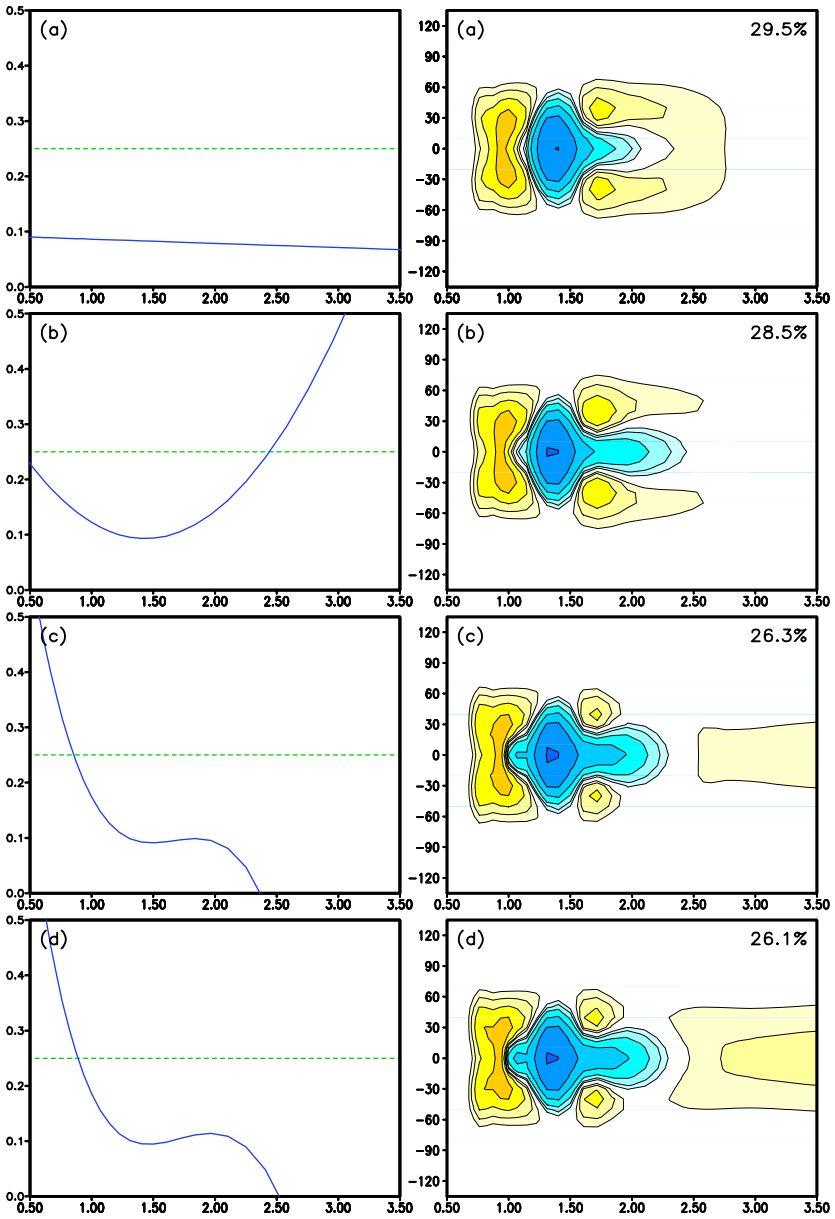

Fig. 3.11 : VDIA, with $\lambda = 0.25$ and $\mu = 0$ and optimized polynomial description of $C(f)$ with polynomials of first order (panel a) increasing to fourth order (panel d). Legend as in Figs. 3.10b,c.

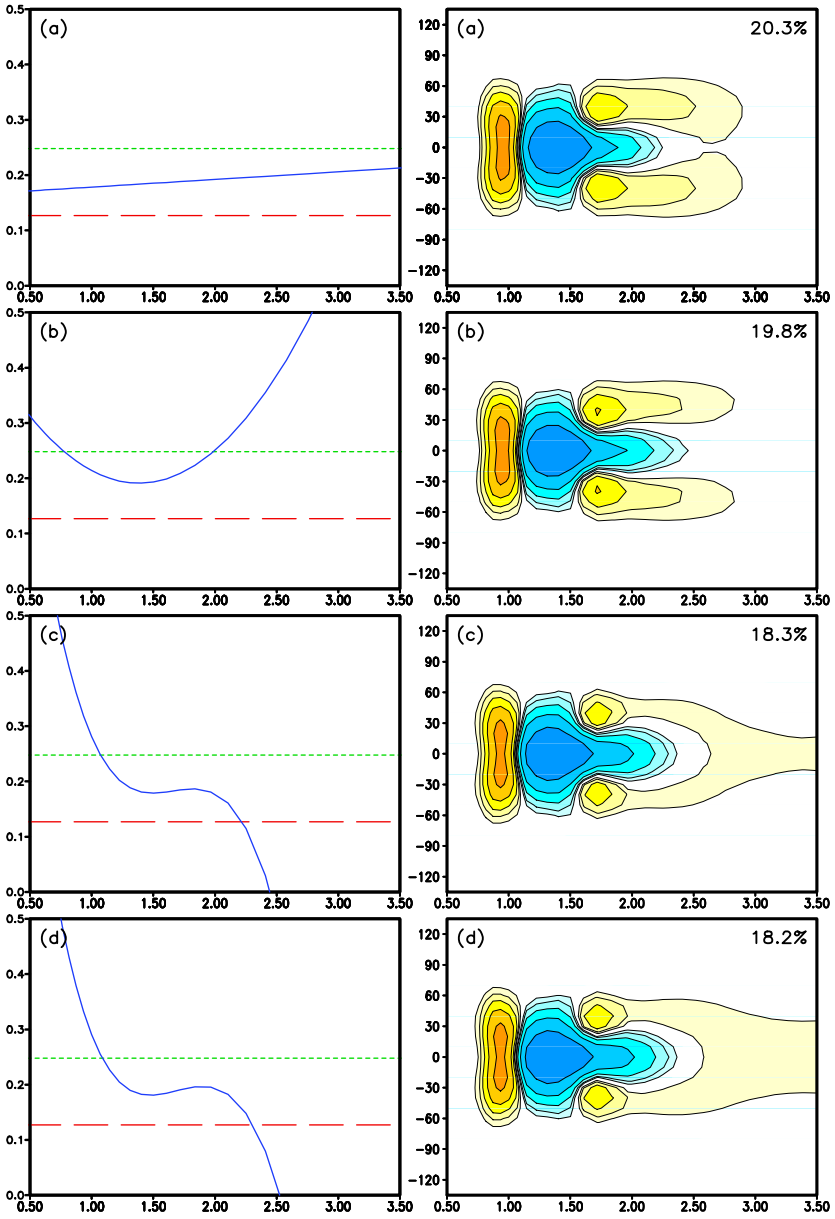

Fig. 3.12 : Like Fig. 3.11, for $\lambda = 0.248$ *and* $\mu = 0.127$.

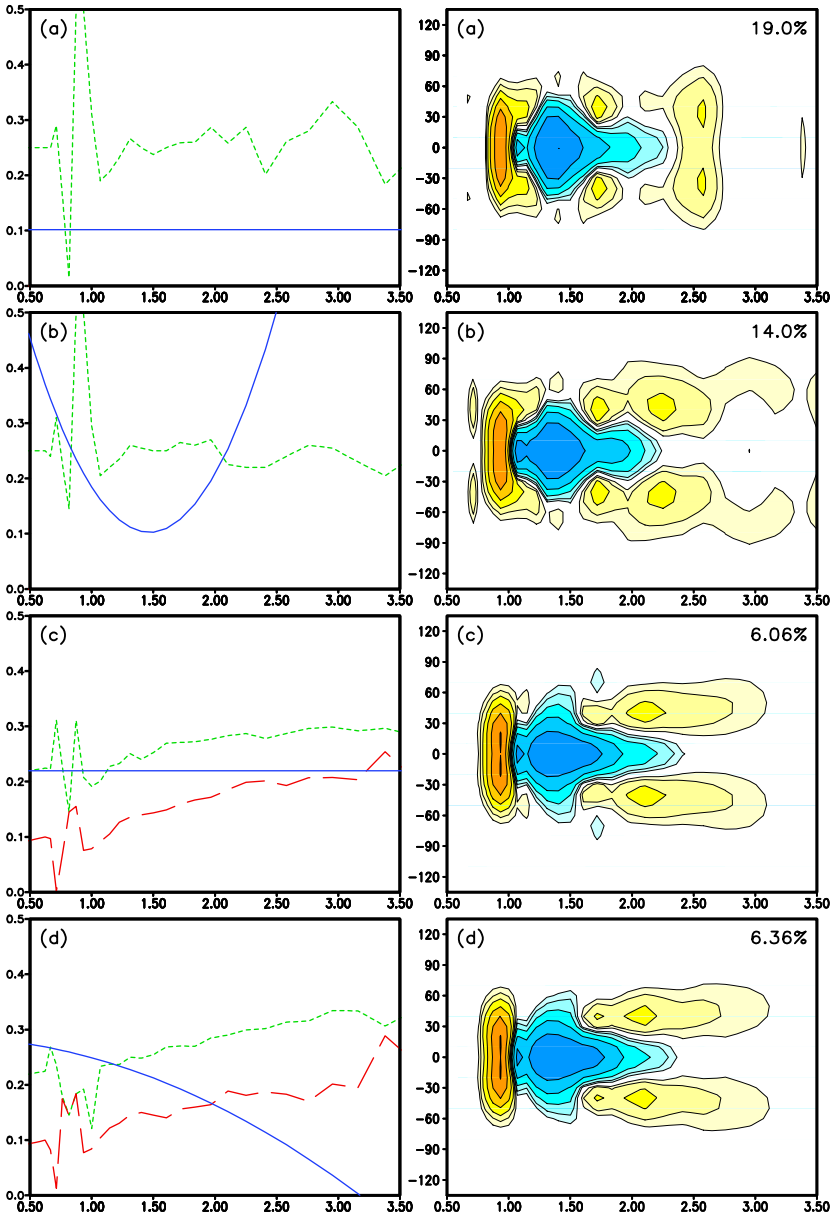

Fig. 3.13 : VDIA, with optimized λ and μ as unrestrained functions of the frequency f (a,b) $\mu \equiv 0$. (a,c) C optimized as a constant. (b,d) C optimized as second order polynomial. Legend as in Figs. 3.10b,c.

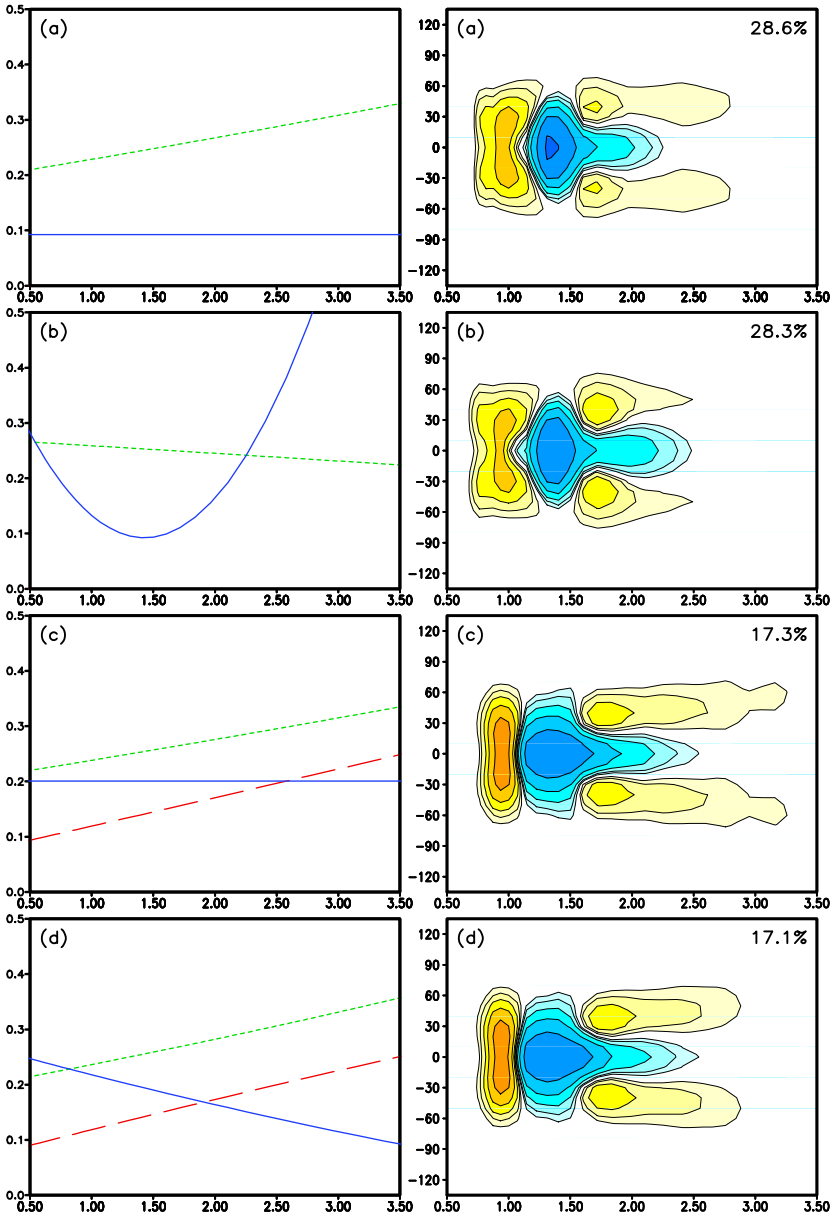

Fig. 3.14 : Like Fig. 3.14, with Pade approximation for λ and μ.

The following conclusion can be drawn from the experiments with the VDIA.

- The VDIA has the potential to significantly reduce errors of the DIA in a quantitative sense, but generally does so at the expense of introducing noise. Hence, the results deteriorate in a qualitative sense.
- VDIAs based on the conventional quadruplet with $\mu \equiv 0$ perform systematically worse than the corresponding single and multiple DIAs with constant parameters.
- VDIAs with λ and μ described with Pade functions, and with C constant but optimized, show moderate improvements over the corresponding MDIA ($N = 1$) in both a qualitative and quantitative sense.

Note that these conclusions are again based solely on accuracy issues. Economy and other issues will be discussed below.

3.4 Comparison of approaches

In the previous sections the most promising MDIA and VDIA have been identified, based on their capability to reproduce exact interactions for a single test spectrum. The most promising MDIA uses approximately four components, the full definition of the quadruplet [Eq. (2.13)], and a single constant C per component [Eq. (2.16)]. The most promising VDIA uses a single quadruplet, Pade approximations to describe λ and μ in Eq. (2.13), and a constant C as in Eq. (2.16). The resulting source terms and model errors are summarized in Fig. 3.15. Before these MDIA and VDIA are applied to an extended set of test cases, and in an actual numerical model, they will be compared in this section with regard to accuracy, economy and the potential for application to arbitrary spectra and water depths.

In terms of accuracy, the MDIA (Fig. 3.15b) is, for all practical purposes, identical to the exact interactions (Fig. 3.15a). The VDIA (Fig. 3.15c) shows a massive improvement over the original DIA (Fig. 3.15d), but also shows some deviations from the exact solutions. Its most obvious errors are an inability to resolve the two separate local minima in the negative lobe of the source term, a moderate underestimation of the intensity of the positive lobe at low frequencies, and a shift in frequency space for the local maxima in the positive lobes at high frequencies. In terms of absolute errors, this VDIA is only 15% more accurate than the MDIA with a single component (Fig. 3.1b). In a qualitative sense, however, this VDIA looks more realistic for higher frequencies in particular. Arguably, this VDIA represents the most balanced, single component DIA approach considered here, and therefore deserves further attention.

Without writing a highly optimized version of the above MDIA and VDIA, their expected economy can be assessed by addressing the required number of

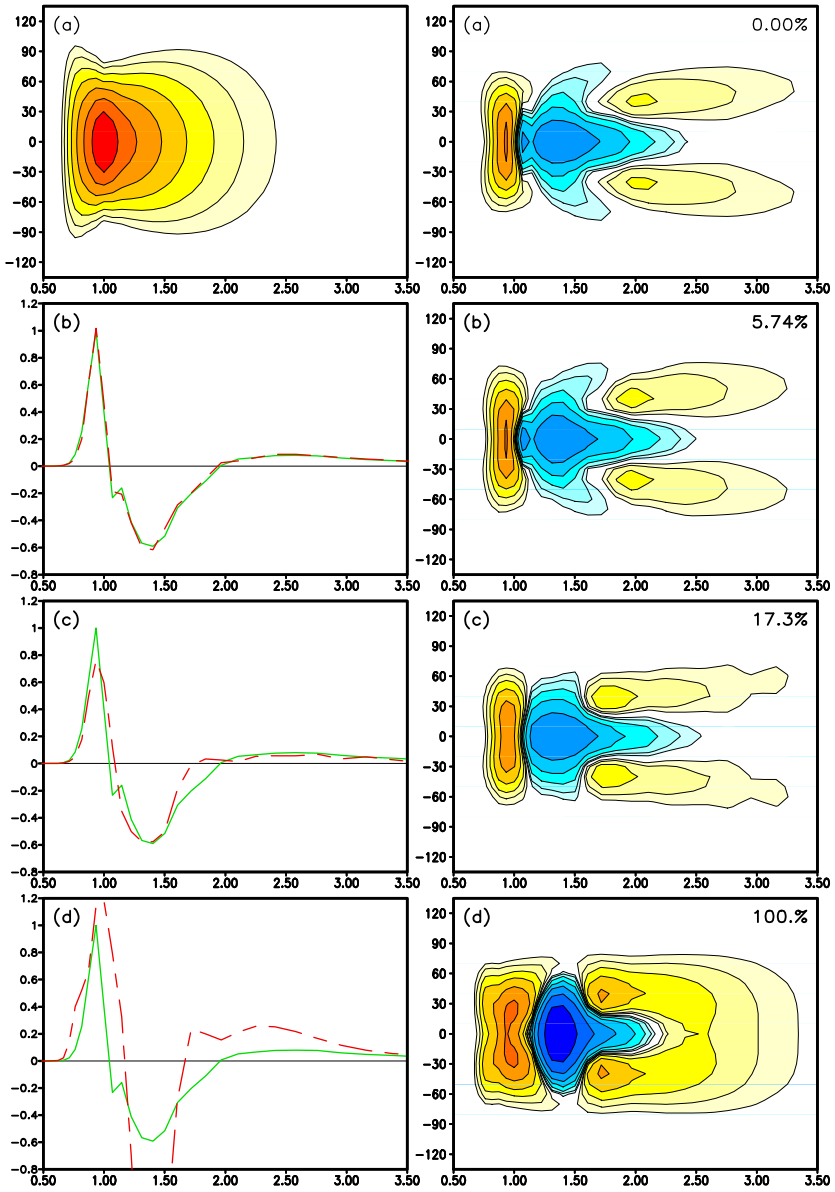

Fig. 3.15 : Review of results of inverse modeling efforts for the test case (a) Spectrum and exact interactions. (b) MDIA with four components with optimum λ, μ and C. (c) VDIA with single component, λ and μ described with Pade functions and constant C. (d) Orriginal DIA without optimization. Legends as in Fig. 2.1. Normalized errors ϵ_n in upper right corner of right panels.

operations in both approaches. A numerical implementation of any DIA consists of four main parts

(i) Preparation of calculations by configuring quadruplets and calculating indices and interpolation weights.
(ii) Calculation by interpolating of the energies at the components of the quadruplet.
(iii) Calculating the strength of the interactions.
(iv) Distributing interactions back to actual grid points.

In the conventional DIA [Eqs. (2.1) and (2.4)], step (i) is performed only once, and hence does not incur computational effort in the actual model run. Steps (ii) and (iv) include gathering and distributing data from 18 surrounding spectral grid points, for each individual spectral grid point to be considered. In step (iii) the interaction strengths for two quadruplets are calculated from four previously interpolated spectral energies. Because the expression to calculate the interaction strengths [Eq. (2.15)] is fairly simple, the main computational effort for the conventional DIA is spent in steps (ii) and (iii).

In the expanded DIA [Eqs. (2.13) and (2.15)], the number of components to be considered in steps (ii) and (iv) is increased from 18 to (up to) 64, increasing the corresponding computational effort by up to a factor of 3.5. In step (ii), the number of interaction strengths to be calculated is increased from two to four, and the expression becomes more complicated, roughly doubling the amount of operations required to calculate the interaction strength. Step (iii), therefore, becomes more expensive by a factor of approximately 4. Dynamic adjustment of the shape of the quadruplet and the strength of the interactions, as envisioned for a final implementation of this DIA, requires step (i) to be performed for every calculation. For fixed quadruplet shapes throughout the spectrum, this represents a single set of computations, which should add negligible effort compared to applying the interactions to each discrete spectral grid point individually. In the VDIA, this layout of the quadruplet needs to be evaluated for each discrete frequency, but not for individual directions. Therefore, step (i) will be more expensive in the VDIA, but even there it is not expected to dominate the computational costs.

Considering the above, the MDIA with one component may require 3.5 to 4 times the run time of a traditional DIA. The corresponding VDIA will be somewhat more expensive, but is not expected to be more than 5 times as expensive as a conventional DIA. An MDIA with several components will require a multiple of the computational effort of an MDIA with one component. However, as was shown by previous authors at the 2002 WISE meeting (see section 2) in an MDIA many individual component contributions can be combined, resulting in an increase in computational effort that is much less than linear. Thus, the MDIA suggested here is expected to be roughly 10 times as expensive as a conventional (single) DIA.

It should be noted that the cost increase for the VDIA and MDIA is in significant part due to the more complex shape of the quadruplet. As is shown in previous sections, the new quadruplet shape is responsible for the much improved (quantitative and qualitative) behavior of the DIA, and is therefore crucial. The factor of 4 increase in computational cost related to this change, therefore, appears well justified.

Finally, the selected MDIA and VDIA should be considered in the context of arbitrary spectra and arbitrary depths. When arbitrary spectra with multiple swell systems are used in the optimization of the MDIA, no specific complications are expected, since constant parameter values are used throughout the spectrum. For the VDIA, however, the functional description of λ and μ will need to be revisited, and might prove less straightforward. The MDIA is, therefore, expected to be more easily applicable to arbitrary spectra than the VDIA. Extension to shallow water mostly involves the assessment of the proper (shallow water) resonance conditions. This implies that the shape of the quadruplet becomes a function of the frequency and depth. In the VDIA this extension is straightforward, because the quadruplet already needs to be evaluated separately for every frequency. For the MDIA, this increases computational costs. Hence, extension to shallow water appears to be somewhat more simple for the VDIA.

This page is intentionally left blank.

4 Sensitivity of optimum parameters

Now that an optimal MDIA and VDIA have been selected, the validity of these methods and their present tuning parameters for spectra other than the test case needs to be assessed. For this reason a set of 20 additional test cases have been considered. Most cases are generated by varying relevant parameters in the JONSWAP / Hasselmann spectrum of Eqs. (2.5) through (2.8). In this way the first 13 cases, as identified in Table 4.1, have been generated. Two additional modifications for test spectra are considered here. First, recent research indicates that the directional distribution at high frequencies is bimodal in many cases. To test the validity for such spectra, two test cases with the bimodal directional distribution of Ewans (1998) are considered. This distribution is given as

$$D(f,\theta) = \frac{1}{\sigma(f)\sqrt{8\pi}} \sum_{n=-\infty}^{\infty} \left\{ \exp\left[-\frac{1}{2} \left(\frac{\theta - \bar{\theta} \pm \bar{\theta}_o(f) - 360n}{\sigma(f)} \right)^2 \right] \right\} \quad , \tag{4.1}$$

$$\bar{\theta}_o(f) = \begin{cases} 14.93 & \text{for} \quad f < f_p \\ \exp\left[5.453 - 2.750 \left(\frac{f}{f_p} \right)^{-1} \right] & \text{for} \quad f \geq f_p \end{cases} \quad , \tag{4.2}$$

$$\sigma(f) = \begin{cases} 11.38 + 5.357 \left(\frac{f}{f_p} \right)^{-7.929} & \text{for} \quad f < f_p \\ 32.13 - 15.39 \left(\frac{f}{f_p} \right)^{-2} & \text{for} \quad f \geq f_p \end{cases} \quad , \tag{4.3}$$

where $\bar{\theta}_o(f)$ is an offset direction, with both the positive and negative value added in the summation. This directional distribution is easily made asymmetric by assigning different weights to the contributions of the positive and negative offset angles. Note that in Eqs. (4.1) through (4.3) all directions are expressed in degrees, whereas Ewans writes (4.1) in radians and the other two in degrees.

Second, nearly every spectrum in nature contains some degree of directional shear, defined as the change of mean direction $\bar{\theta}$ in the directional distribution D with frequency f. For wind seas, the spectrum at high frequencies tends to line up with the wind direction. For lower frequencies, it may deviate progressively. A realistic shear can therefore be obtained by using a mean direction that is a function of $f^{-\beta}$ (for instance, $\beta = 2$). By defining the shear as 0 at f_p, and as θ_s at some high frequency f_h (for instance, $f_h = 3f_p$), the sheared mean direction becomes

$$\bar{\theta} = 1.125\, \theta_s \left[\left(\frac{f}{f_p} \right)^{-2} - 1 \right] \quad . \tag{4.4}$$

Three cases with sheared test spectra have been added to the data set. The data set is completed by arbitrarily choosing some combinations of the perturbation of the original test spectrum.

Table 4.1: Expanded set of test cases to address the sensitivity of the selected MDIA and VDIA to the spectral shape. Changes compared to original test case as described in Eqs. (2.5) through (2.8) unless specified differently.

Case	Description
1	Less peaked spectrum with $\gamma = 1$.
2	More peaked spectrum with $\gamma = 3$.
3	Idem, $\gamma = 5$.
4	Idem, $\gamma = 9$.
5	Modified equilibrium range, $m = 4$.
6	Idem, $m = 6$.
7	Idem, $m = 10$ ('swell transition').
8	Idem, $m = 20$ ('swell transition').
9	Modified low frequency face of spectrum, $n = 2$ (less steep).
10	Idem, $n = 6$ (steeper).
11	Idem, $n = 8$ (steeper).
12	Broader directional distribution, $s = s/2$.
13	Narrower directional distribution, $s = 2s$.
14	Bimodal direction distribution of Ewans (1998), Eqs. (4.1) – (4.3).
15	Idem, asymmetric.
16	Spectrum with directional shear, $\Delta\theta_s = 15°$.
17	Idem, $\Delta\theta_s = 30°$.
18	Idem, $\Delta\theta_s = 60°$.
19	Combination: $\gamma = 1.5$, narrow asymmetric Ewans (1998), $\Delta\theta_s = -25°$.
20	Combination: $\gamma = 3$, $m = 4.5$, $\Delta\theta_s = 35°$.

Several source term parameterizations are applied to all test spectra. The first is the exact (WRT) interaction model, which is used as a benchmark. The second is the original DIA, which provides a normalization for the resulting error of newer methods, and to obtain a picture of qualitative improvements. Of the MDIA and VDIA parameterizations of S_{nl} suggested here, two versions are considered. The first are the parameterizations as tuned for the original test case. These are denoted as the 'frozen' MDIA and VDIA. The second are parameterizations as optimized for the test case under consideration. These models are denoted as the 'optimized' models. The differences in behavior between these two model versions identifies the need for and/or potential of dynamically adjusting the free parameters of the MDIA and VDIA as a function of the spectral shape.

The frozen MDIA is defined by the parameter settings as presented in Table 3.1, for $N = 4$ and with both λ and μ optimized. The optimized MDIA, by definition, also uses $N = 4$. The frozen VDIA is defined by

$$\lambda = \frac{0.20187 + 0.03234\tilde{f}}{1 - 0.01698\tilde{f}} \quad , \quad \mu = \frac{0.06812 + 0.05063\tilde{f}}{1 - 0.00377\tilde{f}} \quad , \quad C = 2.007\ 10^7 \quad , \quad (4.5)$$

where $\tilde{f}$ is the normalized frequency ($\tilde{f} = f/f_p$). Figures for all test cases are gathered in Appendix C (Figs. C.1 through C.20). Figure 4.1a presents the normalized errors ϵ_n of each optimized model as a function of the error of the corresponding frozen model. Figure 4.1b presents the error of the optimized model normalized with the corresponding error of the frozen model ($\epsilon_{n,opt}/\epsilon_{n,frozen}$), as a function of the latter.

Figure 4.1 shows significantly different overall behavior for the selected VDIA and MDIA. As expected from the results in the previous section, the MDIA is much more accurate than the VDIA. The optimized MDIA is always at least a factor of 4 more accurate than the original DIA ($\epsilon_n < 0.25$), and for most cases is more than a factor of 10 more accurate ($\epsilon_n < 0.10$). The optimized VDIA shows better results than the original DIA, but the improvements are much smaller than for the MDIA. More interesting, however, is the overall behavior of the VDIA and the MDIA, and the impact of the optimization on each case, or conversely, their sensitivity to the selected free parameters. This will be discussed separately for the VDIA and MDIA below.

For the VDIA, inspection of the individual cases as presented in Appendix C leads to the following conclusions. Whereas for most cases the qualitative improvement of the VDIA over the original DIA is large, this improvement is smaller (or even absent) for cases with sharply peaked spectra (cases 2, 3, 4 and 20, and corresponding Figures in the Appendix), or for spectra with strongly suppressed equilibrium ranges (cases 6 and 7). In such cases, however, the original DIA also behaves particularly poorly. The original DIA then systematically moves the low frequency lobe of the interactions to much higher frequencies than expected, and

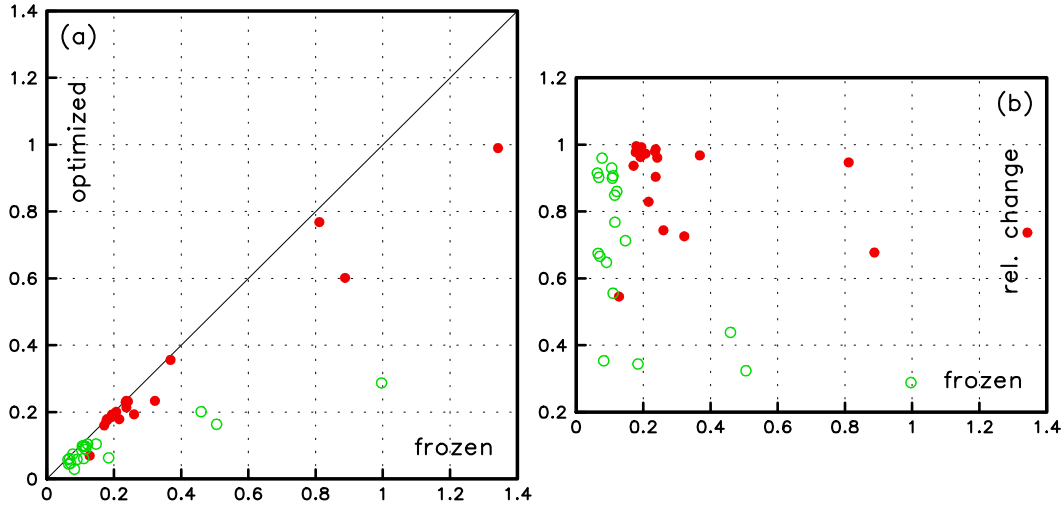

Fig. 4.1 : Resulting normalized errors ϵ_n for all test cases. (a) Error of optimized model as a function of the error of the frozen model. (b) Relative change in error defined as error of optimized model normalized with error of frozen model, as a function of the latter. MDIA: open red circles. VDIA: solid green circles.

the positive lobe at low frequencies also seems to be shifted systematically, compared to more conventional cases. With the exception of the very sharply peaked spectrum in case 4, the VDIA does not appear to display such systematic behavior, and, therefore, should be considered qualitatively much better than suggested by the quantitative error comparison with the original DIA. The systematically narrow and sharp features of the low frequency, positive lobe of the source term are particularly encouraging.

Cases where the retuning of the VDIA has a significant impact on the model errors are isolated in Fig. 4.1b. In only five cases did the retuning reduce the error by more than 20% (relative change less than 0.8). Most of these correspond to the cases identified above in which the VDIA performs relatively poorly. Exceptions are case 1 with the less-peaked spectrum, in which the retuning of the VDIA cuts its rms error nearly in half. Even the frozen VDIA, however performs very well here with $\epsilon_n = 12.7\%$. Another exception is case 9, which has a low frequency face of the spectrum that is much less steep. For most of the remaining cases, the error reduction attained by dynamic optimization of the VDIA is less than 10%. The VDIA thus is surprisingly insensitive to retuning. Furthermore, the improvement from retuning occurs mostly in cases where the VDIA already shows great accuracy, or in sharply peaked spectra which are generally not produced by numerical wave models with relatively poor spectral resolution. Therefore, it appears more sensible to use a frozen VDIA than a dynamically optimized VDIA.

Two additional remarks need to be made regarding the VDIA. First, in the

directionally asymmetric and sheared spectra from cases 15 through 20, the exact interactions tend to result in a much more directionally asymmetric source term than the DIA. The VDIA appears to share this deficiency with the conventional DIA. Second, as discussed in the previous section and in the results presented in Appendix C, the VDIA systematically underestimates the strength of the positive lobe at low frequencies. As in the original DIA, this could be counteracted by systematically increasing C. In the original DIA, an increase by a factor of more than 3 was needed (see discussion of Fig. 3.1). For the VDIA, such a factor only needs to be between 1.1 and 1.2.

For the MDIA, inspection of the individual cases presented in Appendix C leads to the following conclusions. As with the VDIA, the smallest improvement over the original DIA occurs in strongly peaked spectra or in spectra with a strongly suppressed tail. Only in cases 3, 4, 8, and 20, is the improvement of the optimized MDIA over the original DIA less than a factor of 8 ($\epsilon_n > 12.5\%$). The qualitative improvement is perhaps more impressive. Even in the case where the MDIA performs worst in a quantitative sense (case 4), the qualitative improvement is still large. In this case, the frozen MDIA has an rms error that is identical to the rms error of the DIA (see Fig. C.4), yet the frozen MDIA clearly captures the essence of the exact interactions, whereas the original DIA does not. The optimized MDIA, in this case, betters the rms error of the original DIA by a factor of 3.5.

Figure 4.1b indicates that the impact of optimization for individual spectra is much more pronounced for the MDIA than for the VDIA. In half the cases, the optimization of the MDIA reduces the rms error relative to the frozen MDIA by at least 25%; in a quarter of the cases, this error reduction is more than 50%. This result seems to be at least qualitatively consistent with the previous findings of Hashimoto and Kawaguchi (2001), who found that the optimum layout of a quadruplet for a single DIA is a distinct function of the peakedness of the spectrum [i.e., of γ in Eq. (2.5)]. The MDIA is, therefore, a candidate for dynamically adjusting the constants in the parameterization as a function of the actual spectral shape (unlike the VDIA). Note that for strongly peaked spectra, the MDIA with four components generally has one component with a large negative C. As discussed in the previous section, this is not desirable. Hence, the actual number of components in the MDIA could also be dynamically adjusted in the MDIA.

This page is intentionally left blank.

5 Model integration

This final section presents a preliminary assessment of the capability of the selected parameterizations of the nonlinear interactions to result in well behaved model integration. This final step has been omitted in many recent papers in this field. Our recent experience with NN Interaction Approximations, however, has demonstrated the importance of such an assessment. This part of the study is intended only to provide a basis for a second study, in which the robustness of several DIAs in a full wave model integration is addressed in more detail.

The robustness of a DIA, in the context of wave modeling, is evaluated by a time integration of the complete set of source terms in Eq. (1.1). For a first impression of the robustness of the MDIA and VDIA, it is sufficient to use an idealized homogeneous situation, or in other words, a one point wave model without wave propagation. In the present study, these test calculations are made with version 2.22 of the WAVEWATCH III model (Tolman and Chalikov, 1996; Tolman et al., 2002; Tolman, 2002). With the exception of the nonlinear interactions, the default model settings of WAVEWATCH III have been used. The spectral grid consists of 36 directions, with $\Delta\theta = 15°$, and 35 frequencies ranging from 0.0418 through 0.417 Hz ($\alpha = 1.07$). The initial conditions consist of a JONSWAP / Hasselmann spectrum with $f_p = 0.15$ Hz, $\gamma = 3.3$, and the other parameters follow the standard settings for such a spectrum. The wind speed is set to 20 ms^{-1} in the initial mean wave direction, and integration is performed for 6 hours.

Model integration results for various nonlinear parameterizations after 2, 4 and 6 hours of model integration are presented in Figs. 5.1 through 5.4. The spectra and source terms are displayed in polar format, as is common in general purpose wave models. Because at this time only the consistency of spectral shapes in relevant, growth curves and other diagnostics will not be presented and discussed.

Figure 5.1 shows the results of the conventional WAVEWATCH III model, which includes the conventional DIA, retuned to spread the errors of this DIA more evenly over the entire spectrum ($\lambda = 0.25$ and $C = 1.\,10^7$, see Tolman and Chalikov, 1996). Figure 5.2 shows the corresponding spectra and source terms as, obtained by replacing the DIA with the exact WRT algorithm, provided with version 2.22 of WAVEWATCH III. Figures 5.3 and 5.4 show results obtained with the frozen VDIA and MDIA, as defined in the previous section. These algorithms have been implemented in a developmental version of WAVEWATCH III at NCEP.

Figures 5.1 and 5.2 show the well established capability of the DIA and the WRT interaction algorithms to produce realistic, single peaked wind sea spectra, with reasonable corresponding instantaneous estimates of the nonlinear interactions. The MDIA (Fig. 5.4) shows a similar capability, and hence appears to have the potential to also produce robust model integration results. The VDIA

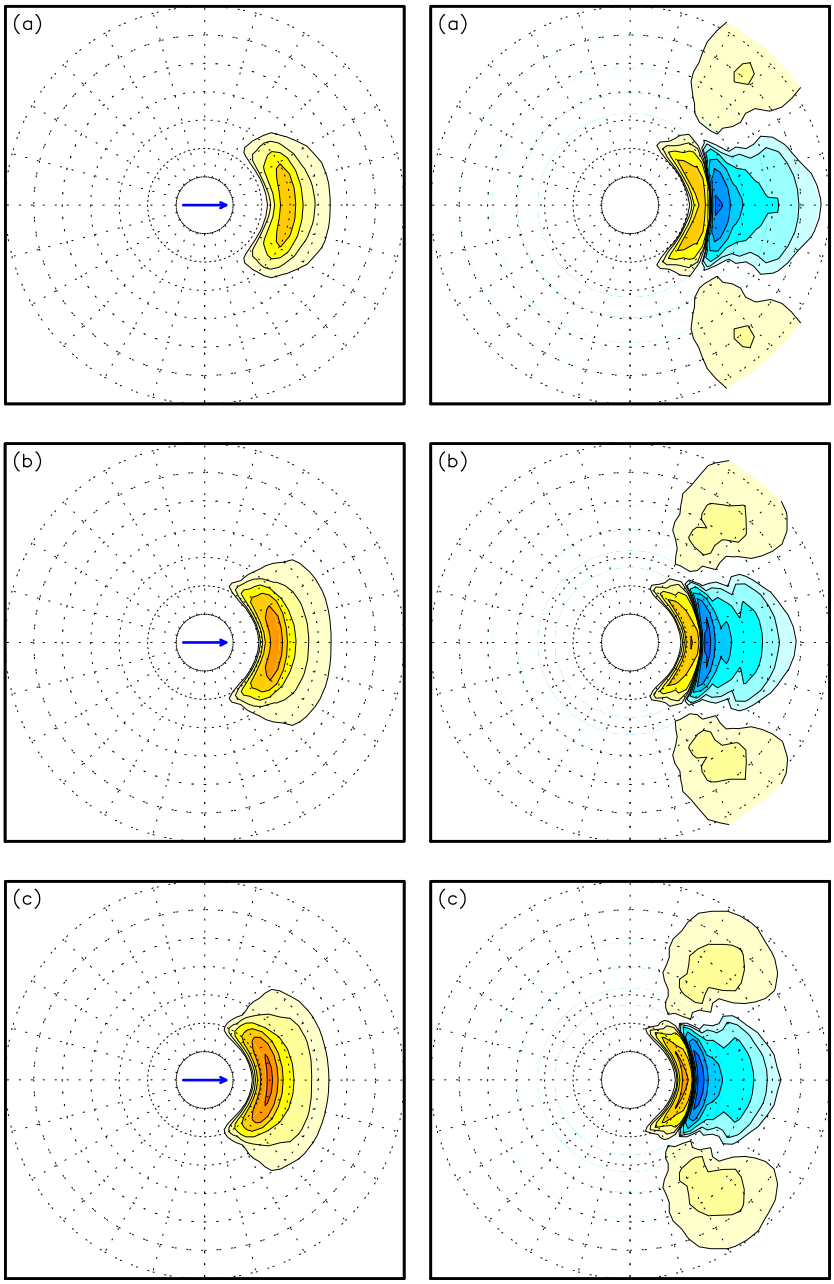

Fig. 5.1 : Spectra (left panels) and nonlinear source terms (right panels) resulting from WAVEWATCH III model integration with DIA ($C = 1 \times 10^7$ as in default WAVEWATCH III) after 2 hours (panel a), 4 hours (panel b) and 6 hours (panel c). Contours increment by factor 2, lowest contour for spectrum 1 $m^2 s^{-1}$ and for source term $\pm$ 10^{-4} $m^2 s^{-1}$. Polar representation with low frequencies in center of plot, and grid lines at 15° and 0.05 Hz intervals. Blue arrow in left panels represents wind direction (20 ms^{-1} at 10 m height).

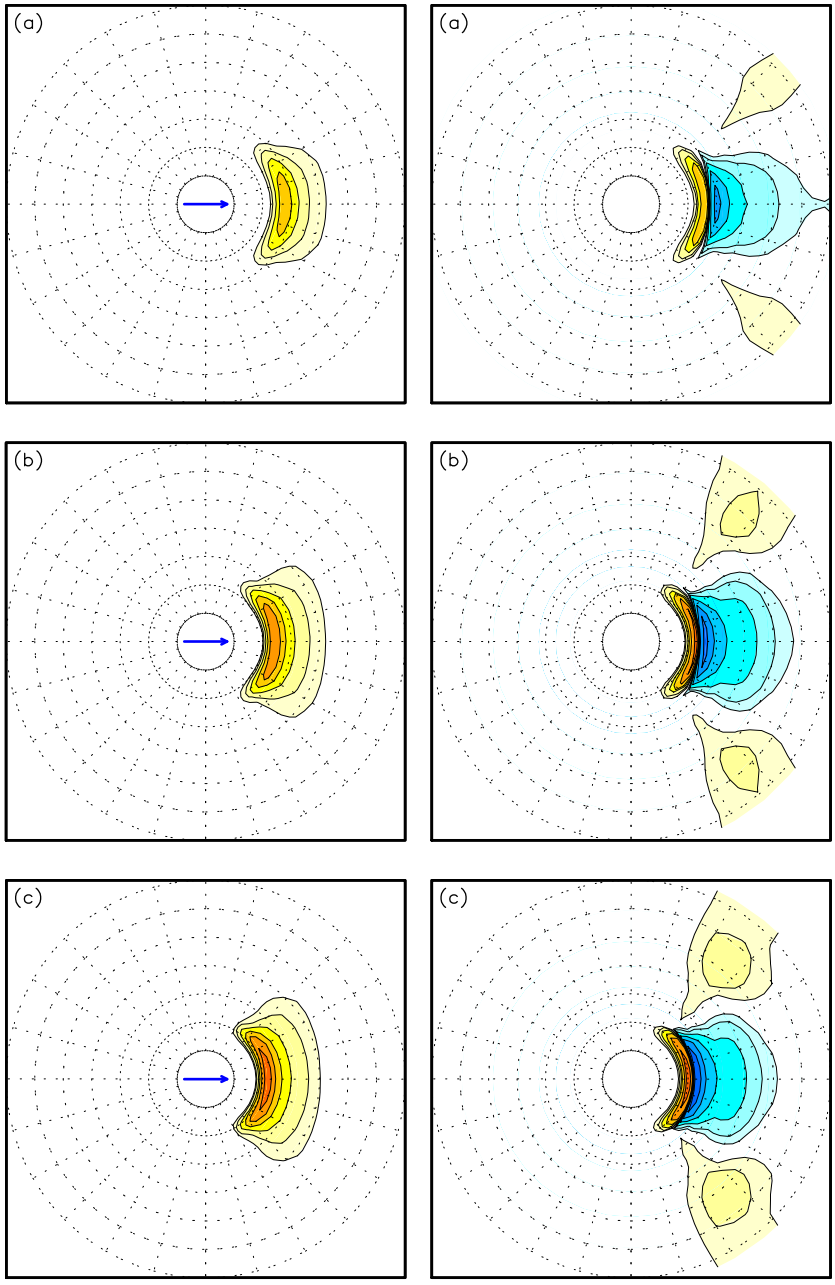

Fig. 5.2 : Like Fig. 5.1, replacing DIA with exact interactions (WRT).

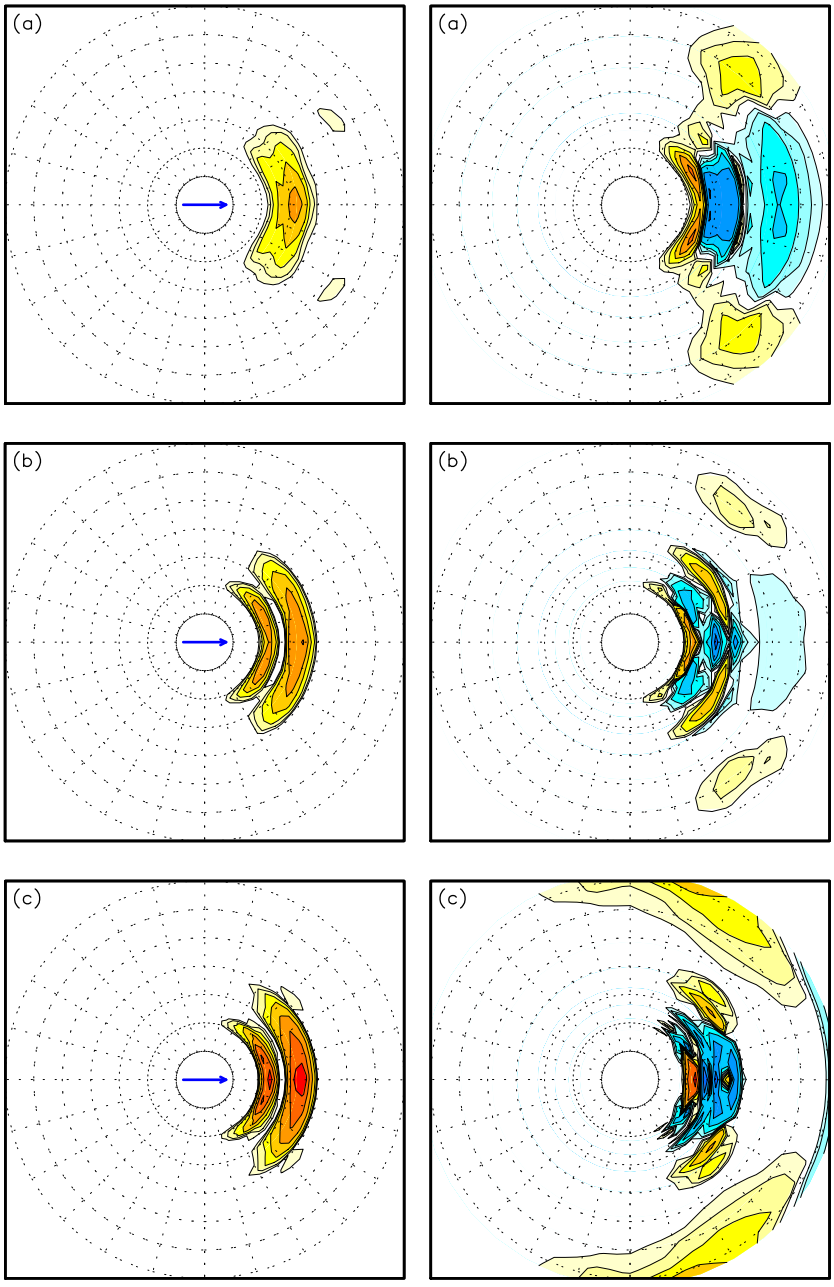

Fig. 5.3 : Like Fig. 5.1, replacing DIA with frozen VDIA.

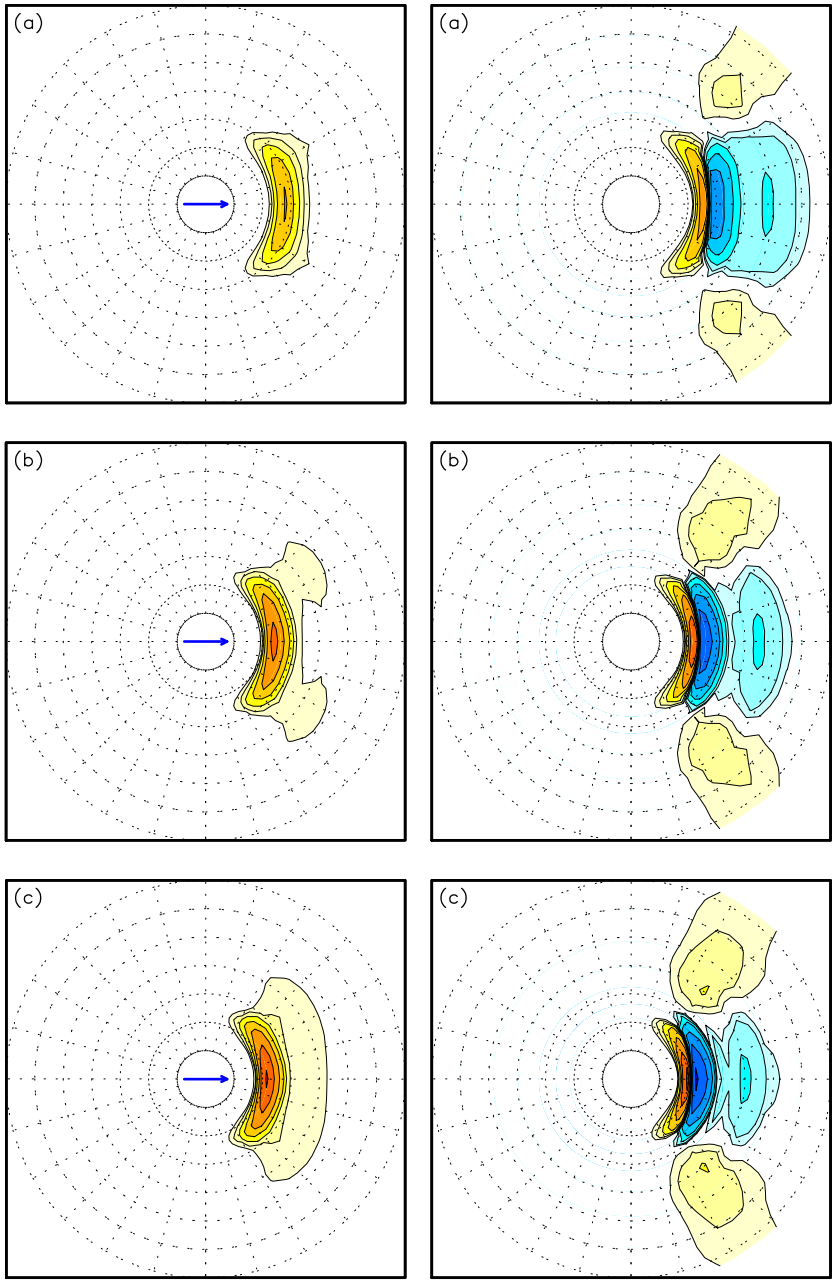

Fig. 5.4 : Like Fig. 5.1, replacing DIA with (frozen) MDIA.

(Fig. 5.3), however, results in unrealistic double peaked spectra. It should be noted that this is not due to the frequency dependence of the free parameters in the VDIA. A single MDIA with $\lambda = 0.248$, $\mu = 0.127$ and $C = 1.81\,10^7$ gives similar results (Figures not presented here).

The inability of the VDIA to produce robust model integration may be considered surprising when considering the established robustness of the conventional DIA. The reasons and possible remedies for this behavior will be discussed in more detail in part two of this study. It clearly demonstrates that any study regarding nonlinear interactions cannot be considered complete without testing the resulting algorithms in realistic wave model integrations.

6 Summary and conclusions

The present study addresses the capability of various Discrete Interaction Approximations (DIAs) to accurately reproduce exact nonlinear interaction source terms as calculated using the Web-Resio-Tracy (WRT) method. This study mostly focuses on inverse modeling, where the free parameters in various DIAs are estimated to optimally reproduce the WRT results for a given spectrum. The following DIAs have been considered :

- The original DIA, with the suggested parameter setting for λ and C as suggested by Hasselmann et al. (1985), or with optimized settings.
- An expanded DIA, with more complex quadruplet configurations than the original quadruplet with one free parameter [Eq. (2.1)], focusing on a new symmetric two-parameter quadruplet [Eq. (2.13)]. A more complex three parameter quadruplet as, suggested by Van Vledder (2001), could have been considered [Eq. (2.9)], but was never investigated after good results were obtained with the two parameter quadruplet.
- An expanded DIA, with additional proportionality constants in the calculation of the strength of the interactions [Eqs. (2.10), (2.12) and (2.15)]], as in Hashimoto and Kawaguchi (2001).
- A new variable DIA (VDIA), where the free parameters in the DIA are no longer constant throughout the spectrum.
- Multiple DIAs (MDIA), consisting of a composite of several DIAs with different quadruplet configurations, as in Ueno and Ishizaka (1997), Hashimoto and Kawaguchi (2001) and Van Vledder (2001).

The potential of many of these methods has been addressed, first by using a single test case which is considered fairly representative for well developed wind waves. Using this test case, two potentially accurate DIA versions have been selected for further investigation. These are a single component VDIA and a four component MDIA, both with the expanded quadruplet definition of Eq. (2.13).

These two methods have been applied to an expanded test set of 20 spectra. Both the initially optimized version of each model and a version optimized to the actual tests spectrum are considered. Results from these tests show that the VDIA is less accurate for sharply peaked spectra, and would benefit little from dynamical adjustment of its parameter. The selected MDIA is more generally applicable, but requires dynamically adjusted parameters for optimum results.

Finally, the two methods are incorporated into the WAVEWATCH III model to test the robustness of these alternative parameterizations of S_{nl} with respect to wave model integration. The VDIA fails this test, whereas the MDIA shows promising results.

In summary, the following conclusions have been drawn :

- Single or multiple DIAs based on the original quadruplet of Eq. (2.1) cannot accurately reproduce the exact interactions.
- DIAs with additional constants C show little or no improvement over optimized DIAs with a single C. The additional complexity of these parameterizations, therefore, is not justified.
- A VDIA requires a constrained variability in its free parameters to avoid an accurate but noisy solutions.
- A VDIA with a single component, and λ, μ and C as a function of the frequency f, with a limited number of free parameters can, improve the qualitative description of the interactions. Such a VDIA seems to have fairly general applicability, without the need for retuning for individual spectra.
- This VDIA is expected to be roughly four times as expensive as the conventional DIA.
- Unfortunately, in its present form, the above VDIA does not result in stable model integration.
- An MDIA with four components, and λ, μ and C optimized for each component (but constant in spectral space), produces a very accurate description of the exact nonlinear interactions.
- For optimum results, the MDIA would require dynamically estimated free parameters.
- In a simple frozen form, the MDIA provided a realistic and stable model integration.
- This MDIA is expected to be about 10 times more expensive than the original DIA.

The inability of the selected VDIA to produce realistic model integration is somewhat surprising. It stresses the importance of addressing the ability of a nonlinear parameterization to perform well in a model environment, which in itself is the ultimate goal in developing new economical yet accurate parameterizations for S_{nl}. It shows that the ability to generate reasonable interactions for a given spectrum does not automatically translate into reasonable behavior when applied in a wave model. For this reason, part two of the present study will be focused on the integration behavior of several DIAs. It should also be noted that the present study, by definition, is limited because it considers single peaked spectra in deep water only. A final study of any nonlinear interaction approximation requires the assessment of the effects of restricted water depth and complicated wave spectra with one or more swell fields present.

References

Ewans, K. C., 1998: Observations of the directional spectrum of fetch-limited waves. *J. Phys. Oceanogr.*, **28**, 495–512.

Hashimoto, N., I. G. Haagsma and L. H. Holthuijsen, 2002: Four-wave interactions in swan. in *Proc. 28th Int. Conf. Coastal Eng., Cardiff, Wales*. ASCE, In Press.

Hashimoto, N. and K. Kawaguchi, 2001: Extension and modification of Discrete Interaction Approximation (DIA) for computing nonlinear energy transfer of gravity wave spectrum. in *Ocean Wave Measurement and Analysis*, pp. 530–539. ASCE.

Hasselmann, D. E., M. Dunckel and J. A. Ewing, 1980: Directional wave spectra observed during JONSWAP 1973. *J. Phys. Oceanogr.*, **10**, 1264–1280.

Hasselmann, K., 1960: Grundgleichungen der seegangsvoraussage. *Schiffstechnik*, **1**, 191–195.

Hasselmann, K., 1962: On the non-linear transfer in a gravity wave spectrum, Part 1. General theory. *J. Fluid Mech.*, **12**, 481–500.

Hasselmann, K., 1963a: On the non-linear transfer in a gravity wave spectrum, Part 2, Conservation theory, wave-particle correspondence, irreversibility. *J. Fluid Mech.*, **15**, 273–281.

Hasselmann, K., 1963b: On the non-linear transfer in a gravity wave spectrum, Part 3. Evaluation of energy flux and sea-swell interactions for a Neuman spectrum. *J. Fluid Mech.*, **15**, 385–398.

Hasselmann, K., T. P. Barnett, E. Bouws, H. Carlson, D. E. Cartwright, K. Enke, J. A. Ewing, H. Gienapp, D. E. Hasselmann, P. Kruseman, A. Meerburg, P. Mueller, D. J. Olbers, K. Richter, W. Sell and H. Walden, 1973: Measurements of wind-wave growth and swell decay during the Joint North Sea Wave Project (JONSWAP). *Ergaenzungsheft zur Deutschen Hydrographischen Zeitschrift, Reihe A(8)*, **12**, 95 pp.

Hasselmann, S. and K. Hasselmann, 1985: Computations and parameterizations of the nonlinear energy transfer in a gravity-wave spectrum, Part I: A new method for efficient computations of the exact nonlinear transfer integral. *J. Phys. Oceanogr.*, **15**, 1369–1377.

Hasselmann, S., K. Hasselmann, J. H. Allender and T. P. Barnett, 1985: Computations and parameterizations of the nonlinear energy transfer in a gravity-wave spectrum, Part II: parameterizations of the nonlinear energy transfer for application in wave models. *J. Phys. Oceanogr.*, **15**, 1378–1391.

Herterich, K. and K. Hasselmann, 1980: A similarity relation for the nonlinear energy transfer in a finite-depth gravity-wave spectrum. *J. Fluid Mech.*, **97**, 215–224.

Komatsu, K. and A. Masuda, 1996: A new scheme of nonlinear energy transfer among wind waves: RIAM method – algorithm and performance. *Journal of*

Oceanography, **52**, 509–537.

Komen, G. J., L. Cavaleri, M. Donelan, K. Hasselmann, S. Hasselmann and P. E. A. M. Janssen, 1994: *Dynamics and modelling of ocean waves*. Cambridge University Press, 532 pp.

Krasnopolsky, V. M., D. V. Chalikov and H. L. Tolman, 2002: A neural network technique to improve computational efficiency of numerical oceanic models. *Ocean Mod.*, **4**, 363–383.

Masuda, A., 1980: Nonlinear energy transfer between wind waves. *J. Phys. Oceanogr.*, **10**, 2082–2093.

Phillips, O. M., 1960: On the dynamics of unsteady gravity waves of finite amplitude. *J. Fluid Mech.*, **9**, 193–217.

Phillips, O. M., 1981: Wave interactions: the evolution of an idea. *J. Fluid Mech.*, **106**, 215–227.

Resio, D. T. and W. Perrie, 1991: A numerical study of nonlinear energy fluxes due to wave-wave interactions. Part 1: Methodology and basic results. *J. Fluid Mech.*, **223**, 609–629.

Snyder, R. L., R. B. Long and W. L. Neu, 1998: A fully nonlinear regional wave model for the Bight of Abaco 1. Nonlinear-transfer computation. *J. Geophys. Res.*, **103**, 3119–3141.

Tolman, H. L., 1992: Effects of numerics on the physics in a third-generation wind-wave model. *J. Phys. Oceanogr.*, **22**, 1095–1111.

Tolman, H. L., 2002: User manual and system documentation of WAVEWATCH III version 2.22. Tech. Note 222, NOAA/NWS/NCEP/MMAB, 133 pp.

Tolman, H. L., B. Balasubramaniyan, L. D. Burroughs, D. V. Chalikov, Y. Y. Chao, H. S. Chen and V. M. Gerald, 2002: Development and implementation of wind generated ocean surface wave models at NCEP. *Wea. Forecasting*, **17**, 311–333.

Tolman, H. L. and D. V. Chalikov, 1996: Source terms in a third-generation wind-wave model. *J. Phys. Oceanogr.*, **26**, 2497–2518.

Tracy, B. and D. T. Resio, 1982: Theory and calculation of the nonlinear energy transfer between sea waves in deep water. WES Report 11, US Army Corps of Engineers.

Ueno, K. and M. Ishizaka, 1997: On an efficient calculation method of the nonlinear energy transfer in wind waves. *Sottukojiho, JMA*, **64**, 75–80, (In Japanese).

Van Vledder, G. Ph., 2000: Improved method for obtaining the integration space for the computation of nonlinear quadruplet wave-wave interaction. in *Proceedings of the 6th International Workshop on Wave Forecasting and Hindcasting*, pp. 418–431.

Van Vledder, G. Ph., 2001: Extension of the Discrete Interaction Approximation for computing nonlinear quadruplet wave-wave interactions in operational wave prediction models. in *Ocean Wave Measurement and Analysis*, pp. 540–549. ASCE.

Van Vledder, G. Ph., 2002a: Improved parameterizations of nonlinear four wave interactions for application in operational wave prediction models. Report 151a, Alkyon, The Netherlands.

Van Vledder, G. Ph., 2002b: A subroutine version of the Webb/Resio/Tracy method for the computation of nonlinear quadruplet interactions in a wind-wave spectrum. Report 151b, Alkyon, The Netherlands.

Van Vledder, G. Ph., T. H. C. Herbers, R. E. Jenssen, D. T. Resio and B. Tracy, 2000: Modelling of non-linear quadruplet wave-wave interactions in operational wave models. in *Proc. 27th Int. Conf. Coastal Eng., Sydney, Australia*, pp. 797–811. ASCE.

WAMDIG, 1988: The WAM model – a third generation ocean wave prediction model. *J. Phys. Oceanogr.*, **18**, 1775–1809.

Webb, D. J., 1978: Non-linear transfers between sea waves. *Deep-Sea Res.*, **25**, 279–298.

Young, I. R. and G. Ph. Van Vledder, 1993: A review of the central role of nonlinear interactions in wind-wave evolution. *Trans. Roy. Soc. London*, **342**, 505–524.

This page is intentionally left blank.

APPENDICES

This page is intentionally left blank.

A Inverse modeling: MDIA

In an MDIA based on Eqs. (1.2), (1.3), (2.13), (2.15) and (2.19), with constant C, λ and μ, only C is an implicit parameter whose optimum value can be estimated directly. Because λ and μ are implicit to the formulation, these parameters can only be optimized by using iterative methods. First, the direct estimate of the N factors C, for given λ and μ, will be discussed, after which the technique for obtaining optimum estimates of the latter two parameters will be discussed briefly.

Consider an MDIA with N components, where j and l are counters from 1 thought N, and let i be a counter covering the entire discrete spectral space. For each component j of the MDIA, the contribution $S_{i,j}$ equals $C_j B_{i,j}$, where B is the normalized or 'base' solution of the DIA with given λ_j and μ_j. The MDIA, as defined in Eq. (2.19), then can be written as

$$S_i = \frac{1}{N} \sum_j C_j B_{i,j} \quad . \tag{A.1}$$

C_j can now be estimated objectively by minimizing the rms error of the resulting MDIA relative to the exact nonlinear interactions. If X_i represents the exact solution to which the MDIA is fit, the rms error ϵ becomes

$$\epsilon = \left[\sum_i \left(X_i - \frac{1}{N} \sum_j C_j B_{i,j} \right)^2 \Delta\theta_i \Delta f_i \right]^{1/2} \quad , \tag{A.2}$$

Considering that the directional increment $\Delta\theta$ is constant, minimizing the rms error corresponds to minimizing the function $\tilde{\epsilon}$

$$\tilde{\epsilon} = \sum_i \left(X_i - \frac{1}{N} \sum_j C_j B_{i,j} \right)^2 \Delta f_i \quad , \tag{A.3}$$

C_l can then be estimated by evaluating the following N equations identified by the counter l

$$\frac{\partial \tilde{\epsilon}}{\partial C_l} = \frac{\partial}{\partial C_l} \sum_i \Delta f_i \left\{ X_i^2 - 2x_i \sum_j C_j N^{-1} B_{i,j} + \left(\sum_j C_j N^{-1} B_{i,j} \right)^2 \right\} =$$

$$\sum_i \Delta f_i \left\{ -2X_i \sum_j \frac{\partial C_j}{\partial C_l} N^{-1} B_{i,j} + 2 \left(\sum_j C_j N^{-1} B_{i,j} \right) \sum_j \frac{\partial C_j}{\partial C_l} N^{-1} B_{i,j} \right\} =$$

$$2N^{-1} \sum_i \Delta f_i \left\{ -X_i B_{i,l} + \left(\sum_j C_j N^{-1} B_{i,j} \right) B_{i,l} \right\} = 0 \quad . \tag{A.4}$$

From this, the following set of N equations identified by l is found

$$\sum_i \Delta f_i B_{i,l} \sum_j C_j N^{-1} B_{i,j} = \sum_i \Delta f_i \; X_i B_{i,l} \quad , \tag{A.5}$$

or

$$\sum_j C_j N^{-1} \sum_i \Delta f_i B_{i,l} B_{i,j} = \sum_i \Delta f_i \; X_i B_{i,l} \quad , \tag{A.6}$$

which can be solved using a simple sweeping technique. Note that this equation gives a direct solution for a single DIA where $N = 1$ (without the need for sweeping a matrix). Note, furthermore, that this technique is trivially expanded for DIAs with multiple proportionality constants (C_1, C_2) or (C_3, C_4), by defining a base function B for each constant separately.

With this direct technique to optimize C_j, a simple algorithm can be designed for optimizing the complete MDIA. First, an initial guess for λ_j and μ_j is given. Typically, λ_j are chosen to equally cover the possible range of λ, and μ initially set to 0. For these parameter estimates, the optimum values for C_j [Eq. (A.5)], and the corresponding error ϵ [Eq. (A.2)] are computed. After this, all λ_j and μ_j are systematically perturbed (one-by-one), the corresponding C_j and ϵ are estimated, and perturbations with reduction of ϵ are retained. In this study, a simple method with alternating signs for the perturbations and with systematic reduction of perturbations was used. Although there is some effect from initial conditions and initial perturbations on the final results, these effects appear irrelevant in the present study.

B Inverse modeling: VDIA

B.1 Fully variable C

For any given λ and μ, $C(f,\theta)$, in principle, contains enough degrees of freedom for the DIA to represent any given $S_{nl}(f,\theta)$. If an exact fit is sought, Eqs. (2.13), (2.15), (2.20) and (2.21) result in a set of equations

$$\mathbf{AC} = \mathbf{X} \quad , \tag{B.1}$$

where $\mathbf{X}$ is an array with the exact source term to be reproduced by the DIA, $\mathbf{C}$ is the corresponding set of coefficients C to be estimated, and $\mathbf{A}$ is a 2-D array with coefficients given by the above equations, having a broad but sparse band structure. This set of equations in principle can be solved with a simple sweep operation. However, two problems occur with this set of equations.

First, quadruplets centered outside the discrete spectral domain contribute to the estimated source term in the discrete domains, making $\mathbf{C}$ larger than $\mathbf{X}$. Thus, additional equations are required for closure. Second, the set of equations is not well conditioned, due to the sensitivity of the fitting away from strong spectral signatures.

The latter problem can be alleviated somewhat by removing equations fitting to $X_{nl}(f,\theta)$ for $F(f,\theta) < \alpha F_{\max}$. The corresponding values of $C(f\theta)$ can be assumed to contribute negligibly to the source term and, therefore, simply be set to 0. A similar approach can be used in the tail of the spectrum, providing a direct estimate for each C for which no X is available. To illustrate the poor conditioning of the equations, Fig. B.1 shows the results of attempting to retrieve C by trying to fit the VDIA to the results of the original DIA, both with $\lambda = 0.25$ and $\mu = 0$. Furthermore, $\alpha = 10^{-5}$ is used. For a large area, C is close to the expected value of 3×10^7. At low frequencies, and for directions far from $\theta = 0°$, however, the retrieved C shows large negative values. This has, nevertheless, no notable impact on the VDIA with the estimated C, which reproduces the original DIA meticulously.

More elaborate schemes with the relaxation of C to neighboring values, proved not to improve results nor to notably impact the results presented in Fig. B.1, unless α of $\mathrm{O}(10^{-2})$ is chosen. In the latter case, the constant C is exactly retrieved, but such a setup is not conducive to give results when the DIA is fitted to other interactions, such as the exact interactions.

B.2 C varying with frequency f only

If the constant C is allowed to be a function of f only, no exact fit of the resulting source term S to the exact solution X can be expected. Instead, a best fit can again be defined in terms of a minimal rms error, as in Appendix A. Counters

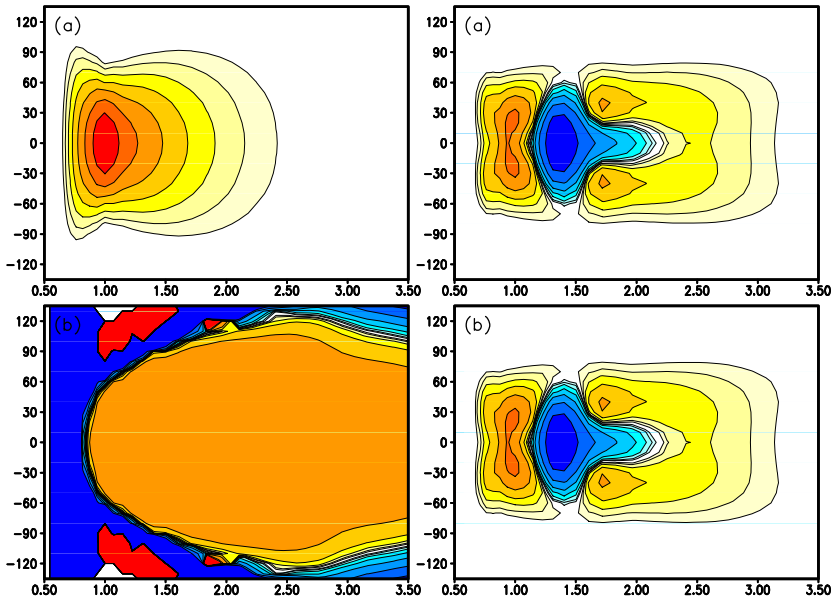

Fig. B.1 : (a) Spectrum for test case (left) and conventional DIA (right). (b) Retrieved constant $C(f,\theta)$ (left) and corresponding DIA (right). Legend for spectra and source terms as in Fig. 2.1. Logarithmic scaling for C with lowest contour levels at $\pm 10^6$

and symbols in this Appendix will be adopted from Appendix A, unless specified differently. If the constant C is assumed to be a function of the frequency f, the source term can be expressed in vector notation as

$$\mathbf{S} = \mathbf{BC} \quad , \tag{B.2}$$

or

$$S_i = \sum_j C_j B_{i,j} \quad , \tag{B.3}$$

where j is a counter over the discrete frequencies (1 through N_f) and B is now a matrix similar to A in Eq. (B.1), yet significantly smaller because C is now a function of f only. Note that this equation is nearly identical to Eq. (A.1), apart from the factor $1/N$ and a completely different definition of B. For the optimization, however, this has no relevance, and hence the optimum estimate of $C(f)$ is similar to Eq. (A.6), with a set of N_f equations identified by the counter l

$$\sum_j C_j \sum_i \Delta f_i B_{i,l} B_{i,j} = \sum_i \Delta f_i \, X_i B_{i,l} \quad . \tag{B.4}$$

This optimization does not assume any coherence between neighboring estimates of C in the discrete frequency space. If C is assumed to be an arbitrary function G of f, $C = G(f)$, Eq. (B.3) becomes

$$S_i = \sum_j G_j B_{i,j} \quad , \tag{B.5}$$

where j is a counter over N_f. The function to be minimized now becomes

$$\tilde{\epsilon} = \sum_i \left(X_i - \sum_j G_j B_{i,j} \right)^2 \Delta f_i \quad . \tag{B.6}$$

If G has N_g free parameters c_1, c_2, ..., optimum parameter settings can again be found by solving N_g equations

$$\frac{\partial \tilde{\epsilon}}{\partial c_l} = 0 \quad , \tag{B.7}$$

where l is now a counter over N_g. This leads to the following set of equations

$$\sum_i \Delta f_i \, X_i \sum_j B_{i,j} \left. \frac{\partial G}{\partial c_l} \right|_j = \sum_i \Delta f_i \left(\sum_j B_{i,j} G_j \right) \sum_j B_{i,j} \left. \frac{\partial G}{\partial c_l} \right|_j \quad , \tag{B.8}$$

which can be used to optimize an arbitrary G. Here, only polynomial functions will be considered

$$G = c_1 + c_2 f + c_3 f^2 + \ldots \quad , \tag{B.9}$$

with

$$\frac{\partial G}{\partial c_l} = f^{l-1} \quad . \tag{B.10}$$

Substitution of (B.9) and (B.10) in Eq. (B.8) then gives a set of N_g equations identified by the counter k

$$\sum_l c_l \sum_i \Delta f_i \left(\sum_j B_{i,j} f^{k-1} \right) \left(\sum_j B_{i,j} f^{l-1} \right) = \sum_i \Delta f_i \, X_i \left(\sum_j B_{i,j} f^{k-1} \right) \quad , \tag{B.11}$$

where l and k are counters over N_g, j represents all frequencies, and i represents all spectral bins.

B.3 Optimizing λ and μ

The free parameters λ and μ remain implicit to the DIA, and, therefore, can only be optimized by simple iterative methods. This is true if parameters are allowed to vary freely for each spectral frequency, or if they are described using functions with a limited number of parameters. In the latter case, the iterative procedure obviously deals with the free parameters in the functions.

C Results for all test cases

In this Appendix, the results of all test cases identified in Table 4.1 are presented in graphical form. Panels (a) represent the test spectrum (left figure) and the exact interactions. The legend is the same as in the main body of this report, with the exception that the source term contour levels are rescaled relative to the absolute maximum of the exact interactions for each case individually. All source term panels in a given figure use the same contour intervals.

Panels (b) show the results for the selected MDIA, with the parameter settings of the initial test case used for the left panel, and the results as optimized for the actual test spectrum in the right panel. Panels (c) show the corresponding results for the selected VDIA. Panels (d) show the resulting conventional DIA on the right, and all the one dimensional source terms $S_{nl}(f)$ on the left.

The one dimensional source term on the left side of the (d) panels is normalized with the absolute maximum of the exact solution. The solid green line represents the exact (WRT) solution, the dotted red line the original DIA, the long dashed, blue lines the two MDIAs and the short dashed, magenta lines, the two VDIAs. Normalized errors ϵ_n are printed in the upper right corner of panels with full source terms. The normalization always takes place with the error of the original DIA, for the test case considered.

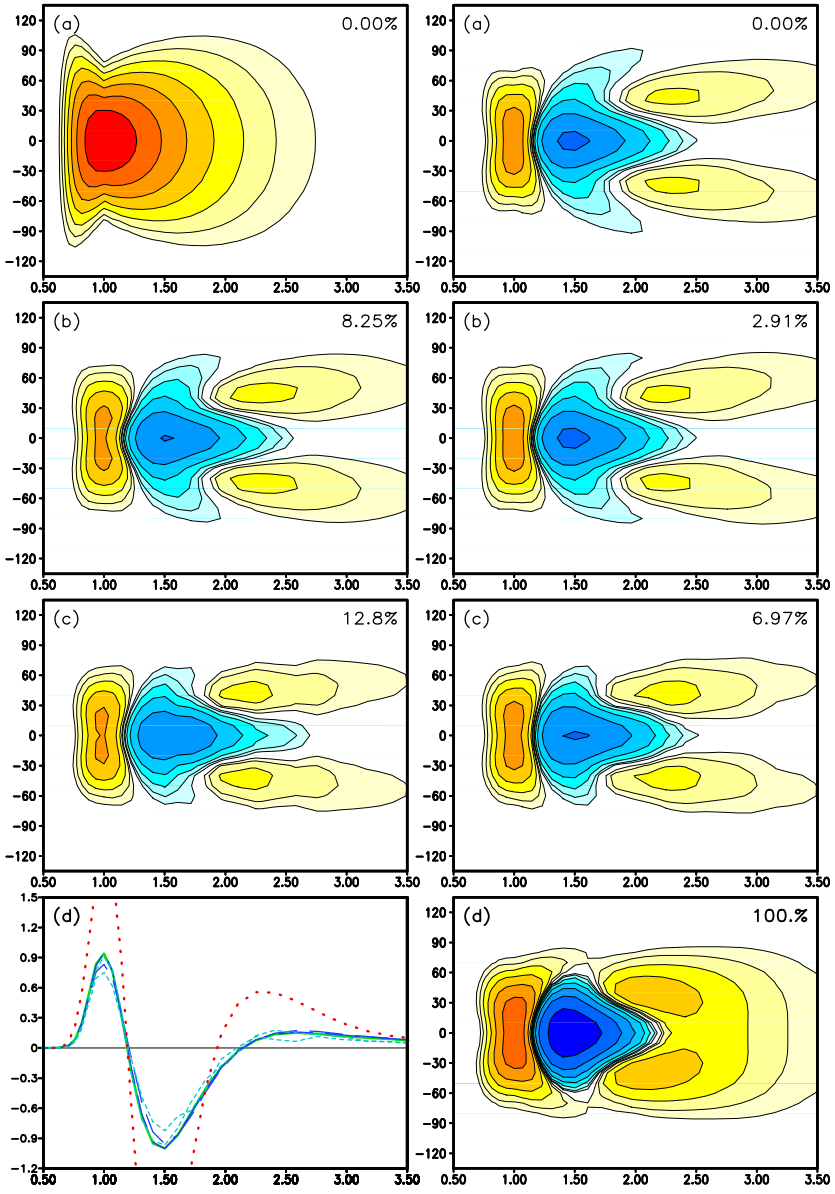

Fig. C.1: Results for test case 1. See text for legend.

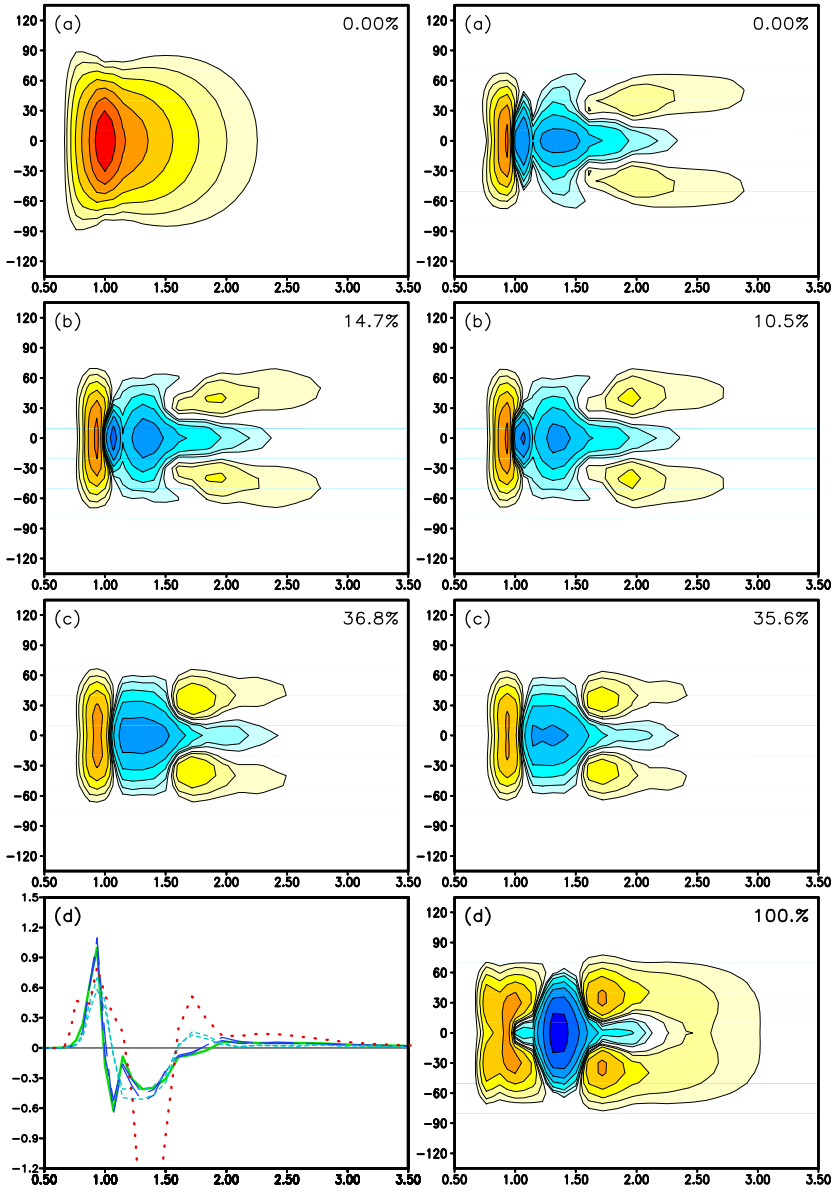

Fig. C.2: Results for test case 2. See text for legend.

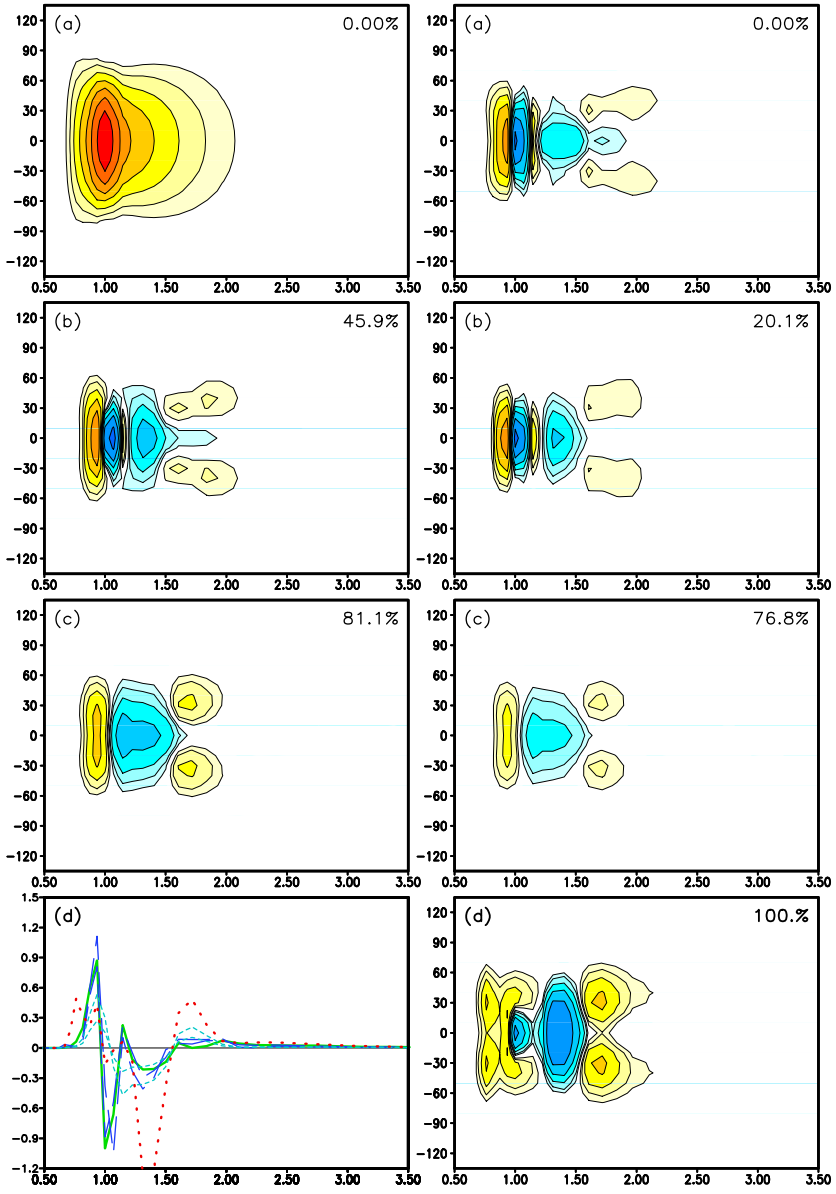

Fig. C.3: Results for test case 3. See text for legend.

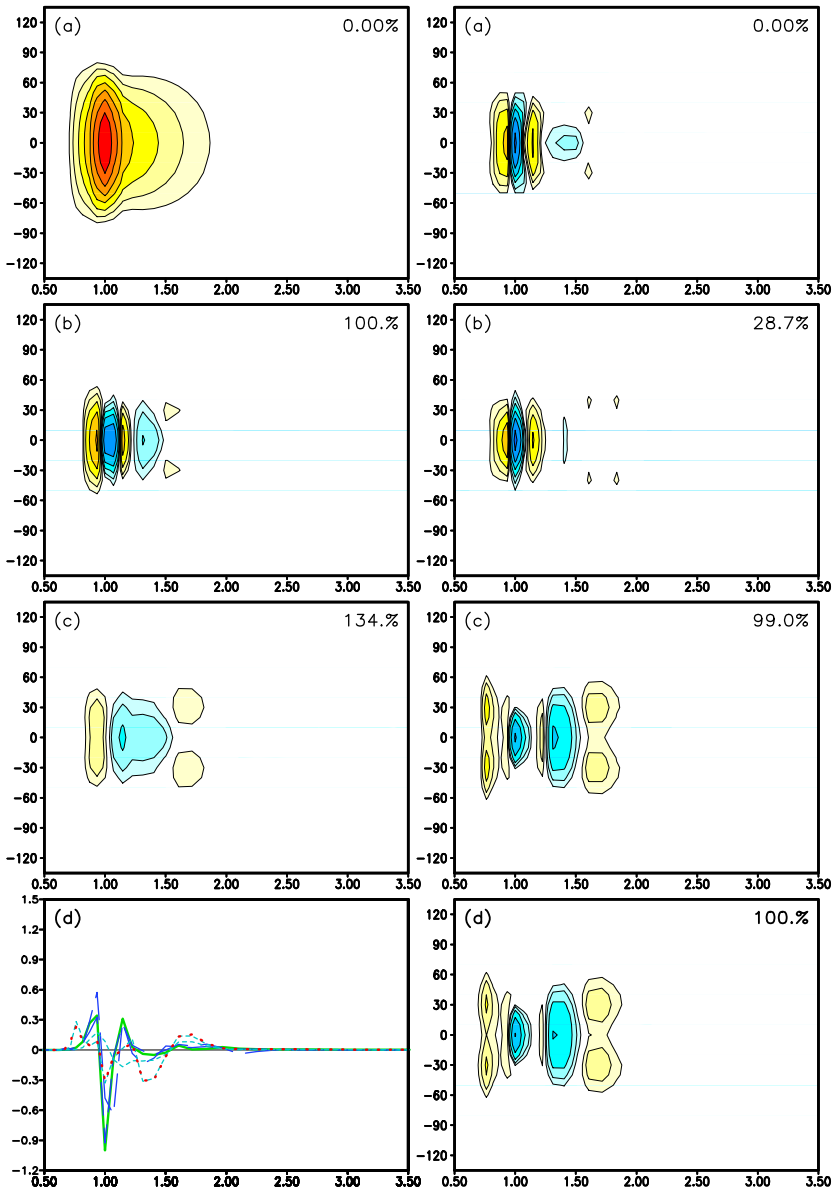

Fig. C.4: Results for test case 4. See text for legend.

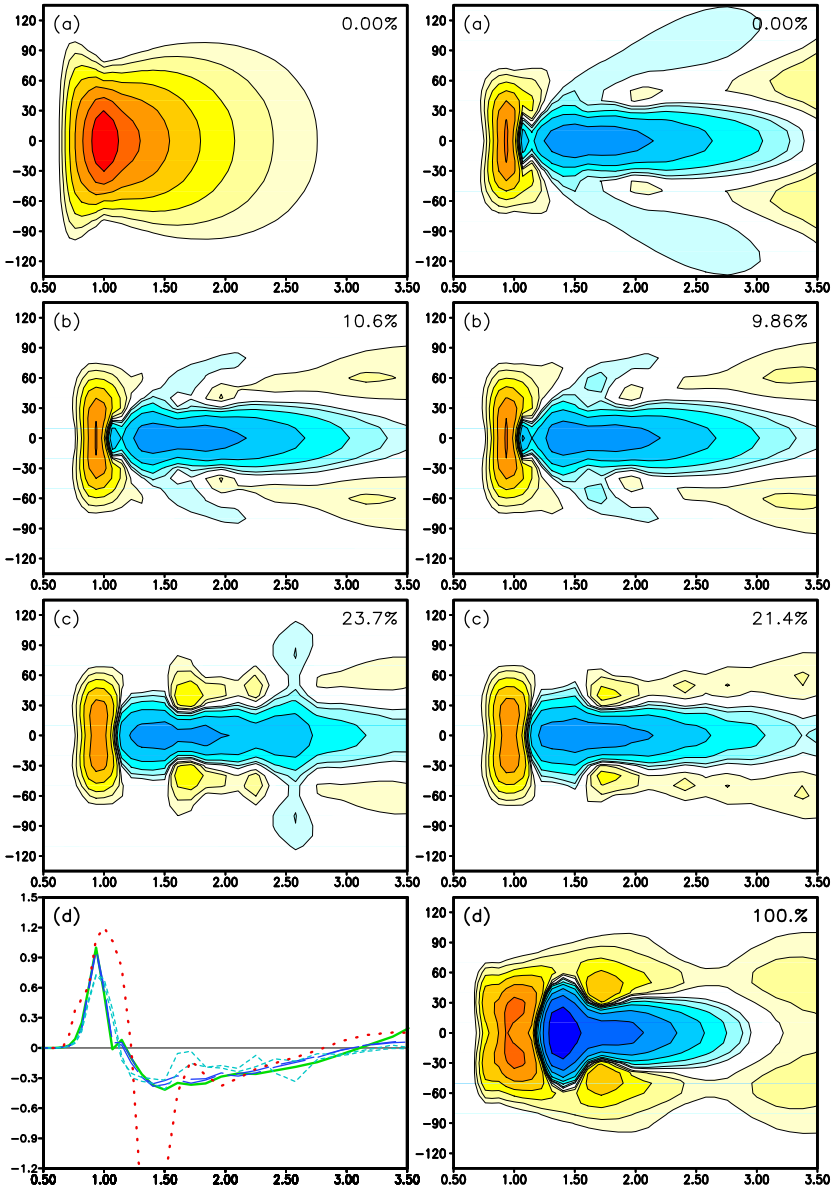

Fig. C.5: Results for test case 5. See text for legend.

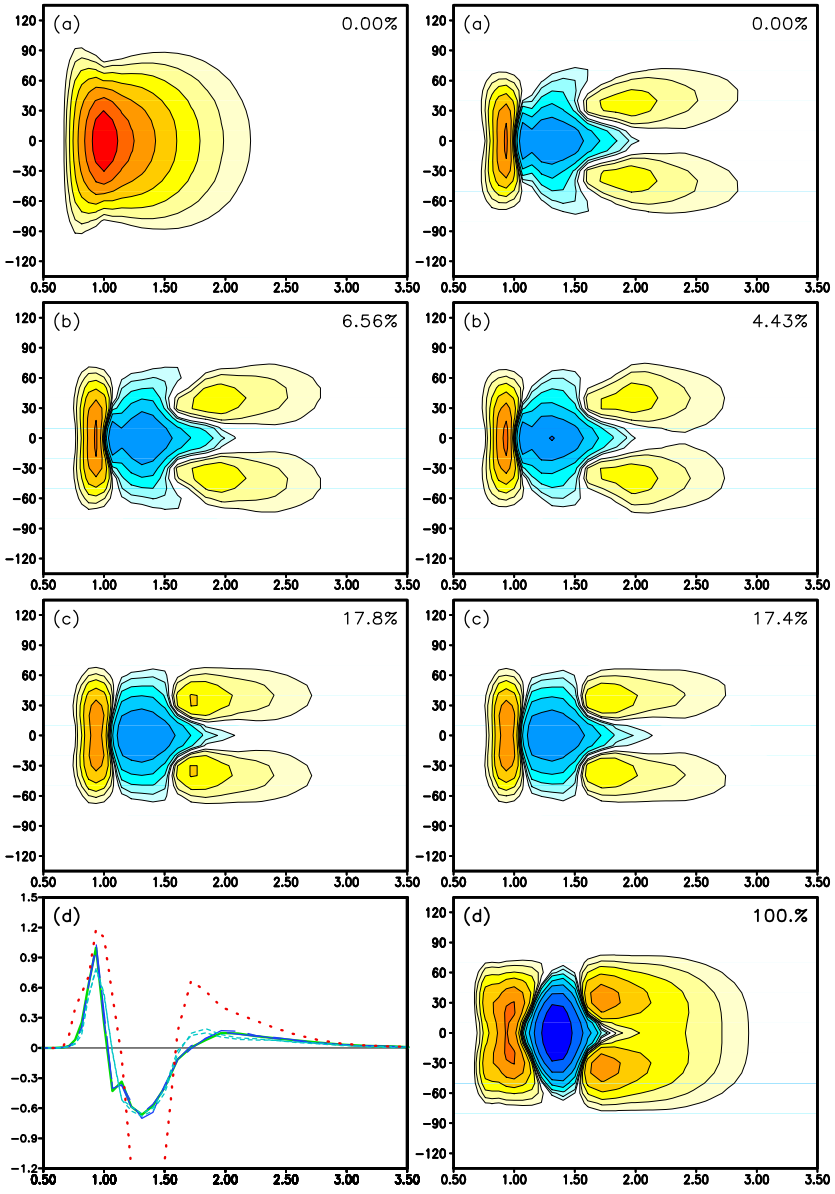

Fig. C.6: Results for test case 6. See text for legend.

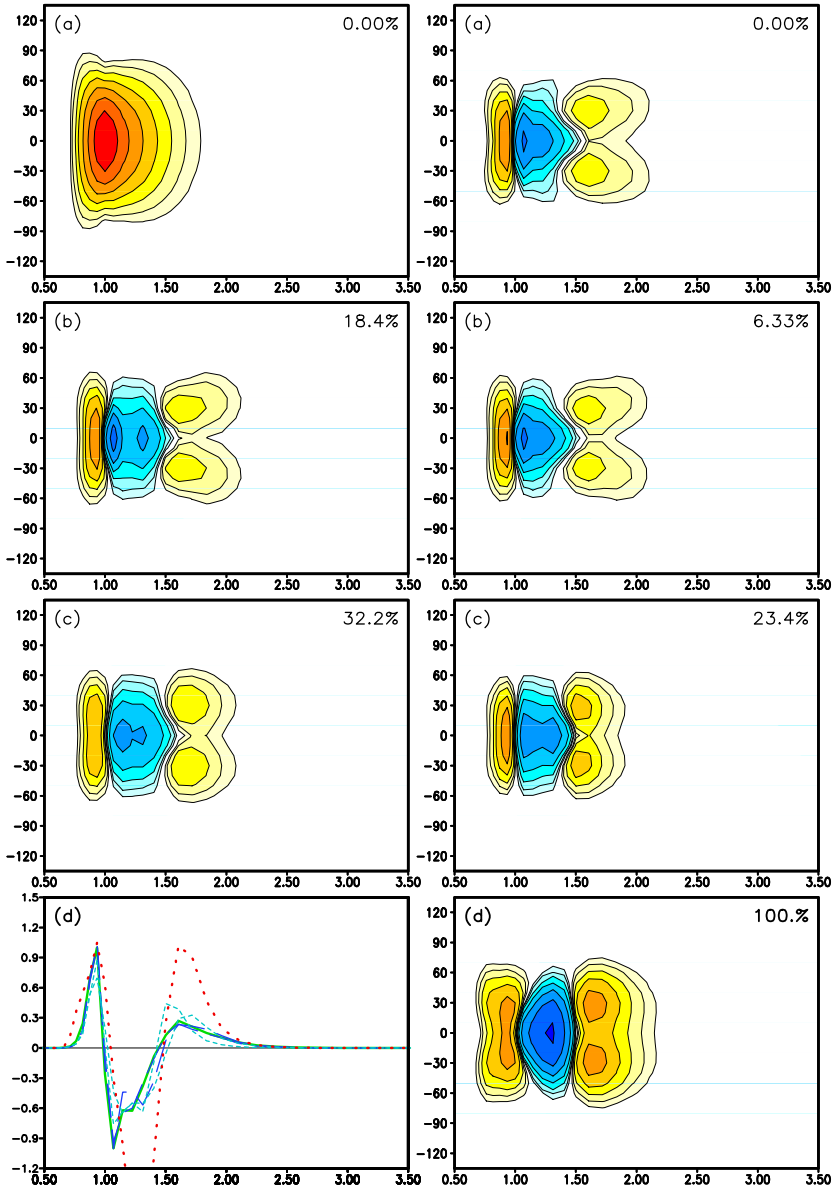

Fig. C.7: Results for test case 7. See text for legend.

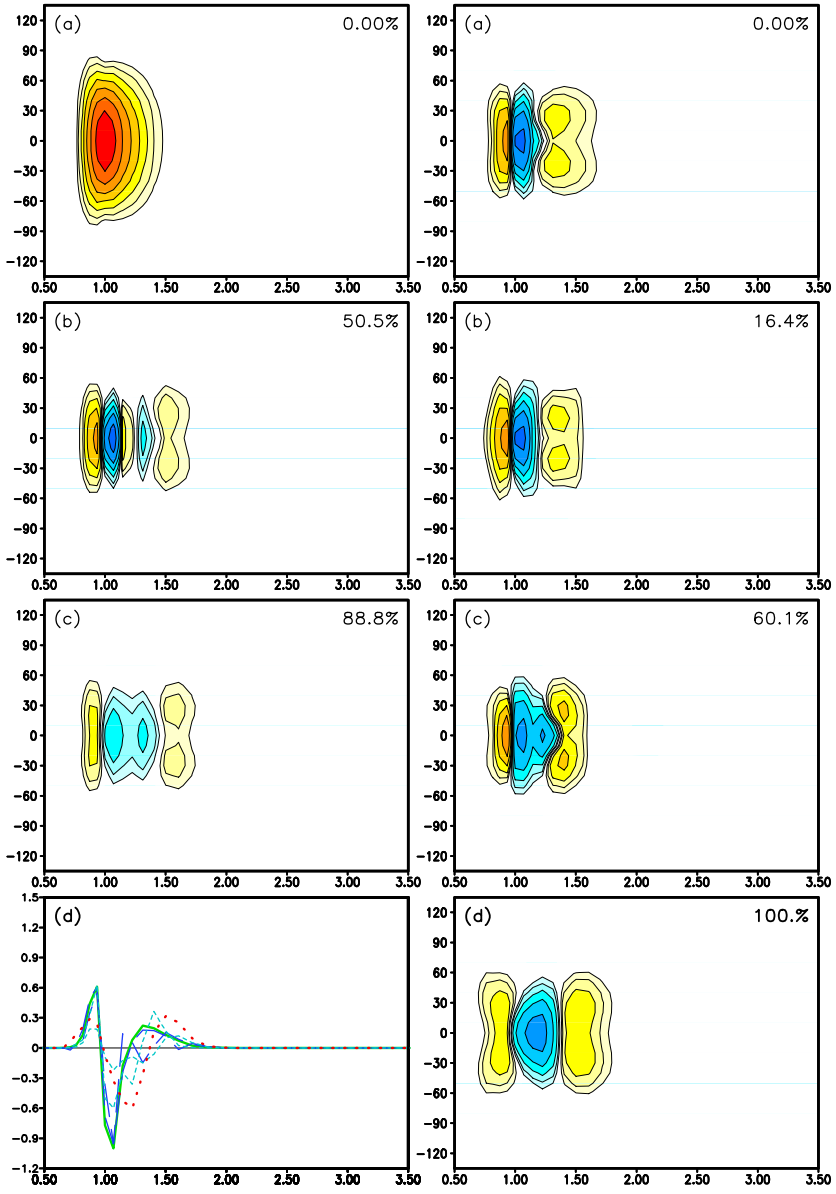

Fig. C.8: Results for test case 8. See text for legend.

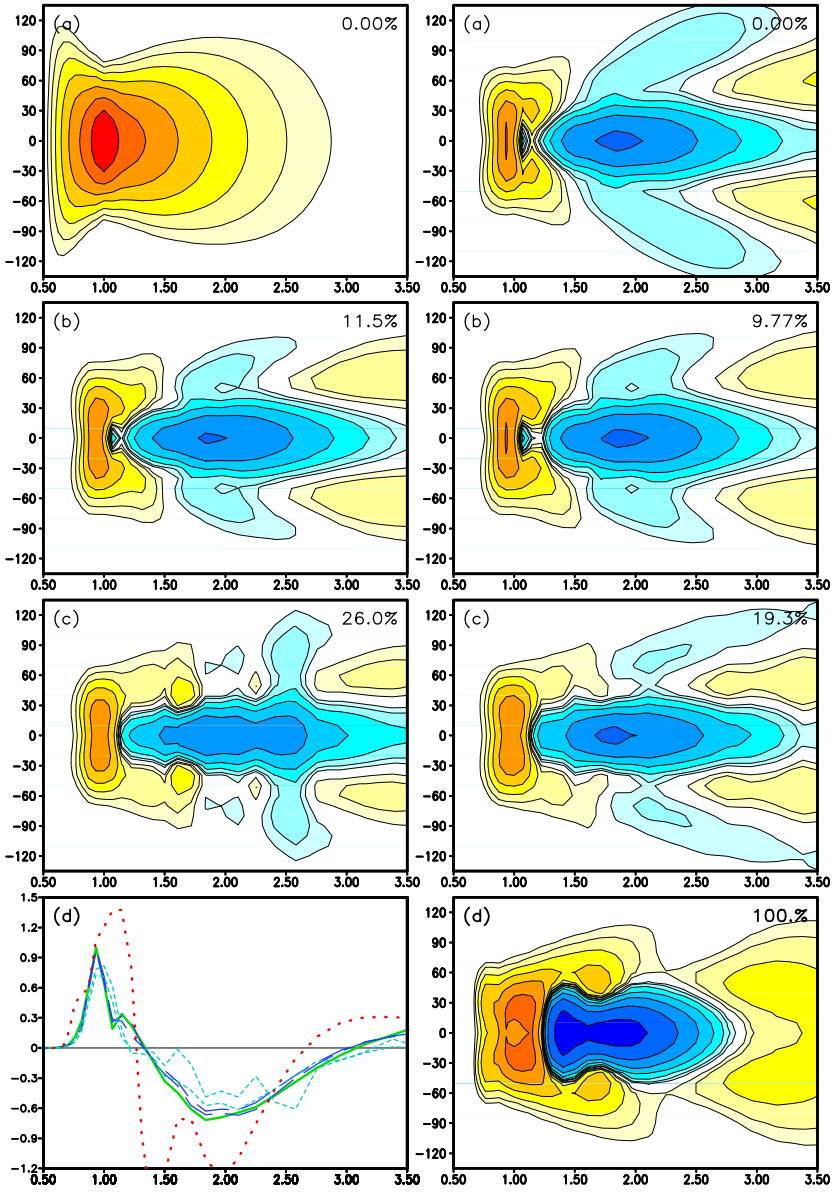

Fig. C.9: Results for test case 9. See text for legend.

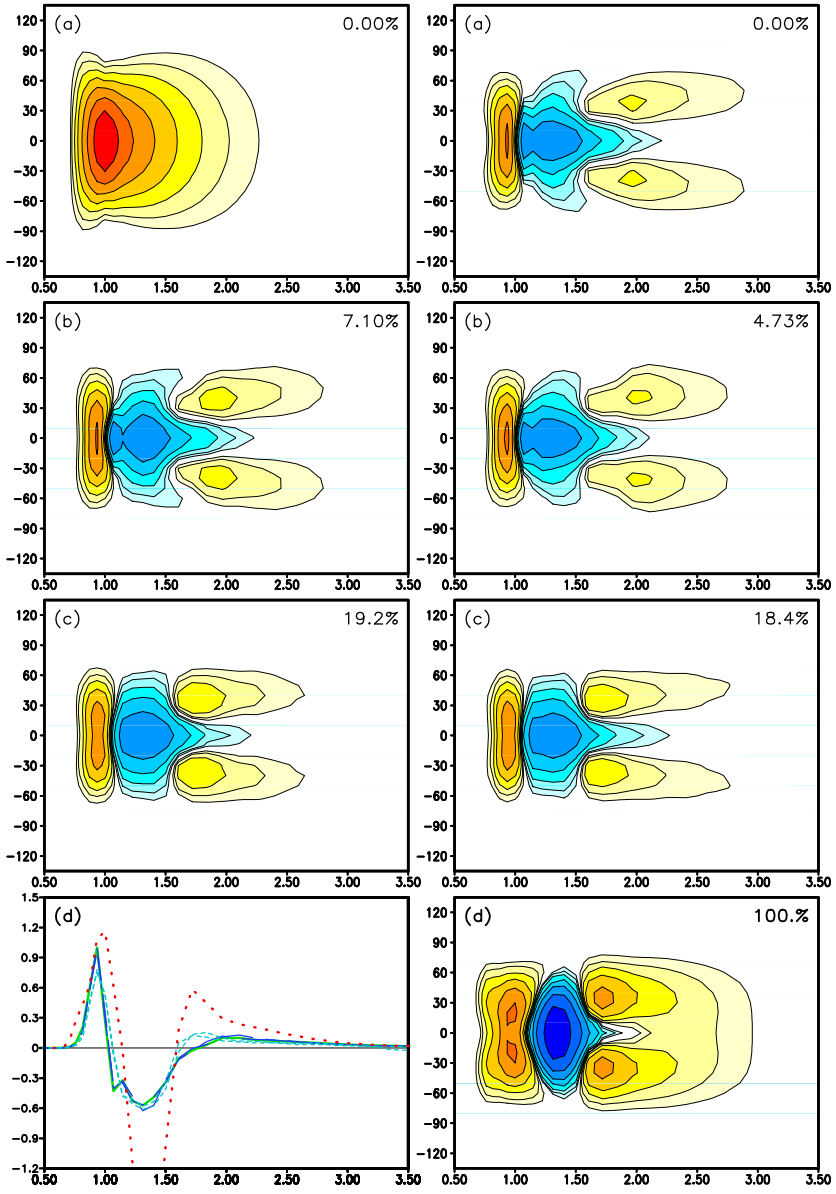

Fig. C.10: Results for test case 10. See text for legend.

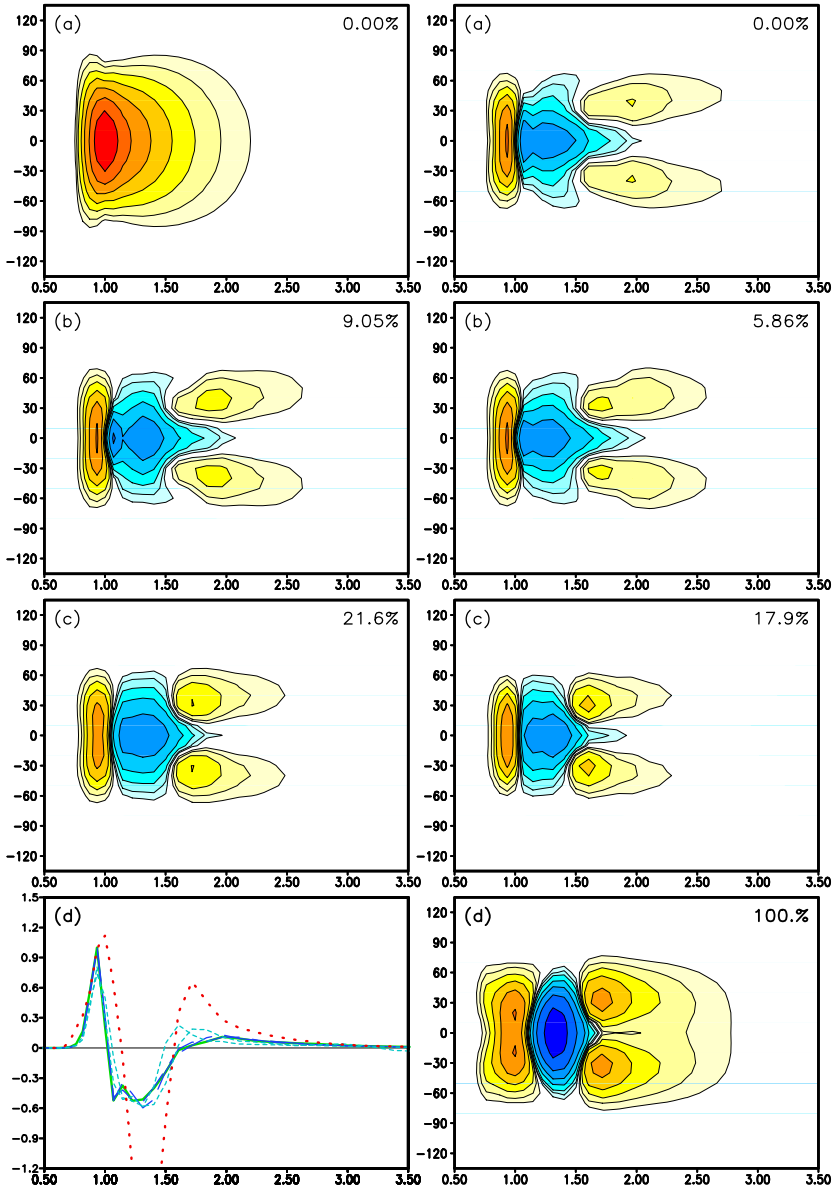

Fig. C.11: Results for test case 11. See text for legend.

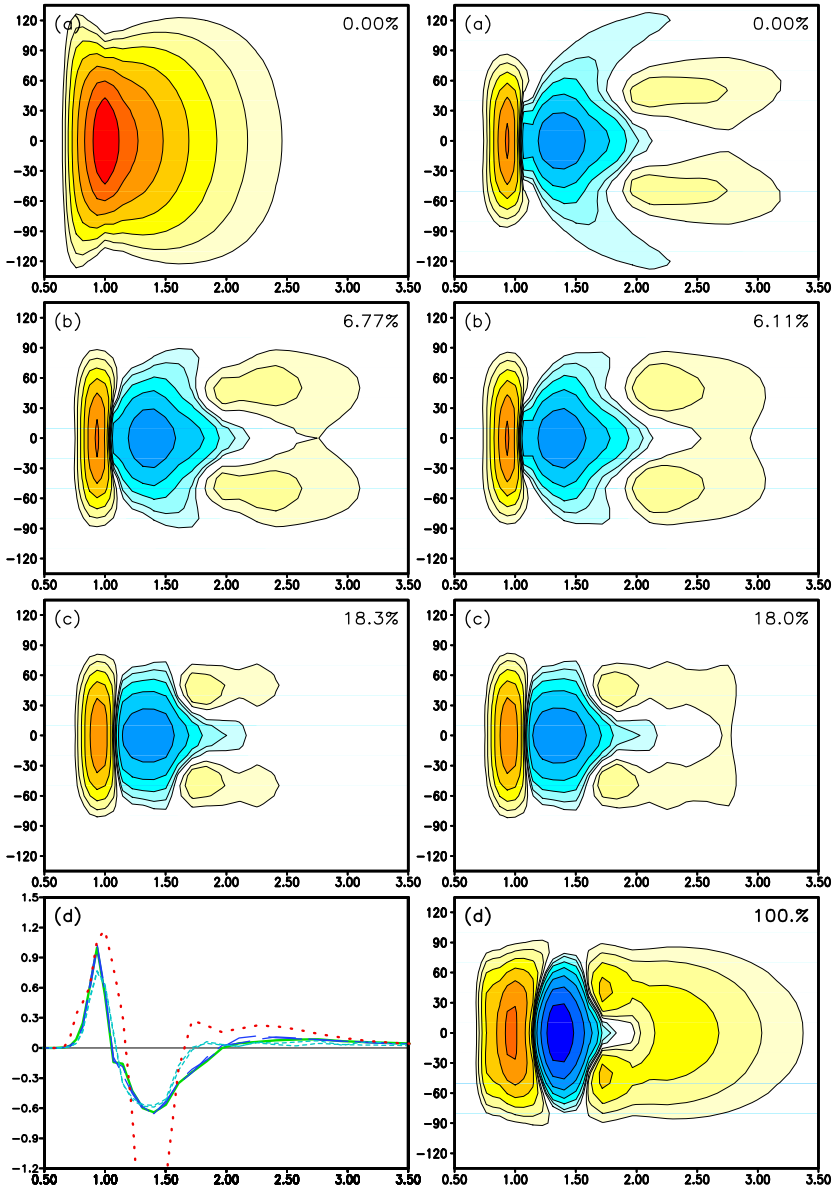

Fig. C.12: Results for test case 12. See text for legend.

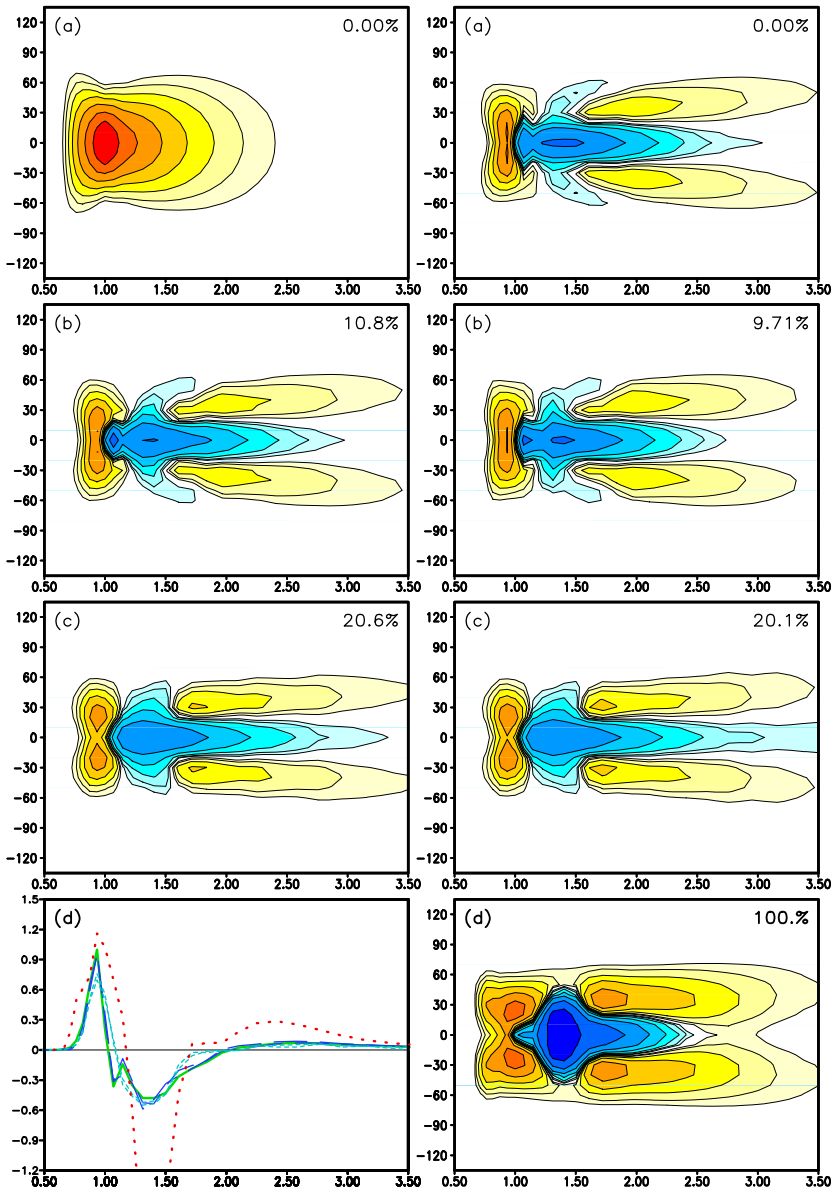

Fig. C.13: Results for test case 13. See text for legend.

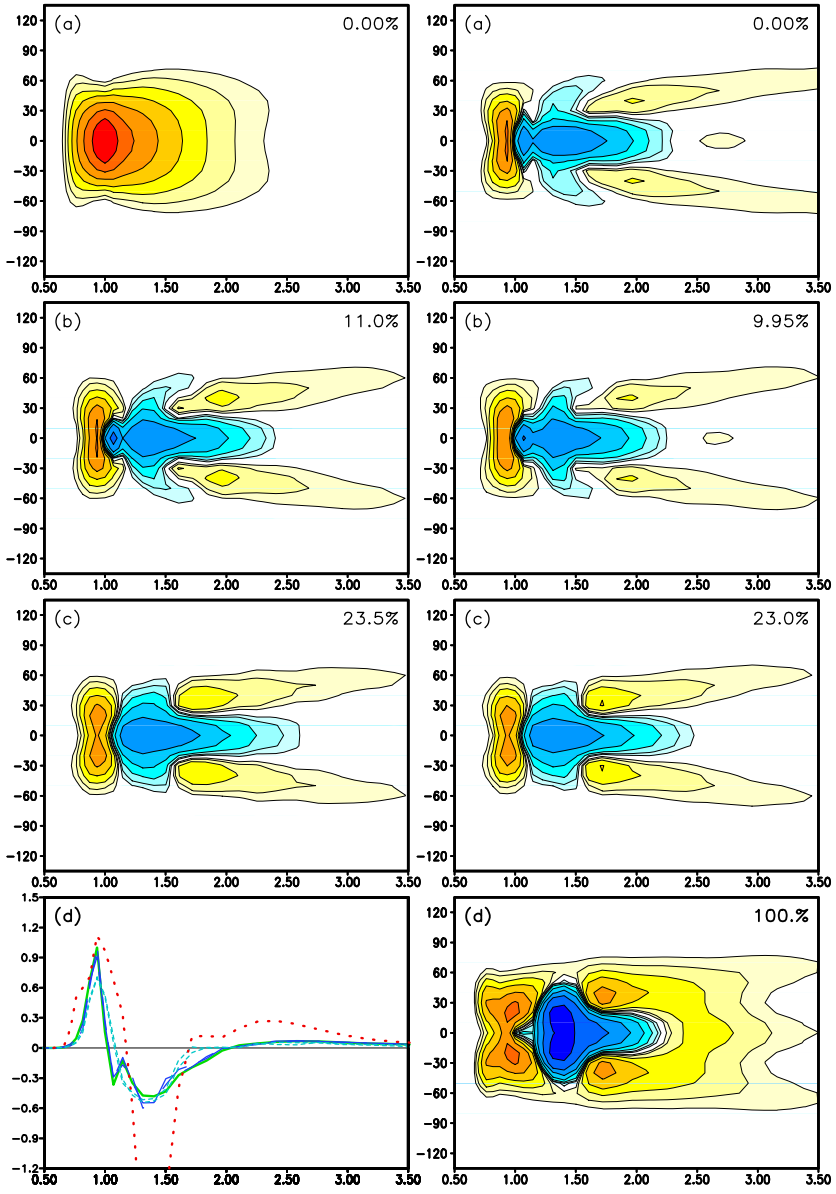

Fig. C.14: Results for test case 14. See text for legend.

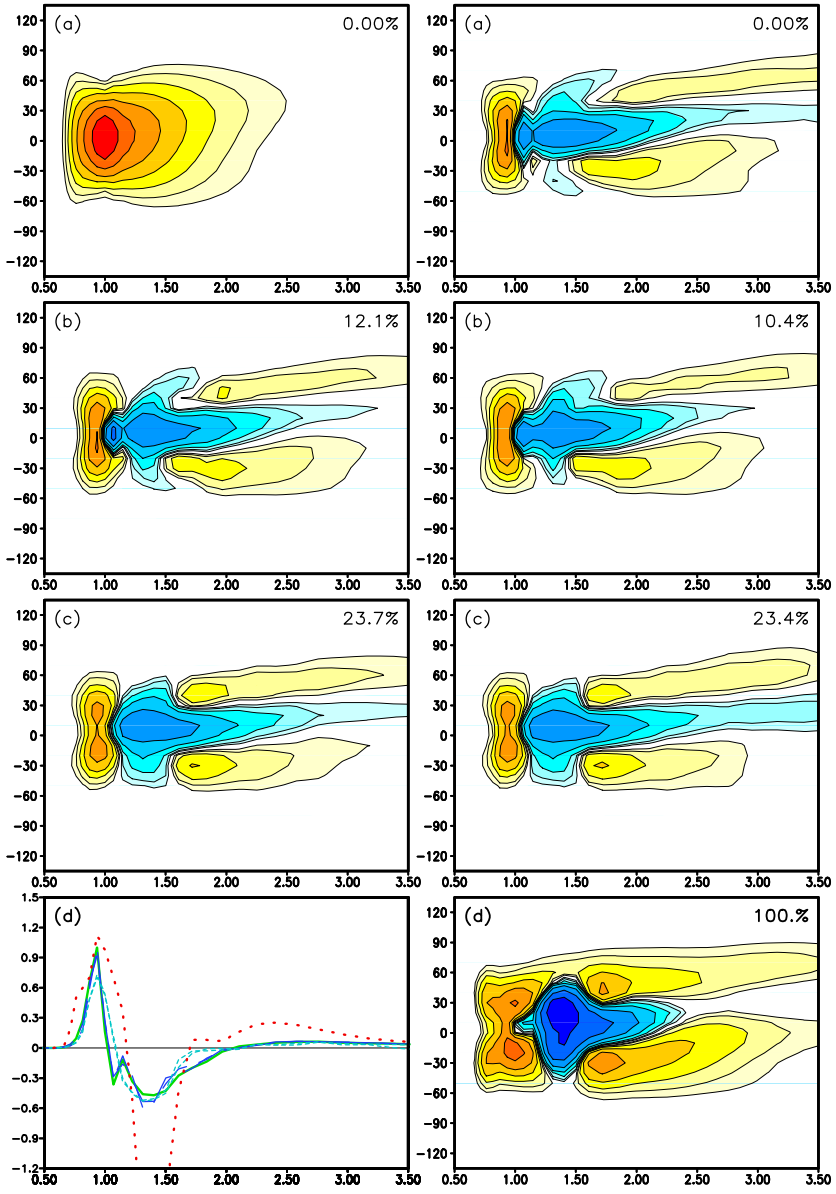

Fig. C.15: Results for test case 15. See text for legend.

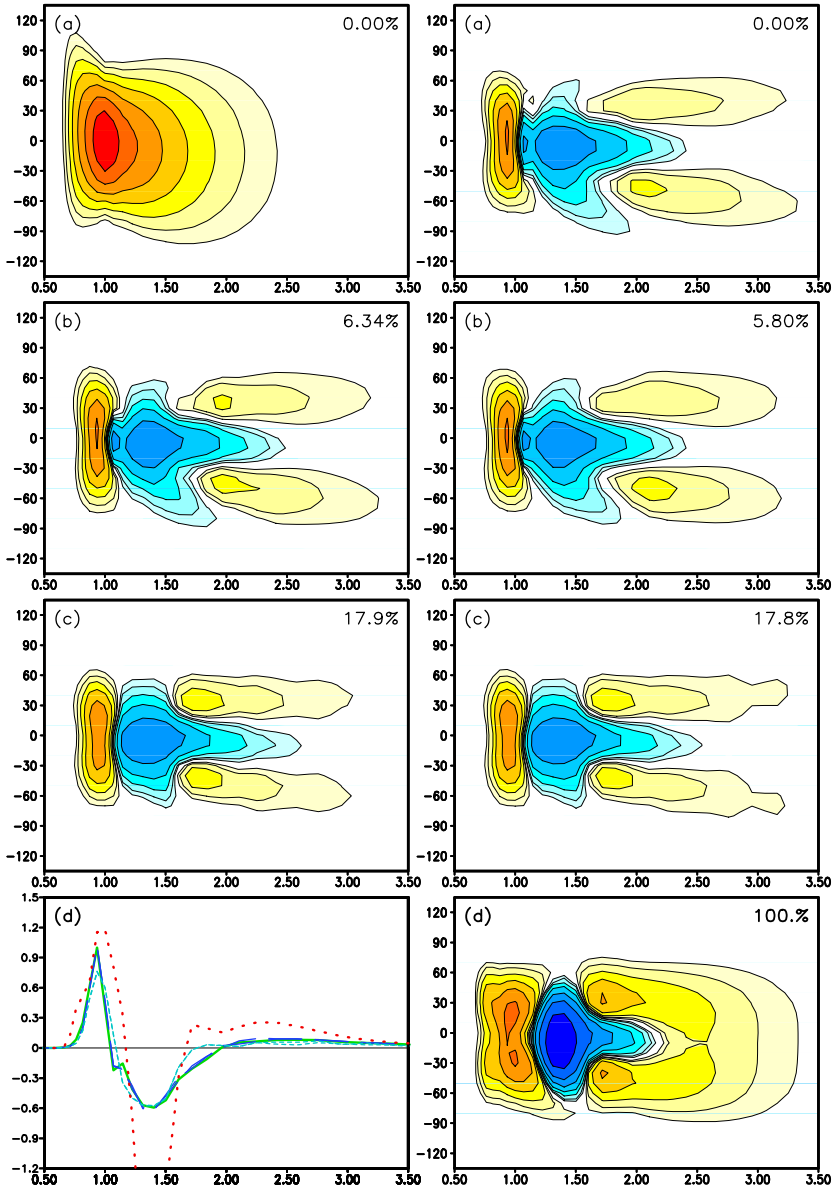

Fig. C.16: Results for test case 16. See text for legend.

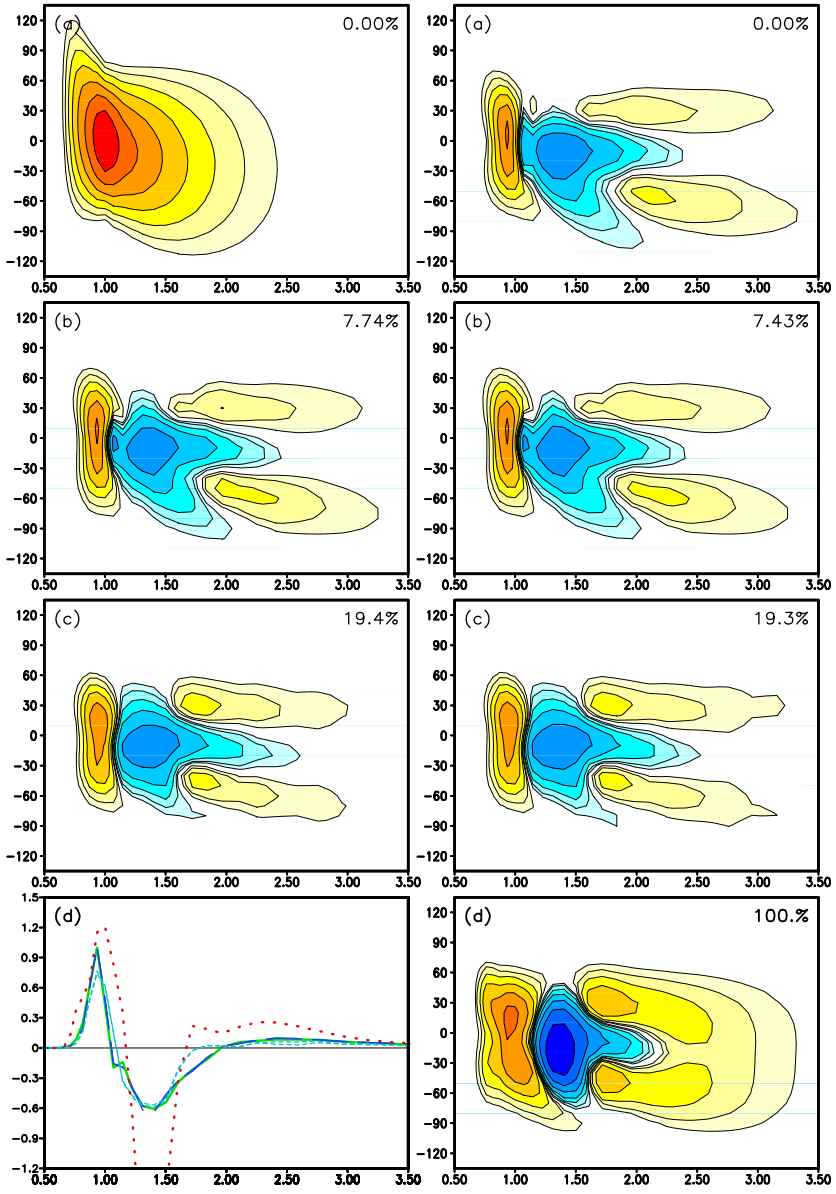

Fig. C.17: Results for test case 17. See text for legend.

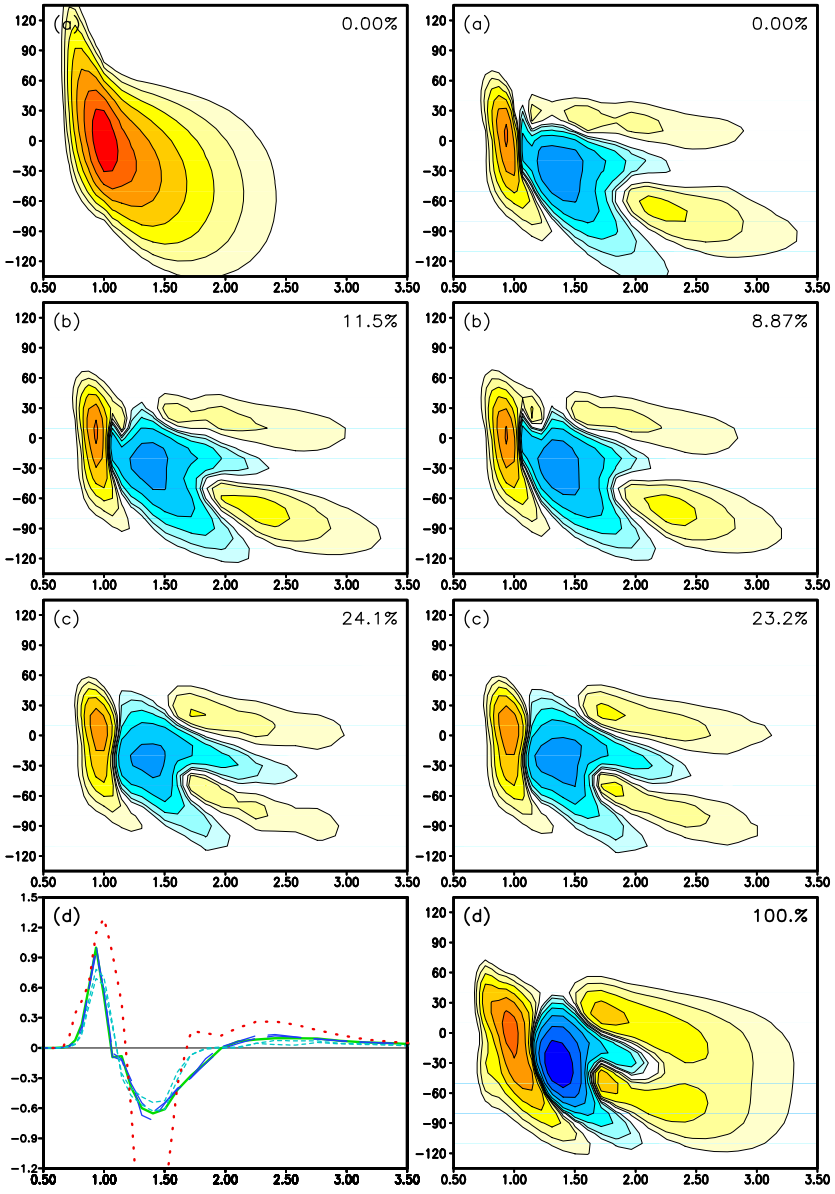

Fig. C.18: Results for test case 18. See text for legend.

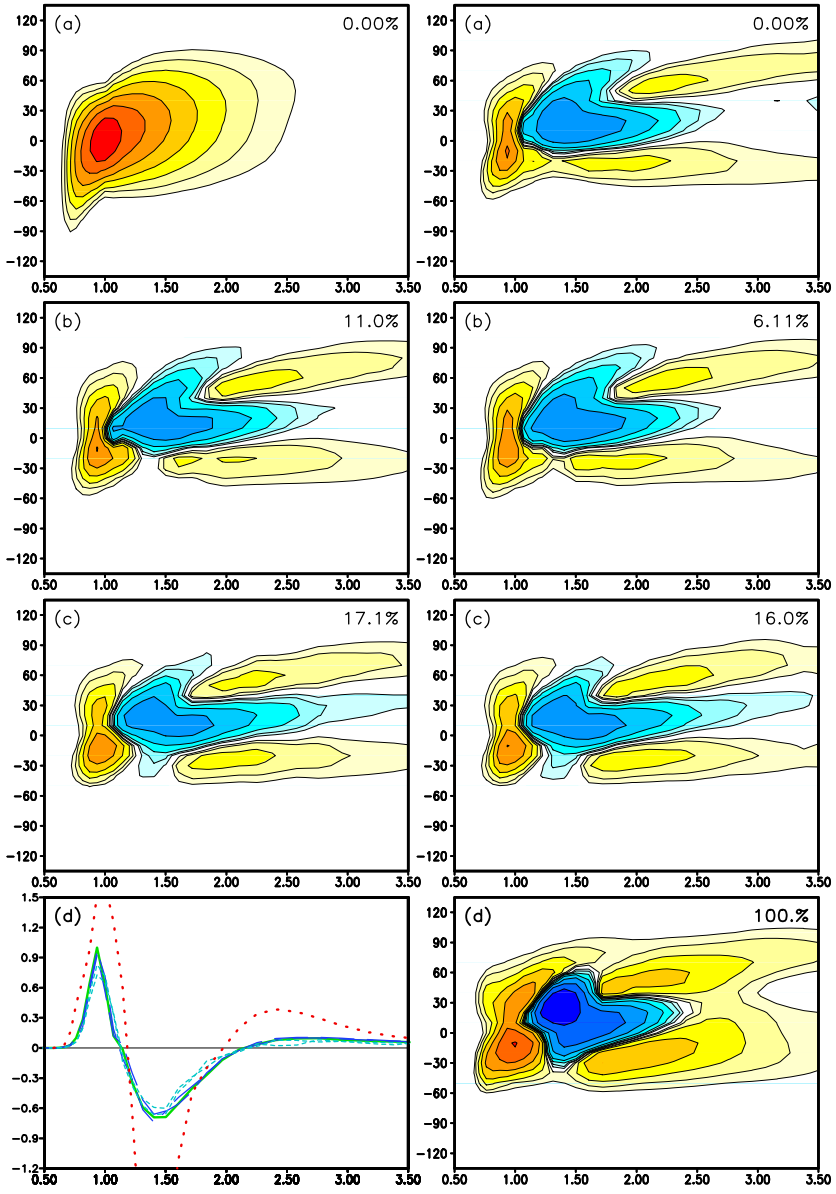

Fig. C.19: Results for test case 19. See text for legend.

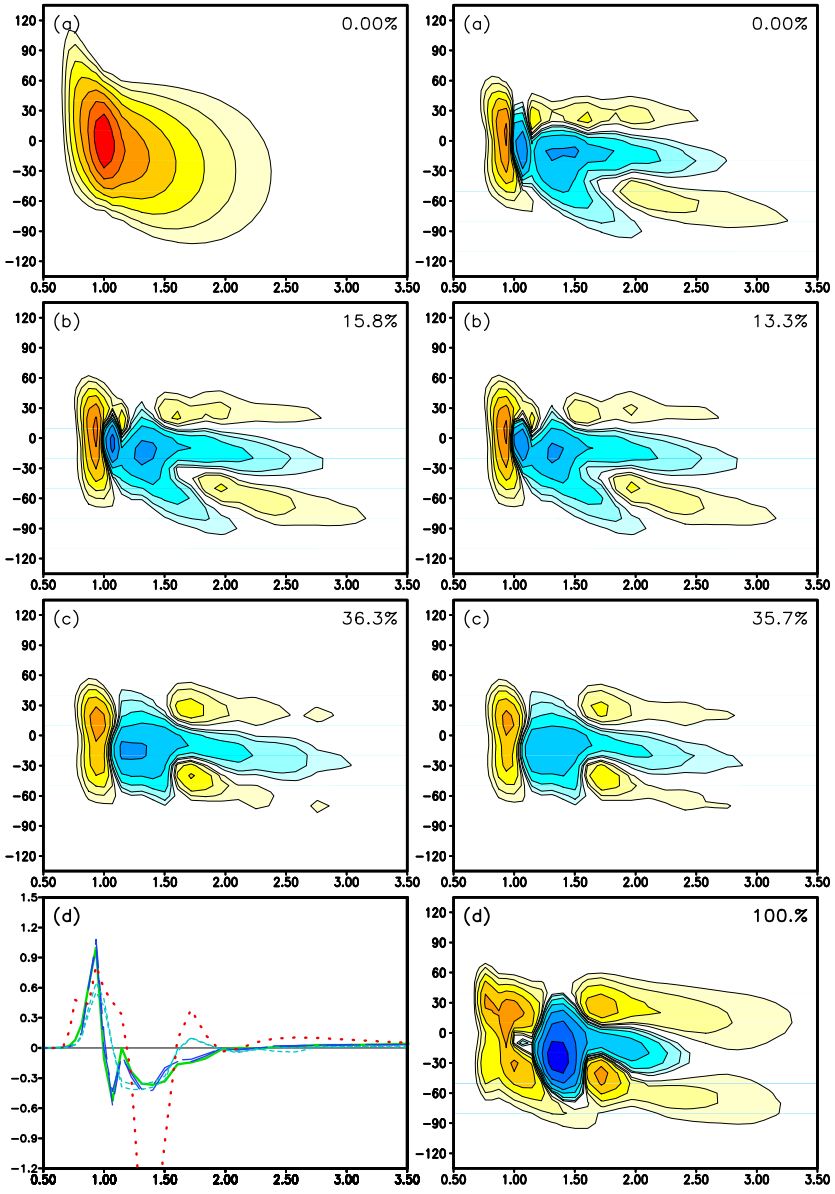

Fig. C.20: Results for test case 20. See text for legend.